

**HIDDEN HIGGSES AND DARK MATTER AT  
CURRENT AND FUTURE COLLIDERS**

*Adarsh Pyarelal*



A Dissertation Submitted to the Faculty of the  
**DEPARTMENT OF PHYSICS**  
In Partial Fulfillment of the Requirements  
For the Degree of  
**DOCTOR OF PHILOSOPHY**  
In the Graduate College  
University of Arizona

2017



THE UNIVERSITY OF ARIZONA  
GRADUATE COLLEGE

As members of the Dissertation Committee, we certify that we have read the dissertation prepared by Adarsh Pyarelal entitled *Hidden Higgses and Dark Matter at Current and Future Colliders*, and recommend that it be accepted as fulfilling the dissertation requirement for the Degree of Doctor of Philosophy.

---

Shufang Su Date

---

William D. Toussaint Date

---

Kenneth A. Johns Date

---

Sean P. Fleming Date

---

Weigang Wang Date

Final approval and acceptance of this dissertation is contingent upon the candidate's submission of the final copies of the dissertation to the Graduate College.

I hereby certify that I have read this dissertation prepared under my direction and recommend that it be accepted as fulfilling the dissertation requirement.

---

Dissertation Director: Shufang Su Date



#### STATEMENT BY AUTHOR

---

This dissertation has been submitted in partial fulfillment of the requirements for an advanced degree at the University of Arizona and is deposited in the University Library to be made available to borrowers under rules of the Library. Brief quotations from this dissertation are allowable without special permission, provided that an accurate acknowledgement of the source is made. Requests for permission for extended quotation from or reproduction of this manuscript in whole or in part may be granted by the head of the major department or the Dean of the Graduate College when in his or her judgment the proposed use of the material is in the interests of scholarship. In all other instances, however, permission must be obtained from the author.

---

SIGNED: Adarsh Pyarelal



## ACKNOWLEDGMENTS

---

I would like to thank my advisor, Shufang Su, for her patient guidance and support throughout my graduate studies. Under her mentorship, I learned to critically examine scientific claims and to hold my own research to the highest standards. I would also like to thank the following:

- Ken Johns, for letting me get a taste of experimental particle physics, career advice, and a fun semester teaching Scientific Computing.
- Doug Toussaint, Sean Fleming, and Weigang Wang for agreeing to serve on my committee.
- Abhay Shastry, Dheeraj Golla, and Rebekah Cross for their steady friendship these past six years.
- Jessie Erikson, for being the most wonderful partner anyone could ask for.

Finally, I would like to thank my family, and especially my parents for their unconditional love and encouragement during this process. It is a huge privilege to be able to pursue a doctorate, and I could not have done it without their support.



## ABSTRACT

---

Despite its indisputable successes, the Standard Model of particle physics (SM) is widely considered to be an effective low-energy approximation to an underlying theory that describes physics at higher energy scales. The class of models known as Two-Higgs Doublet Models (2HDMs) are physically well-motivated extensions to the scalar sector of the SM. Through the addition of an additional  $SU(2)$  Higgs doublet field, they extend the scalar mass spectrum so that it is comprised of two CP-even states  $h$  and  $H$ , a CP-odd state  $A$ , and a charged state  $H^\pm$ . Traditional searches for these states at particle colliders focus on finding them via their decays to SM particles. However, there are compelling scenarios in which these heavy scalars decay predominantly through exotic modes to non-SM final states. In certain regions of parameter space, these exotic modes can dominate the conventional decay modes to SM final states, and thus provide a complementary avenue for discovery. In this work, we present two analyses aimed at discovering new scalar states at the Large Hadron Collider (LHC) and a possible future hadron collider via exotic decay modes. The first is aimed at discovering charged Higgs bosons  $H^\pm$  via top decay at the LHC. We find that the exotic decay modes outperform the conventional decay modes for regions of parameter space with low values of the 2HDM parameter  $\tan\beta$ . The second analysis is aims to systematically cover a number of different exotic decay scenarios at both the 14 TeV LHC and a future 100 TeV hadron collider. We find that the preliminary results are promising, and cover a large swathe of 2HDM parameter space, up to scalar masses of 3.5 TeV, for a wide range of values of  $\tan\beta$ .

In addition, we also present an analysis aimed at discovering pair produced Higgsinos that decay to binos at a 100 TeV collider. Higgsinos and binos are the fermionic counterparts of scalar states in the Minimal Supersymmetric Standard Model. This heavily-studied model can be viewed a special case of a 2HDM that incorporates supersymmetry, a symmetry that connects fermions and bosons. In the scenario we consider, the bino is the lightest supersymmetric partner, which makes it a good candidate for dark matter. This analysis is performed using razor variables and boosted decision trees. We find that we are able to exclude Higgsinos up to 1.8 TeV for binos up to 1.3 TeV with this analysis.



## CONTENTS

---

ABSTRACT	9
LIST OF FIGURES	13
LIST OF TABLES	17
1 INTRODUCTION	19
2 THE STANDARD MODEL AND BEYOND	23
2.1 The Standard Model . . . . .	23
2.2 Two-Higgs Doublet Models . . . . .	28
2.3 The Minimal Supersymmetric Standard Model . . . . .	32
3 COLLIDER PHENOMENOLOGY AND MACHINE LEARNING	39
3.1 Detector design for hadron colliders . . . . .	39
3.2 Anatomy of a collider analysis . . . . .	41
3.3 Statistical significance in particle physics . . . . .	43
3.4 Machine learning in particle physics . . . . .	45
4 LIGHT CHARGED HIGGSES AT THE LHC	49
4.1 Couplings and branching ratios . . . . .	50
4.2 Literature review . . . . .	52
4.3 Collider analysis . . . . .	54
4.4 Implications for the Type II 2HDM . . . . .	58
4.5 Conclusion . . . . .	61
5 EXOTIC HIGGS DECAYS AT 14 AND 100 TEV	63
5.1 Setting the stage . . . . .	63
5.2 Classifying exotic decays . . . . .	64
5.3 Literature review . . . . .	65
5.4 Crafting features for our classifier . . . . .	66
5.5 Preliminary results . . . . .	68
5.6 Conclusions and outlook . . . . .	69
6 A RAZOR SEARCH FOR DARK MATTER AT 100 TEV	71
6.1 Dark matter . . . . .	71
6.2 Model and experimental constraints . . . . .	73
6.3 Analysis Details . . . . .	77
6.4 Conclusion . . . . .	82
7 CONCLUSION	85
BIBLIOGRAPHY	87



## LIST OF FIGURES

---

1.1	Schematic diagram of the Large Hadron Collider, which lies on the border between Switzerland and France. (CERN) . . . . .	19
2.1	A representation of the innards of a proton, showing the dynamic structure. Image source:[11] . . . . .	27
2.2	Feynman diagram for the one-loop fermionic correction to the SM Higgs mass . . . . .	33
2.3	Feynman diagram for the one-loop scalar correction to the SM Higgs mass . . . . .	33
2.4	2-loop RG evolution of inverse gauge couplings in the SM (dashed lines) and the MSSM (solid lines). The sparticle masses are varied between 0.5-1.5 TeV, and $\alpha_3(m_Z)$ is varied between 0.117 and 0.121. Source: [10]. . . . .	34
3.1	Transverse slice of the CMS detector, showing the paths of various particles. Source: [20] . . . . .	41
3.2	Illustration of a non-linear decision boundary in two-dimensional feature space. . . . .	46
4.1	Contours of the branching fraction of the top quark to the charged Higgs, in the $m_{H^\pm} - t_\beta$ plane. We see that it reaches a minimum at $t_\beta = \sqrt{m_t/m_b} \approx 8$ . . . . .	50
4.2	Contours of the branching fraction for the decay ( $H^\pm \rightarrow AW$ ) in the Type II 2HDM in $m_{H^\pm} - t_\beta$ plane. The branching fraction reaches large values for $t_\beta$ between 10 and 30, for $m_{H^\pm}$ . . . . .	51
4.3	The branching fractions of $H^\pm \rightarrow AW$ (red), $\tau\nu$ (green) and $cs$ (blue) as functions of $t_\beta$ for $m_{H^\pm} = 160$ GeV. . . . .	51
4.4	CMS limits on the branching fraction of the top quark to the charged Higgs . . . . .	52
4.5	The excluded region in $m_{H^\pm} - t_\beta$ plane assuming a $BR(H^\pm \rightarrow \tau\nu) = 100\%$ (combined yellow and cyan regions) and the weakened limits with a light neutral Higgs (cyan region only). . . . .	52
4.6	Normalized distribution of $\cos \theta^*$ , for case A with $m_{H^\pm} = 160$ GeV. The imposed cuts are indicated by the vertical dashed lines. . . . .	55
4.7	Normalized distribution of the transverse momentum of the $tj$ system $p_{T,tj}$ , for case A with $m_{H^\pm} = 160$ GeV. The imposed cuts are indicated by the vertical dashed lines. . . . .	55
4.8	Exclusion and discovery limits on $\sigma \times BR(t \rightarrow H^+ b)$ . . . . .	57
4.9	Contours of branching fractions for the benchmark point BP1. . . . .	59
4.10	Contours of branching fractions $BR(H^\pm \rightarrow hW^\pm)$ for the benchmark point BP2. . . . .	59

4.11	The exclusion (yellow and cyan regions combined, bounded by dashed lines) and discovery (cyan region only bound by solid lines) reach achievable in the $t_\beta$ versus $s_{\beta-\alpha}$ plane for the benchmark points 1 and 2, with an integrated luminosity of $300 \text{ fb}^{-1}$ at the 14 TeV LHC. The red lines represent the reach achievable by the top pair production channel, while the blue lines represent the reach achievable by the single top channel. . . . .	60
4.12	Exclusion (yellow regions bounded by solid lines as well as the cyan regions) and discovery (cyan regions bounded by the dashed lines) imposed by the $tj$ -channel (blue) and $tt$ -channel (red) in the $m_{H^\pm} - t_\beta$ parameter space for $300 \text{ fb}^{-1}$ luminosity with $m_A = 70 \text{ GeV}$ . The same limits apply for $m_h = 70 \text{ GeV}$ and $s_{\beta-\alpha} = 0$ if $A$ is decoupled. The black hatched region indicates the region excluded by the CMS search based on $H^\pm \rightarrow \tau\nu$ [33]. . . . .	60
5.1	Branching fractions for exotic decays in Type II 2HDMs, as a function of $t_\beta$ , with $c_{\beta-\alpha} = 0$ . Source: [4]. . . . .	64
5.2	Exclusion and discovery limits for the channel $A \rightarrow HZ \rightarrow \tau\tau ll$ , for the 14 TeV LHC with $100 \text{ fb}^{-1}$ (solid red line) and $300 \text{ fb}^{-1}$ (dashed red line) and a 100 TeV collider with $1000 \text{ fb}^{-1}$ (solid blue line) and $3000 \text{ fb}^{-1}$ (dashed blue line). Here we assume $m_{12}^2 = m_H^2 s_\beta c_\beta$ . The top panel represents the $bb \rightarrow A$ production channel, while the lower one represents the $gg \rightarrow A$ production channel. . . . .	68
5.3	Exclusion and discovery limits for the channel $H \rightarrow AZ \rightarrow \tau\tau ll$ for the 14 TeV LHC with $100 \text{ fb}^{-1}$ (solid red line) and $300 \text{ fb}^{-1}$ (dashed red line) and a 100 TeV collider with $1000 \text{ fb}^{-1}$ (solid blue line) and $3000 \text{ fb}^{-1}$ (dashed blue line). Here we assume $m_{12}^2 = m_H^2 s_\beta c_\beta$ . The left panel represents the $bb \rightarrow H$ production channel, while the right represents the $gg \rightarrow H$ production channel. . . . .	68
5.4	Exclusion and discovery reaches in the $m_{H^\pm} - m_H$ plane for the exotic decay $H^\pm \rightarrow HW^\pm$ , at a 100 TeV collider with an integrated luminosity of $3 \text{ ab}^{-1}$ . Here we assume $m_{12}^2 = m_H^2 s_\beta c_\beta$ . . . . .	69
6.1	DM detection, three ways . . . . .	71
6.2	Feynman diagram for bino-stau coannihilation. . . . .	72
6.3	Feynman diagrams for the signal and background processes (Generated using [102].) . . . . .	74
6.4	Higgsino pair production cross section as a function of $\mu$ , for a $M_1 = 25 \text{ GeV}$ . . . . .	75
6.5	Higgsino decay branching ratios of $\mu$ , for a $M_1 = 25 \text{ GeV}$ . . . . .	75

6.6	Normalized distributions of the razor kinematical variables $M_R$ (top) and $M_T^R$ (bottom) for a 1 TeV higgsino NLSP and 25 GeV bino LSP . . . . .	78
6.7	Distribution of the decision function of the gradient boosted decision tree classifier algorithm for the signal ( $ \mu  = 1$ TeV, $M_1 = 25$ GeV) and backgrounds. . . . .	80
6.8	Discovery (red) and exclusion (blue) contours for the traditional cut-and-count analysis (solid) and boosted decision tree analysis (dashed), for an integrated luminosity of 3000 $\text{fb}^{-1}$ . . . . .	81



## LIST OF TABLES

---

2.1	The fields of the Standard Model, grouped by their charges under the relevant gauge groups. . . . .	23
2.2	The fermion sector of the Standard Model, grouped by generation. . . . .	24
2.3	2HDMs with flavor conservation. . . . .	30
2.4	List of the factors $\xi$ that determine the Yukawa couplings of Higgs bosons in Type II 2HDMs. . . . .	32
2.5	Chiral supermultiplets of the MSSM. . . . .	37
2.6	Gauge supermultiplets of the MSSM. . . . .	37
3.1	The two competing hypotheses for our simple number counting example. Source: [27]. . . . .	43
4.1	Representative cut flow table for the benchmark point with $m_{H^\pm} = 160$ GeV and $m_A = 70$ GeV at the 14 TeV LHC. . . . .	56
4.2	Representative cut flow table for benchmark point with $m_{H^\pm} = 160$ GeV and $m_A = 70$ GeV at the 14 TeV LHC, for the decay mode $A \rightarrow \tau\tau$ . . . . .	57
4.3	Benchmark points used for illustrating the discovery and exclusion limits in the context of the Type II 2HDM. Also shown are the typical favored regions of $s_{\beta-\alpha}$ for each case (see [50]). . . . .	59
5.1	Summary of all the possible exotic decay modes and the dominant final states for non-SM Higgs bosons . . . . .	65
5.2	Summary of benchmark planes for exploring exotic Higgs decays in 2HDMs that survive theoretical and experimental constraints. Source: [4]. . . . .	65
6.1	Comparison of cross-sections for $(\tilde{\chi}_{2,3}^0, \tilde{\chi}_2^\pm)$ and $(\tilde{\chi}_2^0, \tilde{\chi}_3^0)$ , for $ \mu  \approx 1$ TeV, at a 100 TeV $pp$ collider. The pair-production cross sections are taken from [98], and the branching ratios are taken to be the same as the SM ones listed in the PDG [62]. . . . .	74
6.2	Representative cut flow table for the benchmark point $ \mu  = 1$ TeV, $M_1 = 25$ GeV, for a traditional cut-and-count analysis. All cross sections are given in femtobarns, and the units for the missing energy, invariant mass, and razor variable cuts are GeV. The significance, $S/\sqrt{B}$ , is calculated for an integrated luminosity of $3 \text{ ab}^{-1}$ . . . . .	79
6.3	Representative cut flow table for the same benchmark point and integrated luminosity as in table 6.2, but using a boosted decision tree (BDT) analysis instead. The preselection is equivalent to the trigger and identification cuts listed in table 6.2. As before, all the cross sections are in femtobarns.	80

6.4	Discovery reaches and expected exclusion limits (in TeV) for the parameters $( \mu , M_1)$ for the rectangular cuts and boosted decision tree analyses. . . . .	82
-----	---	----

# 1

## INTRODUCTION

---

The Standard Model of particle physics, which describes the fundamental constituents of matter and their interactions, represents an unambiguous triumph of the scientific method. Its predictions have been verified to extraordinary precision. Its last missing piece, the Higgs boson, was discovered in 2012 [1, 2], fifty years after it was predicted. This resulted in a Nobel prize for François Englert and Peter Higgs, and in much jubilation among the particle physics community.

However, many questions still remain unanswered by the Standard Model. For example, it does not explain why neutrinos have masses, and does not contain a viable dark matter candidate. On a more abstract level, the square of the mass of the Higgs boson seems unnaturally finely tuned - this phenomenon is termed the *hierarchy problem*, and we will revisit it in [section 2.3](#). In fact, it is widely believed that the Standard Model is only a low-energy effective approximation to an underlying theory that is valid at higher energy scales.

To answer these questions, we must go beyond the Standard Model with new theories. These new theories often predict new fundamental particles and forces, which we can study using particle colliders, like the Large Hadron Collider (LHC), which lies on the border between Switzerland and France ([figure 1.1](#)).

At these colliders, we collide particles at near-lightspeed, creating new particles that can be detected by extremely sophisticated detectors. One of the main challenges at particle colliders is that there are hundreds of millions of collisions every second, but only a small fraction of these will have signatures of new physics. In addition, there are a multitude of promising theories beyond the Standard Model, each possessing a large

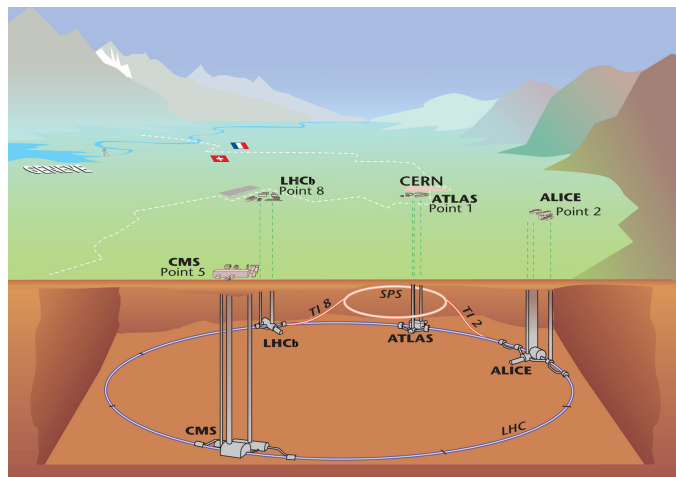


Figure 1.1: Schematic diagram of the Large Hadron Collider, which lies on the border between Switzerland and France. (CERN)

parameter space. However, performing a full experimental analysis for even a single point of this parameter space be very time consuming.

For this reason, existing theories must be constrained (or excluded entirely) by holding them up to the light of experimental evidence. Furthermore, we need to have a rough idea of what the most effective collider search strategies are before going ahead with a complete experimental analysis. This is where phenomenology steps in.

Phenomenology bridges the gap between theory and experiment - connecting the predictions of the former with the measurements of the latter. In this dissertation, we present three phenomenological analyses for finding physics beyond the Standard Model at current and future colliders. The structure of the dissertation is as follows.

*Chapter 2.* This chapter briefly reviews the theoretical background behind the collider analyses presented in this dissertation. We go over the particle content and gauge structure of the Standard Model, followed by a discussion of electroweak symmetry breaking. We briefly touch upon CKM mixing, asymptotic freedom, and quantum chromodynamics as well. This is followed by a discussion of the motivations, mass spectrum, and interactions of Two Higgs Doublet Models and the Minimal Supersymmetric Standard Model.

*Chapter 3.* This chapter describes how to connect theoretical predictions and experimental observables. The design of a generic multipurpose detector for a hadron collider is discussed, followed by discussions of some of the kinematic variables that are relevant to our analyses. The concepts of hypothesis testing and statistical significance are briefly reviewed, and particle physics concerns are recast in the language of machine learning.

*Chapter 4.* A new type of Higgs boson, known as the *charged* Higgs boson  $H^\pm$ , arises naturally in the spectrum of 2HDMs. Finding one of these would be an unmistakable sign of new physics beyond the Standard Model. The mass of this particle,  $m_{H^\pm}$  is a free parameter in the theory. Searches for this particle can be divided into two broad categories - the first involving charged Higgs bosons lighter than the top quark, and the other dealing with charged Higgses heavier than the top quark. In this chapter, we examine the first scenario, with charged Higgses coming from the decay of top quarks that are either produced singly or in pairs.

While experimental results from CMS and ATLAS have placed a lower limit of 160 GeV for the mass of the charged Higgs boson in the context of the MSSM, these limits have been placed assuming that the charged Higgs decays solely via conventional channels to final states with SM particles. However, theories that predict charged Higgs typically predict other BSM particles as well. These can potentially be lighter than the charged Higgs, thus opening up new, ‘exotic’ decay channels for it. For regions of parameter space with low values of the parameter

$\tan \beta$ , the rate of these exotic decays is much larger than the rate of the decays to SM particles, thus significantly weakening the limits set by the LHC. For a complete picture, we must take into account not only the conventional decay channels, but the exotic ones as well.

In this chapter, we investigate the exotic decay of a charged Higgs to a lighter, neutral Higgs boson - either the pseudoscalar  $A$  or the CP-even scalar  $H$ , and a  $W$  boson. We first perform a *model-independent* analysis. That is, *assuming* that  $H^\pm$  decays exclusively to  $AW^\pm/HW^\pm$ , and that  $A/H$  decays to a pair of tau leptons 8.6% of the time, we set out to find the minimum rate of the signal process required for this analysis to discover it with a significance of  $5\sigma$ , or exclude it with a significance of  $1.96\sigma$ . This rate corresponds to the strength of the signal - the weaker the signal that can be probed by the analysis, the more powerful the analysis is. The model-independent limit on the signal strength can be translated into a limit on the branching ratio of the top quark to the charged Higgs,  $\text{BR}(t \rightarrow H^\pm b)$ . We determined that the single top and the top pair channels could potentially set upper limits of 0.2% and 0.3% respectively on this branching ratio . For this analysis to discover the signal process, the branching ratio would have to be about three times higher than the aforementioned upper limits.

These results can be translated into contours in the two-dimensional  $m_{H^\pm} - \tan \beta$  plane in the parameter space of a Type-II 2HDM that delineate regions that can be either discovered or excluded with this analysis. We also found that this analysis would be able to discover points with the charged Higgs mass  $m_{H^\pm}$  between 155 and 165 GeV for  $\tan \beta > 17$ , and the entire viable mass range for  $\tan \beta < 6$ . We also found that almost the entire relevant region of the  $m_{H^\pm} - \tan \beta$  plane can be excluded with this analysis, with the exception of the regions with very small mass differences between the charged Higgs and the top quark. In summary, we found that the exotic decay channel  $H^\pm \rightarrow AW^\pm/HW^\pm$  probes a region of parameter space complementary to the region probed by standard decay channels (such as  $H^\pm \rightarrow \tau\nu$ ), and is thus an important search channel to include in the search for charged Higgs bosons. The results in this chapter have been published in [3].

*Chapter 5*. While the project that [chapter 4](#) is based on dealt with the implications of additional, exotic decay channels opening up for charged Higgs bosons arising from extended scalar sectors at the LHC, the project that this chapter is based on is much more ambitious in scope, aiming for nothing less than a complete prospectus of exotic Higgs decay channels in 2HDMs with large mass hierarchies. The authors of [4] have presented a collection of promising 2HDM benchmark planes for investigation at the LHC that take into account theoretical and experimental constraints, and highlight the complementarity between the different search channels. The end goal of this project is to perform detailed collider analyses to determine exclusion and discovery bounds for both the original benchmark planes at the 14 TeV LHC, as well as extended versions

of them at a 100 TeV collider that, reflecting the higher obtainable mass reach. In this chapter, we present preliminary results based on collider analyses carried out for two of the benchmark planes, corresponding to the mass hierarchies  $m_H < m_A = m_{H^\pm}$  and  $m_A < m_H = m_{H^\pm}$ . The exotic decay channels considered are  $A \rightarrow HZ$  and  $H^\pm \rightarrow HW^\pm$ . The analyses in this chapter are based on boosted decision tree classifiers. Using this technique, we are able to exclude charged Higgses with masses up to 2 TeV, for neutral Higgses  $H$  with masses up to 500 GeV, in the benchmark plane IIB suggested in [4] through the decay mode  $H^\pm \rightarrow AW^\pm$  at a 100 TeV collider. In addition, we are able to exclude neutral Higgses ( $A/H$ ) decaying via the channels  $(A/H) \rightarrow (H/A)Z$  for parent masses up to about 3 TeV for a wide range of values of  $\tan\beta$ , keeping the daughter Higgs mass fixed at 200 GeV. This work is being done in collaboration with Felix Kling, Huayang Song, Honglei Li, and Shufang Su.

*Chapter 6.* A 100 TeV proton-proton collider will be an extremely effective way to probe the electroweak sector of the Minimal Supersymmetric Standard Model (MSSM). In this chapter, we describe a search strategy for discovering pair-produced higgsino-like neutralinos  $\tilde{\chi}_{2,3}^0$  that decay to the lightest neutralino  $\tilde{\chi}_1^0$  (which we assume to be an almost pure bino). The lightest neutralino is a strong candidate for particle dark matter. We investigate the particular case in which the higgsinos decay via intermediate  $Z$  and SM Higgs bosons  $h$ , that in turn decay to a pair of leptons and a pair of  $b$ -quarks respectively:

$$\tilde{\chi}_{2,3}^0 \tilde{\chi}_{3,2}^0 \rightarrow (Z \tilde{\chi}_1^0)(h \tilde{\chi}_1^0) \rightarrow bbll + \tilde{\chi}_1^0 \tilde{\chi}_1^0.$$

We performed two analyses simultaneously - the first using rectangular selection cuts on physically motivated kinematic observables known as razor variables, and the second using the same high-level observables, along with a few lower-level observables as input features for a Boosted Decision Tree Classifier. The results show that the machine learning technique performs substantially better than the regular rectangular selection cuts. With the machine learning analysis, we would be able to discover higgsinos up to a mass of 1.3 TeV, and exclude them up to a mass of 1.8 TeV. Correspondingly, we can discover binos up to 900 GeV, and exclude them up to 1.3 TeV.

Finally, we conclude in [chapter 7](#), where we provide a summary of our findings and discuss prospects for future work.

# 2

## THE STANDARD MODEL AND BEYOND

---

In this chapter, we will provide some of the theoretical background that our research builds upon. We will first provide a lightning-quick review of the Standard Model particle content and gauge structure, followed by an introduction to Two-Higgs Doublet Models and the Minimal Supersymmetric Standard Model. For excellent reviews of the Standard Model, please see [5–8]. For a detailed review of Two-Higgs Doublet Models, see [9]. For a pedagogical introduction to supersymmetry and the MSSM, see [10]. Our treatment of the subjects is adapted from these articles.

### 2.1 THE STANDARD MODEL

The fundamental constituents of matter are fermions. The interactions between them are mediated by particles known as gauge bosons, which arise from the gauge structure of the Standard Model:

$$SU(3) \times SU(2) \times U(1)_Y$$

This means that each fermion transforms in a unique way under transformations corresponding to these gauge groups. In addition to the fermions and gauge bosons, the standard model contains a scalar  $SU(2)$  doublet  $H$ , known as the Higgs field. In [table 2.1](#), we collect the fundamental fields of the SM and their transformation properties under different gauge groups. The fermion labels  $u, d, e$  and  $\nu$  are collective labels for three generations of fermions, shown in [table 2.2](#). The fields  $g$ ,  $W_\mu$ , and  $B_\mu$  are vector bosons that correspond to the  $SU(3)$ ,  $SU(2)$  and  $U(1)$  gauge group respectively.

The ground state that we inhabit spontaneously breaks the larger symmetry  $SU(2) \times U(1)_Y$  to the symmetry  $U(1)_{\text{EM}}$ . The subscript Y

Type	Field	Spin	$SU(3)$	$SU(2)$	$U(1)_Y$
Scalar	$H$	0	<b>1</b>	<b>2</b>	$\frac{1}{2}$
Fermions	$Q = \begin{pmatrix} u_L \\ d_L \end{pmatrix}$	$\frac{1}{2}$	<b>3</b>	<b>2</b>	$\frac{1}{6}$
	$u_R$		<b>3</b>	<b>1</b>	$\frac{2}{3}$
	$d_R$		<b>3</b>	<b>1</b>	$-\frac{1}{3}$
	$L = \begin{pmatrix} e_L \\ \nu_L \end{pmatrix}$		<b>1</b>	<b>2</b>	$-\frac{1}{2}$
	$e_R$		<b>1</b>	<b>1</b>	-1
Vector bosons	$g$	1	<b>8</b>	<b>1</b>	0
	$W_\mu$		<b>1</b>	<b>3</b>	0
	$B_\mu$		<b>1</b>	<b>1</b>	0

Table 2.1: The fields of the Standard Model, grouped by their charges under the relevant gauge groups.

Generation	Quarks		e: Leptons	v: Neutrinos
	u: Up	d: Down		
I	$u$ : up	$d$ : down	$e$ : electron	$\nu_e$ : electron neutrino
II	$c$ : charm	$s$ : strange	$\mu$ : muon	$\nu_\mu$ : muon neutrino
III	$t$ : top	$b$ : bottom	$\tau$ : tau	$\nu_\tau$ : tau neutrino

Table 2.2: The fermion sector of the Standard Model, grouped by generation.

denotes the hypercharge of the field, while the subscript EM denotes electromagnetism. In this process of electroweak symmetry breaking (which we will revisit in more detail in [section 2.1](#)), the three gauge fields  $W_\mu$ , corresponding to the  $SU(2)$  gauge symmetry, combine with the  $B_\mu$  field corresponding to the  $U(1)_Y$  symmetry to form the massive gauge bosons  $W^\pm$  and  $Z$ , and a massless photon,  $A_\mu$  (often denoted by  $\gamma$  instead). The  $W$  and  $Z$  bosons mediate the weak interactions that responsible to phenomena such as radioactive decay, while the photon mediates electromagnetic interactions. The gauge field  $g$  corresponding to the  $SU(3)$  gauge symmetry is known as the gluon, and mediates the strong force between nucleons.

### *Electroweak symmetry breaking*

In 1957, Schwinger proposed the unification of the weak and electromagnetic interactions, citing their vectorial nature. In 1961, Glashow proposed a model for weak interactions governed by symmetry under the product group  $SU(2) \times U(1)$ . The trouble was, experiments had shown that the weak interactions had a short range, implying that the vector bosons that mediated them must be massive. On the other hand, gauge symmetry prohibits mass terms for the intermediate vector bosons. Glashow's theory included these mass terms, but they were put in by hand, and spoiled the renormalizability of the theory. A possible way out was to break the gauge symmetry *spontaneously* rather than explicitly. Spontaneous symmetry breaking refers to the phenomenon where the ground state of a system does not respect the symmetry of the full Lagrangian. However, Goldstone's theorem states that for every spontaneously broken symmetry, there exists a set of massless spin-0 bosons corresponding to the generators of the symmetry group - since such particles have never been observed, this was an undesirable feature of the theory.

Thus we seem to have to choose between two undesirable outcomes: a set of massless gauge bosons, or a set of massless scalars, both of which go against what we actually see in nature. Remarkably, each of these problems would turn out to be the solution for the other, through the marvelous *Higgs mechanism*. This mechanism was first put forth by Philip W. Anderson in the context of condensed matter systems. In 1964, three groups – Peter Higgs, the duo of Francois Englert and Robert

Brout, and the trio of Gerald Guralnik, C. R. Hagen, and Tom Kibble – independently and almost simultaneously proposed that this mechanism could explain how the weak interaction mediators can acquire mass. There is likely a strong case for naming the mechanism after all of these physicists, but for the sake of expediency, we will simply refer to it as the Higgs mechanism.

The Higgs mechanism describes the spontaneous breaking of electroweak symmetry, that is, the breakdown of the product group  $SU(2) \times U(1)_Y \rightarrow U(1)_{EM}$ . This is achieved by adding to the theory a scalar field  $SU(2)$  doublet,  $H$ :

$$H = \begin{pmatrix} H^+ \\ H^0 \end{pmatrix}$$

The terms of the Lagrangian that involve this field can be written as follows:

$$\mathcal{L}_{\text{Higgs}} = \frac{1}{2} |D_\mu H|^2 - V(H) \quad (2.1)$$

$$V(H) = \left( H^\dagger H - \frac{v^2}{2} \right)^2 \quad (2.2)$$

The gauge covariant derivative for the Standard Model takes the form

$$D_\mu = \partial_\mu + ig W_\mu^a \frac{\tau^a}{2} + ig' Y B_\mu.$$

where  $W_\mu^a$  and  $B_\mu$  are the gauge fields corresponding to the  $SU(2)$  and  $U(1)_Y$  symmetries respectively,  $g$  and  $g'$  are coupling constants, and  $\tau^a$  are the Pauli matrices. The potential  $V(H)$  reaches its minimum when  $H^\dagger H = v^2/2$ . We pick a vacuum expectation value (VEV) for  $H$  that breaks the neutral sector symmetry (corresponding to  $H^0$ ) but not the charged symmetry (corresponding to  $H^+$ ), since we wish to keep photons massless. Thus, we can pick the VEV:

$$H = \begin{pmatrix} 0 \\ \frac{v}{\sqrt{2}} \end{pmatrix}$$

Plugging this into the kinetic term of the Lagrangian, and isolating the terms quadratic in the gauge fields, we get

$$\frac{g^2 v^2}{4} W_\mu^- W_\mu^+ + \frac{1}{2} \frac{v^2}{4} (g^2 + g'^2) (\cos \theta_w W_\mu^3 - \sin \theta_w B_\mu)^2$$

where  $W_\mu^\pm = (W_\mu^1 \pm i W_\mu^2)/\sqrt{2}$  and  $\theta_w = \tan^{-1}(g'/g)$  is the *Weinberg angle*, which parameterizes the mixing between the photon  $A_\mu$  and the  $Z$  boson.

$$\begin{pmatrix} Z_\mu \\ A_\mu \end{pmatrix} = \begin{pmatrix} \cos \theta_w & -\sin \theta_w \\ \sin \theta_w & \cos \theta_w \end{pmatrix} \begin{pmatrix} W_\mu^3 \\ B_\mu \end{pmatrix} \quad (2.3)$$

The product  $W_\mu^+ W_\mu^-$  can be interpreted as a mass term for a generic charged vector boson  $W_\mu^\pm$ . Rewriting our mass terms for the vector boson fields with the above redefinitions, we get

$$\mathcal{L}_{\text{mass terms}} = \frac{e^2 v^2}{4 \sin^2 \theta_w} W_\mu W^\mu + \frac{e^2 v^2}{8 \sin^2 \theta_w \cos^2 \theta_w} Z_\mu Z^\mu$$

After accounting for symmetry factors, we get the masses of the W and Z bosons as:

$$m_W = \frac{ev}{2 \sin \theta_w} \quad m_Z = \frac{ev}{\sin 2\theta_w}$$

We see that there is no mass term for  $A_\mu$ , which means that this gauge field remains massless. Thus we see that the W and Z bosons gain mass, limiting their range, while the photon remains massless, corresponding to what is experimentally observed. Remarkably, we have done this without violating gauge invariance. Colloquially, we say that the W and Z bosons have ‘eaten’ the Goldstone boson degrees of freedom to obtain mass.

Peter Higgs was the first to postulate the existence of a physical *Higgs boson* that could be produced by perturbing the vacuum. To see how this plays out, let us parameterize the Higgs doublet field as

$$H = \frac{1}{\sqrt{2}} \exp \left( i \xi^a(x) \frac{\tau^a}{v} \right) \begin{pmatrix} 0 \\ v + h(x) \end{pmatrix}.$$

where  $\tau^a$  are the Pauli matrices,  $\xi^a$  are functions of spacetime,  $\langle \xi \rangle = \langle h \rangle = 0$ , and  $v$  is the vacuum expectation value of the Higgs doublet, experimentally measured to be about 246 GeV. The simplest gauge choice is the unitary gauge, where  $\xi(x) = 0$ . In this gauge, the potential  $V(H)$  from (2.2) becomes:

$$V(H) = -\frac{1}{2} m_h^2 h^2 - \lambda v h^3 - \frac{1}{4} \lambda h^4$$

The field  $h$  is the physical Higgs boson. It is the only fundamental scalar in the Standard Model, and was discovered in 2012, nearly 50 years after it was first predicted. The coefficient of the term quadratic in  $h$  is its mass,  $m_h$ . This mass is a free parameter that had to be determined experimentally. The second and third terms in the above expression represent the trilinear and quartic self-coupling of the Higgs boson.

### Quark mass and gauge eigenstates

While the quarks listed in table 2.2 are gauge eigenstates, with well defined transformations under the gauge groups, the physical states that we observe at a collider will in fact be mass eigenstates. The two are related by the *Cabibbo-Kobayashi-Maskawa* (CKM) matrix:

*The Cabibbo-Kobayashi-Maskawa quark mixing matrix*

$$V_{\text{CKM}} = \begin{pmatrix} V_{ud} & V_{us} & V_{ub} \\ V_{cd} & V_{cs} & V_{cb} \\ V_{td} & V_{ts} & V_{tb} \end{pmatrix} \quad (2.4)$$

The elements of the matrix denote the level of mixing between the gauge eigenstates. Experimentally, the matrix has been determined to be nearly diagonal.

### Asymptotic freedom and QCD

In the 50s and 60s, experiments were devised to unravel the structure of the proton. They found two seemingly incompatible results: on the one hand, colliding protons resulted in the production of a large number of pions collinear with the beam axis, implying that the protons could not absorb a large momentum transfer. However, deep inelastic scattering experiments showed that it was possible for an energetic electron to undergo hard electromagnetic scattering off a proton. These disparate phenomena were reconciled by the introduction of the *parton model* by Bjorken and Feynman. In this model, hadrons were comprised of a collection of loosely bound pieces, known as partons. To an energetic incoming electron, these partons would appear approximately free, allowing it to scatter with a large momentum transfer off of one of them. The struck parton will then exchange momentum softly via the strong interaction among the other partons, which results in the production of a *jet* of hadrons, collinear with the direction of the original struck parton. The deeper reason for this behavior is that these partons are charged under a non-Abelian gauge group,  $SU(3)$ . The phenomenon of the weakening of the strong interaction at large momentum transfers is known as *asymptotic freedom*, and it is a property of non-Abelian gauge theories.

The  $\beta$ -function of a gauge theory describes the evolution of the coupling constant with energy. For non-Abelian gauge theories, it takes the following form (up to leading order):

$$\beta(g_R) = \mu \frac{d}{d\mu} g_R = -\frac{g_R^3}{(4\pi)^2} \left[ \frac{11}{3} C_A - \frac{4}{3} n_f T_F \right] \quad (2.5)$$

where  $\mu$  is the renormalization scale,  $C_A$  is the quadratic Casimir operator for the adjoint representation, and  $T_F$  is the *index* of the fundamental representation. In the case of the strong interaction, the relevant gauge group is  $SU(3)$ . Thus  $C_A = 3$  and  $T_F = \frac{1}{2}$ . If  $n_f$ , the number of quark flavors is less than 17<sup>1</sup>, the  $\beta$  function has a *negative* sign, which means that the coupling *decreases* at higher energies. This is the underlying basis of asymptotic freedom. The theory of the strong interaction is known as *quantum chromodynamics*, or QCD for short. The analogue of electric charge for this theory is a quantity referred to as *color* (hence the name of the theory). The gauge fields that mediate this interaction, that correspond to the generators of  $SU(3)$ , are known as *gluons*. At a hadron collider, it is of crucial importance to understand the physics of gluons and jets.

The Standard Model of particle physics has been remarkably successful, and over the decades has yielded some of the most precise measurements in all of physics. However, as mentioned in [chapter 1](#), there still remain unresolved issues with the SM. In the next two sections we will discuss some of these issues in more depth, and introduce extensions to the SM that potentially resolve them.

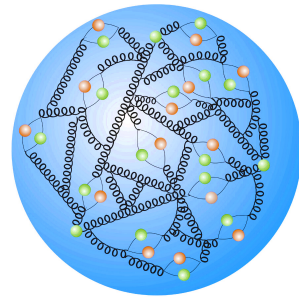


Figure 2.1: A representation of the innards of a proton, showing the dynamic structure.  
Image source:[11]

### Leading order $\beta$ -function for non-Abelian gauge theories

<sup>1</sup>Which it is, since the number of quark flavors is six, as can be seen in [table 2.2](#).

## 2.2 TWO-HIGGS DOUBLET MODELS

Intuitively, it is not too hard to imagine, based on the complex structure of the fermion and gauge sectors, that the scalar sector of the Standard Model might well contain members other than a single  $SU(2)$  doublet. An extended scalar sector can potentially alleviate some of the unresolved issues facing the Standard Model. One of these issues is the *strong CP problem*, which can be summarized as follows. Lagrangians for Yang-Mills theories can have a renormalizable term that is gauge-invariant but violates CP, of the form

$$\mathcal{L}_\theta = \theta \epsilon^{\mu\nu\alpha\beta} F_{\mu\nu}^a F_{\alpha\beta}^a$$

where  $\theta$  is some angle,  $F_{\mu\nu}$  is the field strength tensor, and  $\epsilon^{\mu\nu\alpha\beta}$  is an antisymmetric tensor. This term is a total derivative, since it can be written as  $2\theta \partial_\mu (\epsilon^{\mu\nu\alpha\beta} A_v^a F_{\alpha\beta}^a)$ . Thus, it should not contribute to perturbative effects. However, this term can potentially contribute to non-perturbative effects. Additionally, this term can be modified by chiral rotations of the form  $\psi \rightarrow \exp(i\gamma_5 \theta_F) \psi$ . Since physical observables should be independent of the choice of the basis, i.e.  $\theta_F$ , we should absorb it into  $\theta$  by defining a basis-independent phase:  $\bar{\theta} = \theta - \theta_F$ . For  $SU(2)$  and  $U(1)$  gauge symmetries, this phase can be set to zero by performing appropriate chiral rotations of the fermion fields. However, no such choice exists for the term corresponding to the  $SU(3)$  group, and thus the CP-violating term in the QCD Lagrangian could in principle be non-zero. A non-zero value of  $\bar{\theta}$  would be manifested as non-perturbative effects. For example, the neutron would then have a non-zero electric dipole moment. However, experiments have shown that  $\bar{\theta}$  must be vanishingly small, with a stringent upper bound:  $\bar{\theta} < 10^{-10}$ .

Adding an additional scalar doublet allows us to impose a global  $U(1)$  symmetry on the Lagrangian, known as *Peccei-Quinn* symmetry. If this symmetry is spontaneously broken, a Goldstone boson arises, which can then be chirally rotated such that  $\bar{\theta}$  becomes effectively zero for the ground state. Another motivation for 2HDMs is their ability to explain the observed baryon asymmetry of the universe. That is, the amount of matter in the universe is much larger than the amount of antimatter in it. The CP violation in the weak sector of the Standard Model cannot account for this imbalance, but 2HDMs, with their complex scalar sector and possible new sources of CP violation, can. The strongest motivation for 2HDMs is, however, their connection to supersymmetric models, such as the MSSM, that have the potential to resolve the hierarchy problem, discussed in the next section. The scalar sector of the MSSM has a structure similar to that of a 2HDM - it requires an additional scalar doublet to give mass to both up and down type fermions, and for the cancellation of anomalies. With these motivations in mind, let us look at the scalar potential that results from two scalar  $SU(2)$  doublets.

### The 2HDM scalar potential

The most general renormalizable scalar potential for two scalar doublets  $\Phi_1$  and  $\Phi_2$  with hypercharge +1 is:

$$\begin{aligned} V(\Phi_1, \Phi_2) = & m_{11}^2 |\Phi_1|^2 + m_{22}^2 |\Phi_2|^2 - m_{12}^2 (\Phi_1^\dagger \Phi_2 + \text{h.c.}) \\ & + \frac{\lambda_1}{2} |\Phi_1|^4 + \frac{\lambda_2}{2} |\Phi_2|^4 + \lambda_3 |\Phi_1|^2 |\Phi_2|^2 + \lambda_4 |\Phi_1^\dagger \Phi_2|^2 \\ & + \left[ \frac{\lambda_5}{2} (\Phi_1^\dagger \Phi_2)^2 + \lambda_6 |\Phi_1|^2 (\Phi_1^\dagger \Phi_2) + \lambda_7 |\Phi_2|^2 (\Phi_1^\dagger \Phi_2) + \text{h.c.} \right] \end{aligned}$$

*Scalar potential for a Two-Higgs Doublet Model*

where h.c. stands for the hermitian conjugate of the terms immediately preceding it. The parameters  $m_{11}^2$ ,  $m_{22}^2$ , and  $\lambda_{1,2,3,4}$  are real while  $m_{12}^2$  and  $\lambda_{5,6,7}$  can be complex. Naively, it would seem that this potential has 14 degrees of freedom - six from the real parameters, and eight from the complex parameters. However, it should be noted that we have the freedom to perform basis transformations, that is, we can write the potential in terms of new doublets  $\Phi'_a = \sum_{b=1}^2 U_{ab} \Phi_b$ . where  $U_{ab}$  is a  $2 \times 2$  unitary matrix. The condition of unitarity implies that  $U$  has three degrees of freedom, which can absorb three out of the 14 degrees of freedom listed earlier. Thus, only 11 out of the original 14 degrees of freedom are physical.

In principle, we could proceed with these 11 parameters, however, there are a couple of reasons to attempt to reduce this number. The first is that a large number of free parameters makes a theory less falsifiable, thus reducing its predictive power. The second is that in order to distinguish between pseudoscalars and scalars, CP must be conserved in the Higgs sector. Finally, the potential in (2.6) allows for tree-level flavor-changing neutral currents (FCNC), which are experimentally measured to be highly suppressed. These can be eliminated by introducing discrete or continuous symmetries. Imposing a discrete symmetry such as  $Z_2$ , that is, the Lagrangian is invariant under the reflection of one of the doublets:  $\Phi_i \rightarrow -\Phi_i$ , removes the terms that are odd in  $\Phi_i$ . This effectively sets  $\lambda_6 = \lambda_7 = 0$ . In principle, this should set  $m_{12} = 0$  as well, but we retain this term since it breaks the  $Z_2$  symmetry softly, which relaxes the experimental bounds on the mass spectrum. After imposing these constraints, all the remaining parameters  $\lambda_{1,2,3,4,5}$ ,  $m_{11,12,22}$  are real. From here on, we will only consider 2HDMs with these constraints.

There are four such models, classified based on the coupling patterns of the fermions to the two Higgs doublets. In Type I 2HDMs, all the quarks couple to only one of the Higgs doublets (chosen by convention to be  $\Phi_2$ ). In Type II 2HDMs, the up-type right-handed quarks ( $u, c, t$ ) couple to  $\Phi_2$ , and the down-type right-handed quarks ( $d, s, b$ ) couple to  $\Phi_1$ . In both of these models, the right-handed leptons couple to the same doublet as the down-type quarks. There are two other models that do not have tree-level FCNCs. The lepton-specific model is similar to the Type I model, except in this case, the right-handed leptons couple to  $\Phi_1$ . Similarly, the ‘flipped’ model is similar to the Type II 2HDM, except

Model	$u_R^i$	$d_R^i$	$e_R^i$
Type I	$\Phi_2$	$\Phi_2$	$\Phi_2$
Type II	$\Phi_2$	$\Phi_1$	$\Phi_1$
Lepton-specific	$\Phi_2$	$\Phi_2$	$\Phi_1$
Flipped	$\Phi_2$	$\Phi_1$	$\Phi_2$

Table 2.3: 2HDMs with flavor conservation.

that the leptons couple to  $\Phi_2$ . The coupling patterns for these models are collected in [table 2.3](#).

This potential is minimized for non-zero vacuum expectation values of  $\Phi_i$ :

$$\langle \Phi_i \rangle_0 = \begin{pmatrix} 0 \\ \frac{v_i}{\sqrt{2}} \end{pmatrix} \quad (2.6)$$

The complex scalar  $SU(2)$  doublets  $\Phi_i$  can be expressed in terms of eight real fields as follows:

$$\Phi_i = \begin{pmatrix} \phi_i^+ \\ \frac{1}{\sqrt{2}}(\nu_i + \rho_i + i\eta_i) \end{pmatrix} \quad (2.7)$$

The process of electroweak symmetry breaking causes three of these fields to be ‘eaten’ by the  $W$  and  $Z$  bosons, and the remaining five are manifested as physical scalar fields. These consist of a pair of CP-even neutral scalars  $h$  and  $H$ , a CP-odd pseudoscalar  $A$ , and a charged scalar  $H^\pm$ .

#### *The 2HDM mass spectrum*

In this section, we will analyze the mass spectrum of flavor-conserving 2HDMs. To do so, we construct the mass matrices by taking derivatives of the scalar potential:

$$M_{ij} = \frac{\partial V(\Phi_1, \Phi_2)}{\partial \phi_i \partial \phi_j}$$

where  $\phi_i$  can be any of the fields  $\phi_i^+, \rho_i, \eta_i$  in (2.7). We will also adopt the notation: Applying this procedure to the charged scalar components  $\phi_i^\pm$ , we obtain their mass matrix  $M_{\phi^\pm}$ :

$$M_{\phi^\pm} = [m_{12}^2 - (\lambda_4 + \lambda_5)\nu_1\nu_2] \begin{pmatrix} \nu_2/\nu_1 & -1 \\ -1 & \nu_1/\nu_2 \end{pmatrix}$$

Diagonalizing this matrix gives us the mass of the charged Higgses:

$$m_{H^\pm}^2 = (\nu_1^2 + \nu_2^2)[m_{12}^2/\nu_1\nu_2 - (\lambda_4 + \lambda_5)]$$

Similarly, the mass matrix for the pseudoscalars is given by

$$M_\eta = \frac{m_A^2}{\nu_1^2 + \nu_2^2} \begin{pmatrix} \nu_2^2 & -\nu_1\nu_2 \\ -\nu_1\nu_2 & \nu_1^2 \end{pmatrix}$$

Diagonalizing this matrix gives us a massless Goldstone boson  $G^0$ , corresponding to a zero eigenvalue, and a pseudoscalar Higgs boson  $A$ , with mass given by:

$$m_A^2 = (\nu_1^2 + \nu_2^2)[m_{12}^2/\nu_1\nu_2 - 2\lambda_5]$$

The diagonalization process amounts to a rotation of the basis vectors by some angle. For the CP-odd and the charged scalars, this angle is the same, and is denoted as  $\beta$ . Let us now adopt the notation

$$s_\theta, c_\theta, t_\theta = \sin \theta, \cos \theta, \tan \theta$$

for conciseness. In this notation, the mass eigenstates are given by

$$\begin{pmatrix} A \\ G^0 \end{pmatrix} = \begin{pmatrix} s_\beta & -c_\beta \\ c_\beta & s_\beta \end{pmatrix} \begin{pmatrix} \eta_1 \\ \eta_2 \end{pmatrix} \quad \text{and} \quad \begin{pmatrix} H^\pm \\ G^\pm \end{pmatrix} = \begin{pmatrix} s_\beta & -c_\beta \\ c_\beta & s_\beta \end{pmatrix} \begin{pmatrix} \phi_1^\pm \\ \phi_2^\pm \end{pmatrix}. \quad (2.8)$$

The angle  $\beta$  turns out to be a very important one for studying 2HDMs. It also represents the ratio of the vacuum expectation values of the neutral components of the two Higgs doublets:  $t_\beta = v_2/v_1$ . Finally, the mass matrix for the CP-even scalars is given by:

$$M_\rho = - \begin{pmatrix} m_{12}^2 \frac{v_2}{v_1} + \lambda_1 v_1^2 & -m_{12}^2 + \lambda_{345} v_1 v_2 \\ -m_{12}^2 + \lambda_{345} v_1 v_2 & m_{12}^2 \frac{v_2}{v_1} + \lambda_1 v_2^2 \end{pmatrix}$$

where  $\lambda_{345} = \lambda_3 + \lambda_4 + \lambda_5$ . This matrix is diagonalized by rotation of the basis vectors by the angle  $\alpha$ :

$$\begin{pmatrix} h \\ H \end{pmatrix} = \begin{pmatrix} s_\alpha & -c_\alpha \\ -c_\alpha & -s_\alpha \end{pmatrix} \begin{pmatrix} \rho_1 \\ \rho_2 \end{pmatrix}$$

with the mass eigenstates denoted  $h, H$ . Traditionally,  $h$  is taken to be the lighter of the two particles.

Thus we see that the physical spectrum of 2HDMs contains five mass eigenstates: the CP-even higgses  $h$  and  $H$ , the CP-odd pseudoscalar Higgs  $A$ , and a pair of charged Higgses  $H^\pm$ . Incidentally, the Standard Model Higgs is a combination of the CP-even scalars:

$$h_{\text{SM}} = \rho_1 \cos \beta + \rho_2 \sin \beta = h \sin(\alpha - \beta) - H \cos(\alpha - \beta) \quad (2.9)$$

### Interactions

In this section, we discuss the interactions that are relevant to our analyses. Namely the ones governing the exotic decays of Higgses to other, lighter Higgses, and the subsequent decays of the lighter Higgses to SM fermions. The decays to SM fermions is governed by the Yukawa terms in the Lagrangian:

$$\begin{aligned} \mathcal{L}_{\text{Yukawa}}^{\text{2HDM}} = & - \sum_{f=u,d,l} \frac{m_f}{v} \left( \xi_h^f \bar{f} f h + \xi_H^f \bar{f} f H - i \xi_A^f \bar{f} \gamma_5 f A \right) \\ & - \left\{ \frac{\sqrt{2} V_{ud}}{v} \bar{u} \left( m_u \xi_A^u P_l + m_d \xi_A^d P_R \right) d H^+ + \frac{\sqrt{2} m_l \xi_A^l}{v} \bar{\nu}_L l_R H^+ + h.c. \right\} \end{aligned}$$

*Yukawa terms for flavor-conserving 2HDMs*

where  $f$  is a fermion with mass  $m_f$ , the fields  $u$  and  $d$  are up and down type quarks with masses  $m_u$  and  $m_d$  and CKM mixing  $V_{ud}$ ,  $l$  is a lepton with mass  $m_l$ , and  $\nu_L$  is a neutrino. The factors  $\xi$  in the above expressions

Coefficient	Value		
$\xi_{hVV}$	$s_{\beta-\alpha}$		
$\xi_h^u$	$c_\alpha/s_\beta$		
$\xi_h^d$	$-s_\alpha/c_\beta$		
$\xi_h^l$	$-s_\alpha/c_\beta$		
$\xi_{HVV}$	$c_{\beta-\alpha}$	$g_{AH^\pm W^\mp}$	$= \frac{g}{2}(p_{H^\pm} - p_A)^\mu$
$\xi_H^u$	$s_\alpha/s_\beta$	$g_{hAZ}$	$= is_{\beta-\alpha} \frac{g}{2c_{\theta_w}}(p_A - p_h)^\mu$
$\xi_H^d$	$c_\alpha/s_\beta$	$g_{hH^\pm W^\mp}$	$= -is_{\beta-\alpha} \frac{g}{2}(p_{H^\pm} - p_h)^\mu$
$\xi_H^l$	$c_\alpha/s_\beta$	$g_{HAZ}$	$= ic_{\beta-\alpha} \frac{g}{2c_{\theta_w}}(p_A - p_H)^\mu$
$\xi_{AVV}$	0	$g_{HH^\pm W^\mp}$	$= -ic_{\beta-\alpha} \frac{g}{2}(p_{H^\pm} - p_H)^\mu$
$\xi_A^u$	$1/t_\beta$		
$\xi_A^d$	$t_\beta$		
$\xi_A^l$	$t_\beta$		

Table 2.4: List of the factors  $\xi$  that determine the Yukawa couplings of Higgs bosons in Type II 2HDMs.

### The Type II 2HDM

As mentioned at the beginning of this chapter, The Type II 2HDM is of special interest since it has the same fermion-Higgs doublet coupling pattern as the MSSM. We will examine the MSSM in more detail in the next section, but will note that if we can recover the tree-level MSSM scalar potential from a Type II 2HDM by setting the parameters  $\lambda_i$  to the following values:

$$\lambda_{1,2} = \frac{g^2 + g'^2}{2}, \quad \lambda_3 = \frac{g^2 - g'^2}{4}, \quad \lambda_4 = -\frac{g^2}{2}, \quad \lambda_{5,6,7} = 0. \quad (2.10)$$

It should be noted, however, that these relations do not hold beyond the tree-level for a generic non-supersymmetrized 2HDM. The analyses in chapters 4 and 5 are designed to probe the parameter space of a Type II 2HDM.

### 2.3 THE MINIMAL SUPERSYMMETRIC STANDARD MODEL

Historically, examining nature at increasing energy scales (and correspondingly decreasing length scales) has consistently yielded new physics. For example, higher-energy experiments were able to probe the structure of the weak interactions, precisely at the energy scale that the 4-Fermi theory started to fail. Similarly, the challenges such as the ones listed at the beginning of section 2.2 most likely point to new physics at higher energy scales, between the currently explored weak scale and the reduced Planck scale:

$$M_P = 1/\sqrt{8\pi G} \approx 2.4 \times 10^{18} \text{ GeV}.$$

However, the SM Higgs potential is extremely sensitive to new physics at high energies. The square of the mass of the SM Higgs boson receives

large quantum corrections from any new physics at high energies that couples to the Higgs sector. For example, if the Higgs couples to a heavy fermion  $f$  through a term of the form  $-\lambda_f H \bar{f} f$ , the one-loop correction to the square of the Higgs mass (figure 2.2) takes the form

$$\Delta m_H^2 = -\frac{|\lambda_f|^2}{8\pi^2} \Lambda_{UV}^2 + \dots \quad (2.11)$$

where  $\Lambda_{UV}$  is some cutoff momentum where the effects of the new physics are expected to manifest themselves. Similarly, the one-loop correction from a heavy scalar  $S$  through the term  $-\lambda_S |H|^2 |S|^2$  (figure 2.3) takes the form

$$\Delta m_H^2 = \frac{\lambda_S}{16\pi^2} [\Lambda_{UV}^2 + \dots] \quad (2.12)$$

In both these cases, the size of the correction scales quadratically with the momentum cutoff  $\Lambda_{UV}$ . Higher-order loop corrections can be shown to be similarly large as well. Thus the ‘natural’ mass of the Higgs would seem to be on the order of  $\Lambda_{UV}$ , which could even be as high as the Planck scale. In contrast, the actual mass that we measure is only about 126 GeV. Thus there is a *hierarchy* between the observed and the ‘natural’ mass of the SM Higgs, one of many orders of magnitude.<sup>2</sup> Thus it would seem that any UV completion of the SM would have to come with a host of parameters to tune the counterterms enough to cancel out the quadratic divergences and result in the physical mass we observe experimentally. It is obviously undesirable to have to manually tune a large number of parameters to be able to come up with UV completions of the Standard Model - it would be analogous to the geocentric Ptolemaians adding an ever-increasing number of epicycles to explain what would ultimately be more simply and accurately described by Copernicus’s heliocentric theory. Looking at the forms of the one-loop corrections in (2.11) and (2.12), we can see that the contribution from the fermion  $f$  will be exactly canceled out by the contributions from two complex scalars with  $\lambda_S = |\lambda_f|^2$ , the corrections from the scalar and the fermion will cancel out exactly. This suggests that the simplest way to ensure that all quadratic divergences from new physics at high energy scales cancel out is to require some kind of symmetry between fermions and scalars, ensuring that there is a scalar partner for each fermion, or vice versa.

This symmetry is known as *supersymmetry*. It is a rich mathematical structure with far-reaching consequences, a lot of which are beyond the scope of this work. For a pedagogical review of supersymmetry, we refer the reader to [10]. This section provides a necessarily condensed version of the treatment there. The term ‘supersymmetry’ refers to the invariance of the Lagrangian under supersymmetry transformations of the form<sup>3</sup>

$$Q|Boson\rangle = |Fermion\rangle \quad \text{and} \quad Q|Fermion\rangle = |Boson\rangle.$$

The minimal phenomenologically viable supersymmetric extension to the Standard Model is known as the *Minimal Supersymmetric Standard*

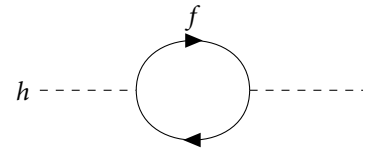


Figure 2.2: Feynman diagram for the one-loop fermionic correction to the SM Higgs mass

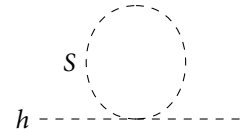


Figure 2.3: Feynman diagram for the one-loop scalar correction to the SM Higgs mass

<sup>2</sup>Note that even though only the mass of the SM Higgs is directly sensitive to  $\Lambda_{UV}$ , this sensitivity is propagated to all the other SM particles through their couplings to the SM Higgs.

<sup>3</sup>Of course, this is not the precise form of the transformation - as can be seen by performing some rudimentary dimensional analysis. We write down more precise transformations later.

*Model*, or the MSSM. Although the hierarchy problem has been the main driving force behind the development of supersymmetry, there are other benefits that the MSSM provides as well. One of them is that the MSSM has the right particle content to unify the strong and electroweak couplings at a high energy scale, as seen in [figure 2.4](#).

The third major motivation (and the one most relevant to this dissertation) is the fact that the MSSM results in a viable dark matter candidate. The MSSM admits a new kind of discrete symmetry known as *R-parity*. It is an analogue of baryon and lepton number conservation. The Lagrangian of the MSSM is defined to be invariant under the action of the operator  $P_R$  on the fields. The eigenvalues of this operator are  $(-1)^{3(B-L)+2s}$ , where  $B$ ,  $L$ , and  $s$  represent the baryon number, lepton number, and spin of the particle, respectively. The consequence of this is that the lightest supersymmetric particle (LSP) must be absolutely stable, that is, it cannot decay further into other particles, thus making it a good candidate for particle dark matter.

### *The supersymmetry algebra*

In 1967, Coleman and Mandula [\[13\]](#) showed that, given certain assumptions, the only possible Lie group symmetries allowed for relativistic interacting field theories in four dimensions are direct products of the Poincaré group and an internal symmetry group (i.e. a gauge symmetry) [\[14\]](#). A Lie algebra is defined by the commutation relations of its generators. If we extend the notion of a Lie algebra to include *anticommutation* relations [\[15\]](#), the theorem no longer applies. These kinds of algebras are known as *graded Lie algebras*, or *superalgebras*. The trio of Haag, Łopuszanski, and Sohnius [\[16\]](#) applied a similar treatment as Coleman and Mandula to determine the most general superalgebra consistent with relativistic quantum field theory. The generators  $Q_\alpha$  of this algebra are known as fermionic operators, and must transform as Weyl spinors. The anticommutation (and commutation) relations take the form

$$\begin{aligned} \{Q_\alpha, \bar{Q}_\beta\} &= 2(\sigma^\mu)_{\alpha\dot{\beta}} P^\mu \\ \{Q_\alpha, Q_\beta\} &= \{\bar{Q}_{\dot{\alpha}}, \bar{Q}_{\dot{\beta}}\} = 0 \\ [P^\mu, Q_\alpha] &= [P^\mu, \bar{Q}_{\dot{\alpha}}] = 0 \end{aligned} \tag{2.13}$$

where  $P_\mu = i\partial_\mu$  is the generator of translations.

The first supersymmetric Lagrangian density in four-dimensions was formulated by Wess and Zumino [\[17\]](#). The approach taken was to define infinitesimal ‘supergauge’ transformations for scalars and spinors that generated a closed algebraic structure. Soon afterwards, Salam and Strathdee [\[18\]](#) created a more systematic approach to constructing these transformations, by giving them a geometric interpretation.

In this picture, supersymmetric transformations can be viewed as translations in a manifold known as *superspace*, which is obtained by adding the ‘fermionic’ coordinates  $\theta^\alpha$ , and  $\bar{\theta}^{\dot{\beta}}$  to the regular spacetime

coordinates  $x^\mu$ . Thus, the generators of these translations are represented by

$$Q_\alpha = \frac{\partial}{\partial \theta^\alpha} - i(\sigma^\mu \bar{\theta})_\alpha \partial_\mu \quad \text{and} \quad \bar{Q}_\beta = \frac{\partial}{\partial \bar{\theta}^\beta} - i(\sigma^\mu \bar{\theta})_\beta \partial_\mu. \quad (2.14)$$

These transformations act on objects known as superfields, which are complex scalar fields parameterized by the coordinates  $(x^\mu, \theta, \bar{\theta})$ . Under an infinitesimal supersymmetry transformation, a general superfield  $S(x, \theta, \bar{\theta})$  transforms as

$$S \rightarrow S' = (1 + i\xi^\alpha Q_\alpha + i\bar{\xi}_\beta \bar{Q}^\beta)S \quad (2.15)$$

The fermionic coordinate  $\theta$  has two components:  $\theta^\alpha = (\theta^1, \theta^2)$ . Each of these two components is a *Grassmannian* variable, satisfying the anticommutation relation  $\{\theta^i, \theta^j\} = 0$ . This implies that  $(\theta^i)^2 = 0$ . This means that a Taylor expansion in powers of a fermionic coordinate must always terminate with a finite number of terms. For a general superfield  $S$ , the Taylor expansion about the fermionic coordinates  $\theta, \bar{\theta}$  takes the form

$$S(x, \theta, \bar{\theta}) = a + \theta\xi + \bar{\theta}\chi^\dagger + \theta\theta b + \bar{\theta}\bar{\theta}c + \bar{\theta}\bar{\sigma}^\mu\theta\nu_\mu + \bar{\theta}\bar{\theta}\theta\eta + \theta\theta\bar{\theta}\zeta^\dagger + \theta\theta\bar{\theta}\bar{\theta}d, \quad (2.16)$$

*Generators of superspace translations*

*Infinitesimal SUSY transformations*

*General superfield expansion*

where  $a, b, c$  and  $d$  are complex-valued scalar fields,  $\xi, \chi, \eta$  and  $\zeta$  are spinor fields, and  $\nu_\mu$  is a vector field. These coefficients in the Taylor expansion will be identified with the regular (non-super) fields that we see in the SM and its supersymmetrized version, the MSSM. The matter content of the MSSM can be derived from expanding superfields of a particular type, known as *chiral* superfields. The expansion of a generic chiral superfield  $\Phi$  takes the form:

$$\begin{aligned} \Phi(y, \theta) = & \phi(x) + \sqrt{2}\theta\psi(x) + \theta\theta F(x) \\ & + i\theta\sigma\bar{\theta}\partial_\mu\phi(x) - \frac{1}{2}\theta\sigma\bar{\theta}\theta\sigma^\nu\bar{\theta}\partial_\mu\partial_\nu\phi(x) + \sqrt{2}i\theta\sigma\bar{\theta}\partial_\mu\psi(x) \end{aligned} \quad (2.17)$$

*Chiral superfield expansion*

Similarly the gauge bosons come from the expansion of *vector* superfields  $V$ , obtained by imposing the condition  $V = V^\dagger$ . The expansion of  $V$  takes the form:

$$V = \bar{\theta}\bar{\sigma}^\mu\theta A_\mu + \bar{\theta}\bar{\theta}\theta\lambda + \theta\theta\bar{\theta}\lambda^\dagger + \frac{1}{2}\theta\theta\bar{\theta}\bar{\theta}D \quad (2.18)$$

*Vector superfield expansion*

We see that the expansion of the chiral superfield  $\Phi$  contains a scalar field  $\phi$ , a Weyl fermion  $\psi$ , and a field  $F$ . Thus, choosing values of  $\phi, \psi$ , and  $F$  fixes  $\Phi$ . These fields, known as the *component fields* of  $\Phi$  can be naturally placed in a collection known as a *supermultiplet*. The scalar superpartners  $\phi$  are referred to as *sfermions*. Similarly, the fields  $A_\mu, \lambda$ , and  $D$  form another natural grouping, called a *vector* supermultiplet. The fields  $A_\mu$  and  $\lambda$  are superpartners of each other, and fields such

<sup>4</sup>After the co-inventor of the Wess-Zumino model, Bruno Zumino.

as  $\lambda$  are generically known as *gauginos*<sup>4</sup>. The particle content of the MSSM, grouped into supermultiplets, is shown in tables 2.5 and 2.6. For brevity, we have not shown all three fermion generations. Also, the fields  $F$  and  $D$  are not included, since they are *auxiliary* fields, serving only to make sure that supersymmetry holds off-shell. The gauge structure of the MSSM is the same as that of the SM - there are no new gauge interactions.

The mass terms and Yukawa terms of the MSSM Lagrangian come from the collection of terms known as the *superpotential*. In terms of the chiral superfields in table 2.5, we can write the MSSM superpotential as:

### The MSSM superpotential

$$W_{\text{MSSM}} = \bar{u} \mathbf{y}_u Q H_u - \bar{d} \mathbf{y}_d Q H_d - \bar{e} \mathbf{y}_e L H_d + \mu H_u H_d$$

We have abbreviated terms such as  $\mu(H_u)_\alpha(H_d)_\beta e^{\alpha\beta}$  to  $\mu H_u H_d$ , and the matrices  $\mathbf{y}$  are  $3 \times 3$  matrices of Yukawa couplings, with indices representing the fermion generations. Note also that we now see the necessity of having two Higgs doublets - one that couples to the up-type fermions, and the other to the down-type fermions. A term like  $\bar{u} \mathbf{y}_u Q H_d^*$  would lead to a non-conserved hypercharge.

### Softly broken supersymmetry

The component fields of a superfield have the same mass, as can be seen from expansions of the chiral and vector superfields in (2.17) and (2.18). This means that, if supersymmetry holds, the superpartners of the SM particles should have been discovered by now. Evidently, if this symmetry exists, it is not evident in the ground state that we inhabit - that is, it must be spontaneously broken. The exact mechanism by which it is broken is still unknown - there are a number of competing models which introduce new physics at high energy scales. To remain model-agnostic, we can simply perform a parameterized explicit breaking by inserting the relevant terms into the Lagrangian by hand. The form of these terms is constrained by the requirement that the quadratic divergences in the radiative corrections to scalar masses must still vanish.

The soft supersymmetry breaking terms, written in terms of component fields, are as follows.

### Soft supersymmetry breaking terms

$$\begin{aligned} \mathcal{L}_{\text{soft}}^{\text{MSSM}} = & -\frac{1}{2} (M_1 \tilde{B} \tilde{B} + M_2 \tilde{W} \tilde{W} + M_3 \tilde{g} \tilde{g} + \text{h.c.}) \\ & - \left( \tilde{\bar{u}} \mathbf{a}_u \tilde{Q} H_u - \tilde{\bar{d}} \mathbf{a}_d \tilde{Q} H_d - \tilde{\bar{e}} \mathbf{a}_e \tilde{L} H_d + \text{h.c.} \right) \\ & - \tilde{Q}^\dagger \mathbf{m}_Q^2 \tilde{Q} - \tilde{L}^\dagger \mathbf{m}_L^2 \tilde{L} - \tilde{\bar{u}}^\dagger \mathbf{m}_{\bar{u}}^2 \tilde{\bar{u}}^\dagger - \tilde{\bar{d}}^\dagger \mathbf{m}_{\bar{d}}^2 \tilde{\bar{d}}^\dagger - \tilde{\bar{e}}^\dagger \mathbf{m}_{\bar{e}}^2 \tilde{\bar{e}}^\dagger \\ & - m_{H_u}^2 H_u^* H_u - m_{H_d}^2 H_d^* H_d - (b H_u H_d + \text{h.c.}) \end{aligned}$$

The tildes denote superpartners of the corresponding SM field - for example,  $\tilde{g}$  is a gluino,  $\tilde{e}$  is the scalar superpartner of a right-handed electron, and so on. The parameters  $M_1$ ,  $M_2$ ,  $M_3$  govern the masses of the gauginos  $\tilde{g}$ ,  $\tilde{W}$ , and  $\tilde{B}$ .

Superfield	Components		Group representation		
	Spin-0	Spin-½	$SU(3)_c$	$SU(2)_L$	$U(1)_Y$
	Squarks	Quarks			
Q	$\begin{pmatrix} \tilde{u}_L \\ \tilde{d}_L \end{pmatrix}$	$\begin{pmatrix} u_L \\ d_L \end{pmatrix}$	3	2	$\frac{1}{2}$
$\bar{u}$	$\tilde{u}_R^*$	$u_R^\dagger$	$\bar{\mathbf{3}}$	$\mathbf{1}$	$-\frac{2}{3}$
$\bar{d}$	$\tilde{d}_R^*$	$d_R^\dagger$	$\bar{\mathbf{3}}$	$\mathbf{1}$	$\frac{1}{3}$
Sleptons		Leptons			
L	$\begin{pmatrix} \tilde{v}_L \\ \tilde{e}_L \end{pmatrix}$	$\begin{pmatrix} v_L \\ e_L \end{pmatrix}$	1	2	$-\frac{1}{2}$
$\bar{e}$	$\tilde{e}_R^*$	$e_R^\dagger$	$\bar{\mathbf{1}}$	$\mathbf{1}$	1
Higgses		Higgsinos			
$H_u$	$\begin{pmatrix} H_u^+ \\ H_u^0 \end{pmatrix}$	$\begin{pmatrix} \tilde{H}_u^+ \\ \tilde{H}_u^0 \end{pmatrix}$	1	2	$\frac{1}{2}$
$H_d$	$\begin{pmatrix} H_d^0 \\ H_d^- \end{pmatrix}$	$\begin{pmatrix} \tilde{H}_d^0 \\ \tilde{H}_d^- \end{pmatrix}$	1	2	$-\frac{1}{2}$

Table 2.5: Chiral supermultiplets of the MSSM.

Components		Group representation		
Spin-½	Spin-1	$SU(3)_c$	$SU(2)_L$	$U(1)_Y$
Gluinos: $\tilde{g}$	Gluons: $g$	8	1	0
Winos: $\tilde{W}^0$	W bosons: $W^\pm$	$\bar{\mathbf{1}}$	3	0
Binos: $\tilde{B}^0$	B bosons: $B^0$	$\bar{\mathbf{1}}$	3	0

Table 2.6: Gauge supermultiplets of the MSSM.

*Phenomenological approximations*

The MSSM has a number of simplifying assumptions motivated both by convenience and compatibility with observed experimental data. For example, it is convenient to take the Yukawa matrices  $\mathbf{y}_u, \mathbf{y}_d, \mathbf{y}_e$  in a simplified limit, where only the heaviest generations have non-zero Yukawa couplings.

$$\mathbf{y}_u \approx \begin{pmatrix} 0 & 0 & 0 \\ 0 & 0 & 0 \\ 0 & 0 & y_t \end{pmatrix}, \quad \mathbf{y}_d \approx \begin{pmatrix} 0 & 0 & 0 \\ 0 & 0 & 0 \\ 0 & 0 & y_b \end{pmatrix}, \quad \mathbf{y}_e \approx \begin{pmatrix} 0 & 0 & 0 \\ 0 & 0 & 0 \\ 0 & 0 & y_\tau \end{pmatrix}$$

Furthermore, to suppress excessive CP-violation and FCNCs in the MSSM, the following approximations are often made. First, we assume that there is minimal mixing among the sfermions:

$$\mathbf{m}_Q^2 = m_Q^2 \mathbf{1}, \quad \mathbf{m}_u^2 = m_u^2 \mathbf{1}, \quad \mathbf{m}_{\bar{d}}^2 = m_{\bar{d}}^2 \mathbf{1}, \quad \mathbf{m}_e^2 = m_e^2 \mathbf{1}, \quad \mathbf{m}_{\bar{L}}^2 = m_{\bar{L}}^2 \mathbf{1}$$

We also suppress the cubic scalar couplings of the first two families of sfermions by imposing the conditions:

$$\mathbf{a}_u = A_{u0} \mathbf{y}_u, \quad \mathbf{a}_d = A_{d0} \mathbf{y}_d, \quad \mathbf{a}_e = A_{e0} \mathbf{y}_e.$$

Finally, requiring that the soft SUSY breaking parameters are real enables us to suppress excessive amounts of CP violation:

$$\text{Im}(M_1) = \text{Im}(M_2) = \text{Im}(M_3) = \text{Im}(A_{u0}) = \text{Im}(A_{d0}) = \text{Im}(A_{e0}) = 0.$$

With the above ingredients, one can work out myriad phenomenological consequences. In [chapter 6](#), we examine the neutralino sector of the MSSM in slightly more detail, and present an analysis aimed at exploring it at a 100 TeV collider.

# 3

## COLLIDER PHENOMENOLOGY AND MACHINE LEARNING

---

In this chapter, we will discuss how to connect theory and experiment. We will begin by connecting scattering amplitudes and physically observed cross sections, after which we will briefly discuss detector components of the LHC, and then move on to the question of how we establish statistical significance given experimental data from detectors.

To observe physics at subatomic length scales, it is necessary to produce interactions on those scales. This requires colliding particles at speeds close to the speed of light. The energy of these collisions is so high that not only do the colliding particles scatter off of each other, but new particles can be created as well. The physical observable at particle colliders is a quantity known as the scattering cross section, denoted by  $\sigma$ . It is defined by the relation

$$R = \sigma \mathcal{L}$$

where  $R$  is the rate of collisions per unit time, and  $\mathcal{L}$  is the luminosity of the collider, that is, the number of particles passing through some cross-sectional area per unit time. The scattering cross-section  $\sigma$  for a generic process with particles 1 and 2 colliding to produce a set of particles  $X$  as the final state is given by the integral of the scattering amplitude for the process,  $|\mathcal{M}_{12 \rightarrow X}|^2$  over the phase space of  $X$ <sup>1</sup>.

$$\sigma_{12} = \int d\Pi_X |\mathcal{M}_{12 \rightarrow X}|^2 \quad (3.1)$$

The dynamics of the collision event are contained in the matrix element  $\mathcal{M}$ , which will be influenced by the presence of BSM physics. Thus, the typical quantities of interest are the *differential* cross sections,  $d\sigma/dx$ , where  $x$  represents some kinematic variable. Particle colliders are broadly categorized as either lepton or hadron colliders. Each one has its advantages and disadvantages. Lepton colliders have cleaner signals than hadron colliders due to the lack of large QCD backgrounds. On the other hand, hadron colliders are able to reach much larger center-of-mass energies, since leptons lose large amounts of energy via synchrotron radiation when forced along a circular path. In this work, we will focus on the phenomenology of hadron colliders, both present and future.

### 3.1 DETECTOR DESIGN FOR HADRON COLLIDERS

Particle detectors can be thought of as sophisticated videocameras with extremely high framerates. Conversely, the digital cameras that we use in our daily lives can be thought of as particle detectors, except designed for only one kind of particle, the photon. The response of a detector to an incident particle can take on a variety of forms. In a gaseous detector such as a Geiger-Muller tube, an energetic incident particle will lead to

<sup>1</sup>Here we omit the form factors that would come into play at a hadronic collider, without affecting our narrative.

the ionization of a large fraction of the gas molecules, followed by rapid recombination. This is manifested as an electrical pulse. The analogue of ionization for a solid-state detector (such as the ones used in regular digital cameras) is the creation of a large number of electron-hole pairs. The design of a particle detector will be based upon the particles it aims to detect as well as the desired precision and accuracy. At the Large Hadron Collider at CERN, the two major detectors are ATLAS (A Toroidal LHC Apparatus) and CMS (Compact Muon Solenoid). They differ slightly in construction, but essentially probe the same physics. The components common to them are the following.

*Tracking chamber.* The innermost part of the detector is the tracking chamber. It consists of layers of solid-state detectors that can accurately measure the paths of charged particles that are formed in the particle collision events. The presence of a strong magnetic field bends the paths of these particles, enabling us to learn about their charge and mass.

*Calorimeter(s).* If a particle is energetic enough to go beyond the tracking chamber, it enters the calorimeter region. A calorimeter consists of materials dense enough to completely absorb the energy of an incident particle and stop it in its tracks. At ATLAS and CMS, the calorimeter is actually a combination of two layers that are designed to stop different kinds of particles. The electromagnetic calorimeter is designed to measure the energy of electrons and photons, while the hadronic calorimeter is designed to stop (and you might have guessed this already) hadrons.

*Muon Detectors.* The muon, being about 200 times heavier than the electron, experiences much less energy loss through bremsstrahlung, and is able to bypass both the tracking chamber and calorimeter layers. For this reason, muon detectors form the outermost layer of a particle detector.

A transverse slice of the CMS detector is shown in [figure 3.1](#), depicting the trajectories taken by different kinds of particles through the layers of the detector. The specific design of a detector depends upon the vision of the collaboration running it. With a finite construction and operation budget, tradeoffs must inevitably be made. Although ATLAS and CMS are both state of the art multipurpose detectors, they have their strengths and weaknesses relative to each other based upon different sets of priorities. For this reason, we do not provide the specifics of their construction, and instead point the reader to [\[19\]](#) for a detailed review and comparison of the two. For our purposes, the features of the collision events that we use to perform our analyses (particle momentum, missing transverse energy, etc.) can be measured with either of these detectors.

*Trigger.* As mentioned in [chapter 1](#), there are hundreds of millions of collisions every second at the LHC. Recording and analyzing all of these

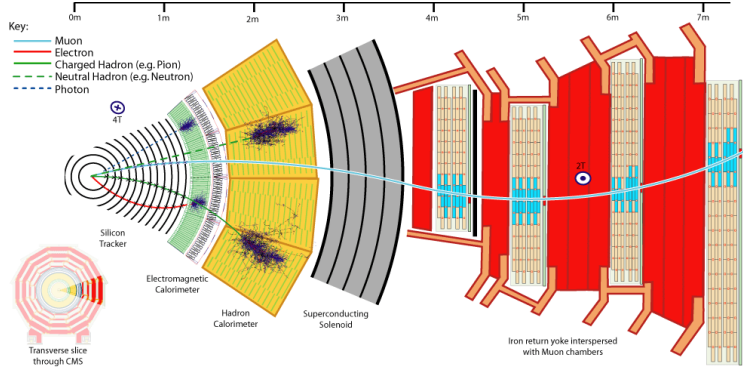


Figure 3.1: Transverse slice of the CMS detector, showing the paths of various particles. Source: [20]

events would be impractical, given that most of the collisions simply involve small deflections. What we are really interested in are the *hard* collisions, with the final state particles having a high amount of momentum in the transverse plane. To filter out the uninteresting events, we employ a *trigger* - that is, a condition that an event must satisfy to be stored for further analysis. For example, in [chapter 6](#), we choose to trigger on a hard lepton, that is, one with a high transverse momentum.

*Invisibles.* An important point to note is that certain particles, such as neutrinos and dark matter candidates, escape the detector entirely, leaving no tracks or energy deposits. The existence of one of these ‘invisible’ particles in a collision event can only be inferred from an observed imbalance of momenta of the final state particles in the transverse direction. Thus, for analyses involving neutrinos or dark matter, the kinematic quantity known as *missing transverse energy*, denoted by  $\cancel{E}_T$ , is of utmost importance.

### 3.2 ANATOMY OF A COLLIDER ANALYSIS

At its heart, the goal of a collider analysis is to compare the predictions of the SM and BSM theories with actual experimental data, and estimate the level of compatibility between them. To do this well, we need precise theoretical predictions of the differential cross sections that we can expect to see at the collider. This is done with the help of Monte Carlo methods and detector simulations, as described below.

#### Parton-level event generation

As mentioned earlier, the cross section for a scattering process is an integral of the scattering amplitude over the phase space of the final state particles. In general, these integrals do not have a closed form solution, and so we must resort to numerical integration. The simplest Monte

Carlo integration method, the *acceptance-rejection* method, involves randomly sampling points within the limits of integration with a uniform probability distribution, and testing whether they lie under the ‘curve’ specified by the integrand. The fraction of points that pass this test, multiplied by the volume of this ‘bounding box’ specified by the integration limits, gives the definite integral. This method is difficult to view in multiple dimensions, but not too hard to grasp in one or two dimensions - see [21] for a brief overview and implementation. However, drawing the random samples from a uniform probability distribution is not the most efficient method for performing Monte Carlo integrals - programs such MadGraph5 and MadEvent [22] do this in more sophisticated ways, determining the roughly most important regions of phase space and concentrating the sampling within those regions. These ‘points’ are simply the particle collision events themselves, with coordinates given by the four-momenta of the final state particles.

#### *Showering and hadronization*

At hadron colliders, dealing with the matrix element  $\mathcal{M}$  alone will not suffice. We must also take into account nonperturbative QCD effects, such as the radiation of soft gluons, and the formation of complex hadronic final states. For example, even if an energetic quark is contained in an event generated by MadEvent, it will not be detected as an elementary particle. It will radiate gluons that themselves split to form new quarks, that subsequently form bound states. This collection of hadronic bound states is termed a jet, and has a momentum collinear with the momentum of the original quark. The identity of this quark can be determined (with a finite efficiency) from the properties of the jet. To handle these non-perturbative effects, we interface MadEvent with the program Pythia[23] which performs the steps of parton showering and hadronization.

#### *Detector simulation and reconstruction*

A full collider analysis carried out by experimentalists will involve detailed simulations of the detector response, using programs such as GEANT4 [24]. For our purposes, however, it is enough to parameterize the detector response at a higher level - for example, specifying a fixed probability for identifying a certain particle. This is done using the Delphes 3 framework [25], which provides a way to perform a fast, modular simulation of the detector response.

#### *Hypothesis testing*

After signal and background samples have been generated using Monte Carlo methods and passed through a detector simulation, they are compared to actual experimental data. Doing this enables us to do one or more of the following:

Symbol	Statistical name	Physics name	Probability model
$H_0$	Null	Background-only	$\text{Pois}(n_{SR} v_B)$
$H_1$	Alternate	Signal+Background	$\text{Pois}(n_{SR} v_S + v_B)$

Table 3.1: The two competing hypotheses for our simple number counting example. Source: [27].

- Estimate some parameter, for example the mass of a particle, or a coupling strength.
- Set upper limits on the rate of occurrence of a process, and translating those limits into limits on the parameter space of BSM theories.
- Discover a new particle
- Compare theoretical and experimental differential cross sections using a goodness-of-fit test.

As it turns out, all of these can be subsumed into the larger framework of *hypothesis testing* [26]. In the following section, we will address how we answer the question “Does this experimental data imply the existence of new physics (or conversely, rule it out)?”. This discussion is adapted from the one in [27].

### 3.3 STATISTICAL SIGNIFICANCE IN PARTICLE PHYSICS

A hypothesis is a claim about what the experimental data will look like, given some model parameters. Let us consider hypothesis testing in the context of a simple counting experiment, in the frequentist interpretation. In this experiment, we examine the subset of a dataset  $\mathcal{D}$  that resides in a region of the ‘data space’ labeled the *signal region* (SR), and contains  $n_{SR}$  events. Our competing hypotheses are the ‘background-only’ and ‘signal plus background’ hypotheses, described in table 3.1. The probability models associated with these hypotheses are Poisson models<sup>2</sup>. The model for the ‘background-only’ hypothesis is  $\text{Pois}(n_{SR}|v_B)$ , that is, the probability of obtaining  $n_{SR}$  events in the signal region when  $v_B$  events are expected from the background process. The competing hypothesis, ‘signal plus background’, on the other hand, predicts  $v_S + v_B$  events in the signal region, with  $v_S$  events from the signal process and  $v_B$  events from the background process. The probability that the background-only hypothesis will produce at least  $n_{SR}$  events is given by

$$P_{\text{background only}} = \sum_{n=n_{SR}}^{\infty} \text{Pois}(n|v_B)$$

The lower this probability is, the less likely it is that the background-only hypothesis can account for the observed number of events in the signal region. This quantity is also known colloquially as the *p*-value - in this case, it is the *p*-value for the background-only hypothesis. The corresponding *p*-value for the signal + background hypothesis is given by:

$$P_{\text{signal + background}} = \sum_{n=n_{SR}}^{\infty} \text{Pois}(n|v_S + v_B)$$

<sup>2</sup>The exact probability distribution for counting experiments is given by the binomial frequency function. In the limit of a large number of events, this approaches the Poisson frequency function, given by

$$\text{Pois}(n|v) = v^n \frac{e^{-v}}{n!}$$

which describes the probability of observing  $n$  events given that the mean expected number of events is  $v$ .

For phenomenology, there are usually two  $p$ -value thresholds of interest. The first is the exclusion threshold - if  $p_{\text{signal} + \text{background}} < 0.05$ , we consider the signal + background hypothesis ‘excluded’. The second is the discovery criterion,  $p_{\text{background only}} < 2.87 \times 10^{-7}$ . When this condition is satisfied, we choose to reject the background-only hypothesis, and claim discovery of new physics. In practice,  $p$ -values are reported in terms of equivalent  $Z$ -values. The  $Z$  value corresponding to a  $p$ -value  $p_0$  is given by

$$Z = \Phi^{-1}(1 - p_0)$$

where  $\Phi^{-1}$  is the inverse of the cumulative distribution function of the standard normal distribution (a Gaussian distribution with mean 0 and variance 1). The equivalent  $Z$ -values for the exclusion and discovery  $p$ -value thresholds are 1.96 and 5, respectively. In particle physics parlance, the equivalent  $Z$  value is known as the *significance*, and is reported as  $Z\sigma$ . The significance is maximized by choosing signal regions with low values of  $n_B$ . This can be seen from the expressions for  $p_{\text{background only}}$ . Lower values of  $n_B$  lead to lower values of  $p_{\text{background only}}$ , minimizing the probability, denoted  $\alpha$ , that we will wrongly reject the background-only hypothesis when it is true. This is known as a Type-I error. However, in general, there can be multiple, or even an infinite number of such regions in data space. Moreover, this criterion does not let us say anything about the signal + background hypothesis. Thus, we also require that the choice of the signal region leads to a low probability (denoted  $\beta$ ) of wrongly accepting the background-only hypothesis when the signal + background hypothesis is true (a Type-II error).

In the language of hypothesis testing, then, the job of a collider phenomenologist like myself is to find regions of data space that *minimize* the probability of wrongly accepting the null hypothesis when the alternate hypothesis is true, given a *fixed* probability of wrongly rejecting the null hypothesis when the alternate hypothesis is true.

Whew, that is a mouthful! In more concise terms, we would like to minimize  $\beta$  for a given value of  $\alpha$ . The quantity  $\alpha$  is known as the *size* of the test, and the quantity  $1 - \beta$  is known as the *power* of the test. And more importantly, in practical terms, this task boils down to finding regions of the data space that are densely populated by signal events (minimizing  $\beta$ ) and sparsely populated by background events (minimizing  $\alpha$ ). After isolating a promising signal region, we calculate the maximum achievable value of  $Z$ . In general, the value of  $Z$  will be calculated differently for claiming exclusion or discovery. However, we are not performing a full collider analysis, but rather a sort of ‘feasibility study’, for which we simply use the asymptotic formula for  $Z$  obtained by taking limit in which the probability distributions are Gaussian, and the signal rates are much smaller than the background rates.

$$Z \approx \frac{n_S}{\sqrt{n_B}}$$

where  $n_S$  and  $n_B$  are the number of signal and background events observed in the signal region respectively.

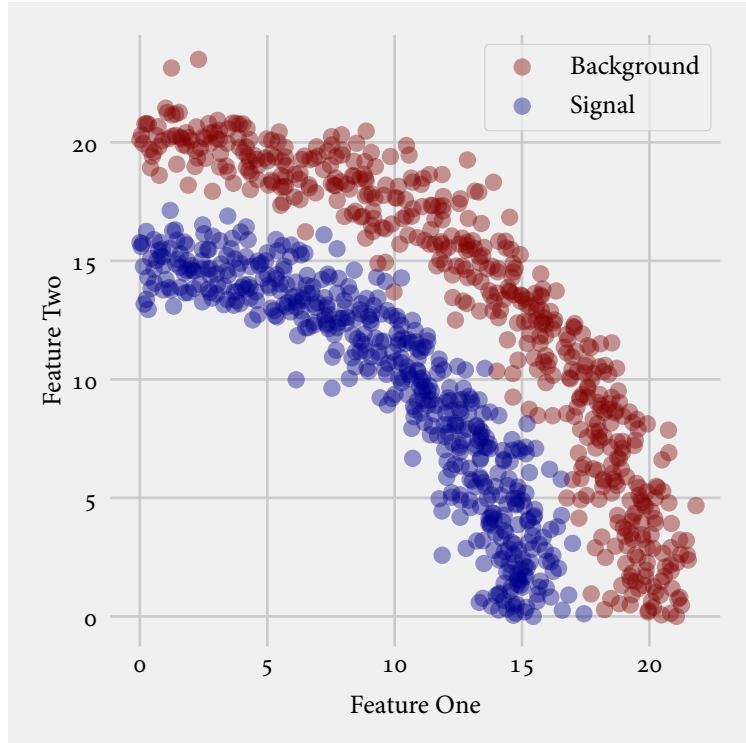
Traditionally, promising signal regions are found by formulating kinematic variables that can efficiently discriminate between signal and background events. These variables are designed based on our knowledge of the kinematics of the final state particles in the signal and background events. They include variables such as invariant mass, missing transverse energy, and transverse mass. While this approach has served us well so far, the models being examined are grown increasingly complex, with large parameter spaces, and with the increase in collision energy comes a much larger rate of background event production. The boundary of the optimal signal region in data space, can potentially be highly non-linear. The traditional ‘cut-and-count’ strategy finds the signal region by applying a series of one or two dimensional selection cuts on the data. This approach can potentially miss higher-dimensional correlations in the data space. These correlations can be found efficiently through the use of *machine learning* techniques, which we discuss in section 3.4.

*Reach in parameter space.* As mentioned earlier, new physics theories such as Two Higgs Doublet Models can have extremely large parameter spaces. Each point of a theory’s parameter space can be considered as a new physics hypothesis. In our analyses, we aim to perform hypothesis tests for a large number of points in parameter space, and ascertain which of the points, or hypotheses, can be rejected, or alternatively, discovered. Doing this, we find contours of the the equivalent  $Z$  values in the parameter space. Typically we show only the contours for  $Z = 1.96$  and  $Z = 5$ , that is, the discovery and exclusion contours. We term the area bounded by these contours the *reach* of our analysis in parameter space.

### 3.4 MACHINE LEARNING IN PARTICLE PHYSICS

Separating signals and backgrounds in particle physics is, in the language of machine learning, a *classification* problem. One can consider particle collision events as residing in a space, where the coordinates of each event are represented by various *features* of the event. This is equivalent to the ‘data space’ discussed in the previous section. These features could be high-level ones such as invariant masses, or low-level ones, such as the momentum components of individual final state particles. What we do when we perform a cut-and-count analysis is to try and isolate a region of this space that is rich in signal events. Typically, the most straightforward approach is to define a sort of ‘box’ in feature space using rectangular, one-dimensional cuts. However, there is no guarantee that signal events are confined to such a box — correlations between the features can distort the distribution of events in feature space. If we consider a two or three dimensional feature space, this distribution of the

Figure 3.2: Illustration of a non-linear decision boundary in two-dimensional feature space.



events is typically easy to visualize, and can often be explained through a simple kinematical relation between the features. Thus, instead of a box, we might draw a ring, or perhaps some other shape as a ‘lasso’ around the events. This kind of delineation between signal and background events is known in machine learning terms as a *decision boundary*. As we go to higher dimensional feature spaces, choosing this decision boundary by visual inspection becomes virtually impossible - instead, we resort to looking at one and two dimensional slices of the space.

However, inspecting these lower dimensional slices may fail to fully capture the potentially complicated correlations among the features, and we might end up rejecting too many signal events, or accepting too many background events. Take for example the distribution of data from a toy experiment in figure 3.2. The decision boundary that separates the signal events (blue) and the background events (red) is curved. Applying rectilinear cuts in this feature space would clearly be suboptimal. Machine learning (ML) techniques (or, as they are sometimes referred to in the particle physics literature, multivariate techniques) can harness the correlations between features more efficiently than manually attempting to find the optimal decision boundary in feature space.

In the context of particle physics, a *binary classifier* is a function that takes as input various features of an event, and outputs a score for the event corresponding to whether it is more signal-like or more background-like. The form of the function itself depends on a number of parameters, which are *a priori* unknown. In *supervised learning* (which

encompasses the most commonly-used ML techniques), these parameters are set by feeding the classifier a set of *labeled training data*. After the parameters are determined, we can evaluate the performance of the classifier by using it on *test data*, which are unlabeled. While there are a number of commonly-used classifiers to choose from, for our study, we chose the Gradient Boosted Decision Tree classifier<sup>3</sup>, since it performs quite well ‘out-of-the-box’, with minimal tuning. This classifier is actually an example of an *ensemble method* — it combines the results from a large number of weak classifiers to assign scores to events. This combination is much more resistant to *overtraining*, that is, the combined classifier will not be too specialized to the training set and can perform well on test sets as well.

While the analysis in chapter 4 does not employ ML techniques, the analyses in chapters 5 and 6 do.

<sup>3</sup>For a description of this classifier and a good review of statistical learning in general, see [28].



# 4

## LIGHT CHARGED HIGGSES AT THE LHC

In [section 2.2](#), we introduced a well-motivated class of extensions to the scalar sector, known as Two-Higgs Doublet Models (2HDMs). In these models, the mass spectrum of the scalar sector contains, in addition to the SM Higgs, a CP-even scalar  $H^1$ , a CP-odd pseudoscalar  $A$ , and a charged scalar  $H^\pm$ .

The discovery of one or more of these new particles would be a clear indication of an extended Higgs sector as the source of electroweak symmetry breaking (EWSB). A number of experimental searches have been carried out to find these particles at the Large Electron-Positron Collider (LEP), the Tevatron experiment at Fermilab, and most recently, at the LHC. [[29–36](#)]. These searches were performed assuming that these new scalar states decay solely through conventional channels, that is, into SM particles. However, if they are kinematically allowed, ‘exotic’ decay channels, in which a heavy Higgs boson decays into either a pair of lighter Higgses, or a Higgs and a gauge boson, can be the dominant decay channels for certain regions of parameter space, thus reducing the reach of the conventional search channels. Some of these channels have already been studied both theoretically [[37–45](#)] and experimentally [[46–48](#)]. With the increase in center of mass collision energy of the LHC from 7 to 14 TeV, more of those exotic decay channels will be accessible at the LHC. It is therefore timely to study the LHC reach of those channels more carefully.

In this study, we examine the prospects of detecting a light (that is, lighter than the top quark) charged Higgs boson through the exotic decay channel

$$H^\pm \rightarrow (A/H) W^\pm \rightarrow (\tau\tau) W^\pm$$

and produced via the decay of the top quark,  $t \rightarrow H^+ b$ . The collider analysis in [[40](#)] studies the same exotic decay channel, but for a charged Higgs heavier than the top quark, produced in  $H^\pm tb$  associated production. The large rate of production of top quarks at the LHC should enable us to observe a sizable number of signal events. Current search strategies for light charged Higgses at the LHC assume that they decay either leptonically to the  $\tau\nu$  final state, or hadronically, to the  $cs$  final state. The null search results obtained by both the ATLAS and CMS experiments exclude a light charged Higgs below a mass of about 160 GeV for most of the two-dimensional  $m_{H^\pm} - t_\beta$  plane<sup>2</sup> in parameter space [[32, 33](#)]. However, if there exists a neutral Higgs ( $A/H$ ) light enough such that the  $H^\pm \rightarrow AW^\pm/HW^\pm$  channel is kinematically open, the branching fractions into the conventional final states  $\tau\nu$  and  $cs$  are suppressed and the exclusion bounds can be significantly weakened. Due to experimental challenges at low energies, such a light neutral Higgs has not been fully excluded yet. A relatively large region of  $m_H^\pm > 150$  GeV and  $t_\beta \lesssim 20$  is still allowed, while no limits exist for  $m_H^\pm > 160$  GeV.

<sup>1</sup>Note that we use  $h$  and  $H$  to refer to the lighter or the heavier CP-even Higgs for models with two CP-even Higgs bosons. When there is no need to specify, we use  $H$  to refer to the CP-even Higgses.

<sup>2</sup>Here we use the abbreviated notations for trigonometric functions introduced in [section 2.2](#)

The exotic decay channel of  $H^\pm \rightarrow AW/HW$ , on the other hand, offers an additional opportunity for the detection of a light charged Higgs, closing the loophole of the current light charged Higgs searches. While there are strong constraints on the mass of the light charged Higgs from flavor [49, 50] and precision [51–55] observables, those limits are typically model dependent and could be relaxed when there are contributions from the other sectors of the model [56]. A direct search for a light charged Higgs, on the other hand, provides a model-independent and complementary reach. It is thus timely and worthwhile to fully explore the discovery or exclusion potential of the light charged Higgs at the LHC.

In this chapter we study the exotic decay of a charged Higgs  $H^\pm \rightarrow AW/HW$  with  $A/H$  decaying into  $\tau\tau$ . We focus on the light charged Higgs produced via top decay, considering both the single top and top pair production channels. We obtain model-independent exclusion and discovery limits that are subsequently interpreted in the context of the Type II 2HDM.

The rest of the chapter is structured as follows. In section 4.1, we briefly introduce the relevant couplings and branching ratios for our decay channel for the type II 2HDM and present scenarios that permit a large branching fraction for the process  $H^\pm \rightarrow AW/HW$ . In section 4.2, we summarize the current experimental constraints on a light charged Higgs. In section 4.3, we present the details of our collider analysis, and in section 4.3, the model independent 95% C.L. exclusion and  $5\sigma$  discovery limits for the 14 TeV LHC with various luminosities. In section 4.4, we discuss the implications of our analysis for the Type II 2HDM and translate our results into reaches in parameter space. We conclude in section 4.5.

#### 4.1 COUPLINGS AND BRANCHING RATIOS

##### *Decays of the top quark*

If the charged Higgs is light enough, the top quark can either decay to  $W^\pm b$  or to  $H^\pm b$ . The first decay is controlled by the SM gauge coupling

$$g_{W^\pm tb} = \frac{g}{\sqrt{2}} \gamma^\mu \frac{1 - \gamma_5}{2}, \quad (4.1)$$

with  $g$  being the SM SU(2) coupling, while the second is a function of the parameter  $t_\beta$  (see the form of the Yukawa coupling in (??)). More specifically, for a type-II 2HDM, it takes the form (see table 2.4)

$$g_{H^\pm tb} = \frac{g}{2\sqrt{2}m_W} [(m_b t_\beta + m_t/t_\beta) \pm (m_b t_\beta - m_t/t_\beta) \gamma_5]. \quad (4.2)$$

This coupling is enhanced for both small and large values  $t_\beta$ . In figure 4.1, we present contours of the branching fraction  $\text{BR}(t \rightarrow H^\pm b)$  in the  $m_{H^\pm} - t_\beta$  plane, calculated using the Two-Higgs Doublet Model Calculator (2HDMC) [57]. We see that it can reach values of 5% and above

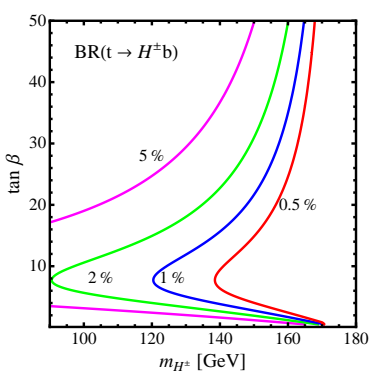


Figure 4.1: Contours of the branching fraction of the top quark to the charged Higgs, in the  $m_{H^\pm} - t_\beta$  plane. We see that it reaches a minimum at  $t_\beta = \sqrt{m_t/m_b} \approx 8$ .

for both large and small  $t_\beta$ , but reaches a minimum at  $t_\beta = \sqrt{m_t/m_b} \sim 8$ . It also decreases rapidly as the charged Higgs mass approaches the mass of the top quark.

### Decays of the charged Higgs

Conventionally, a light charged Higgs is assumed to either decay into the  $\tau\nu$  or  $cs$  final states, with the corresponding couplings given by

$$g_{H^\pm\tau\nu} = \frac{g}{2\sqrt{2}m_W} m_\tau t_\beta (1 \pm \gamma_5) \text{ and}$$

$$g_{H^\pm cs} = \frac{g}{2\sqrt{2}m_W} [(m_s t_\beta + m_c \cot \beta) \pm (m_s t_\beta - m_c \cot \beta) \gamma_5].$$

If there exists an additional neutral Higgs boson  $h$  or  $A$  that is lighter than the charged Higgs, then additional decay channels into  $hW/AW$  open up. The couplings are determined by the gauge coupling structure, as well as the mixing angles [58]

$$g_{H^\pm h W^\mp} = \frac{gc_{\beta-\alpha}}{2} (p_h - p_{H^\pm})^\mu \quad \text{and} \quad g_{H^\pm AW^\mp} = \frac{g}{2} (p_A - p_{H^\pm})^\mu,$$

where  $p_\mu$  is the incoming momentum for the corresponding particle.

The  $H^\pm \rightarrow hW$  channel for a light charged Higgs is open only if we demand the heavy CP-even neutral Higgs  $H$  to be the SM-like Higgs. In this case  $|c_{\beta-\alpha}| \sim 1$  is preferred by experiments and the  $H^\pm h W^\mp$  coupling is unsuppressed. The  $H^\pm AW^\mp$  coupling is independent of  $s_{\beta-\alpha}$  and always unsuppressed. In this scenario, there is no  $H^\pm \rightarrow HW$  channel since it is kinematically forbidden.

In the generic 2HDM, there are no mass relations between the charged scalars, the scalar and pseudoscalar states. Therefore, both the decays  $H^\pm \rightarrow hW$  and  $H^\pm \rightarrow AW$  can be accessible or even dominant in certain regions of the parameter space. It was shown in [50] that in the Type II 2HDM with  $Z_2$  symmetry, imposing all experimental and theoretical constraints still leaves large regions in the parameter space that permit such exotic decays with unsuppressed decay branching fractions.

In figure 4.2, we show the contours of the branching fraction of the charged Higgs to the  $AW$  final state in the  $m_{H^\pm} - t_\beta$  plane, with  $h$  being the SM-like Higgs and  $H$  being heavy enough to be decoupled. This branching fraction reaches large values for  $t_\beta$  between 10 and 30 and charged Higgs masses between 155 and 170 GeV. For small charged Higgs masses close to the  $m_A + m_W$  threshold, the decay is kinematically suppressed. In figure 4.3, we show the same branching fraction, but this time as a function of  $t_\beta$ , for a fixed charged Higgs mass of 160 GeV. For large values of  $t_\beta$ , the branching fraction of the  $\tau\nu$  mode dominates that of the  $AW$  mode. In both plots, we assume the existence of a pseudoscalar  $A$  with mass 70 GeV. Similar results can be obtained for  $H^\pm \rightarrow hW$  with  $m_h = 70$  GeV,  $s_{\beta-\alpha} \sim 0$  and  $A$  decoupled.

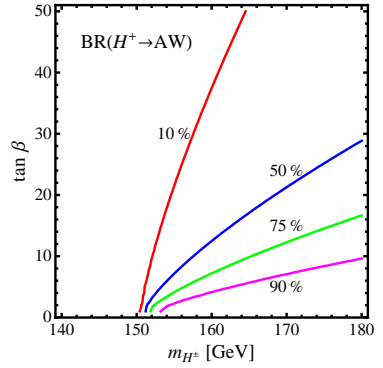


Figure 4.2: Contours of the branching fraction for the decay ( $H^\pm \rightarrow AW$ ) in the Type II 2HDM in  $m_{H^\pm} - t_\beta$  plane. The branching fraction reaches large values for  $t_\beta$  between 10 and 30, for  $m_{H^\pm}$ .

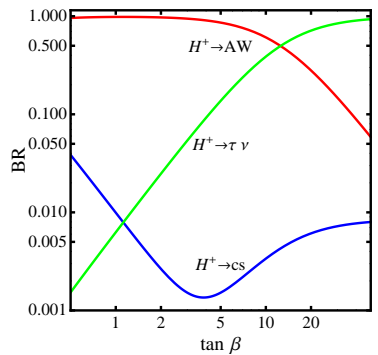


Figure 4.3: The branching fractions of  $H^\pm \rightarrow AW$  (red),  $\tau\nu$  (green) and  $cs$  (blue) as functions of  $t_\beta$  for  $m_{H^\pm} = 160$  GeV.

The MSSM Higgs mass spectrum is more restricted. At tree level, the mass matrix depends on  $m_A$  and  $t_\beta$  only, and the mass of the charged Higgs mass is related to that of the pseudoscalar  $A$  by  $m_{H^\pm}^2 = m_A^2 + m_W^2$ . Large loop corrections are therefore needed to increase the mass splitting enough that the decay  $H^\pm \rightarrow AW$  becomes kinematically permitted. In the non-decoupling region of MSSM with  $H$  being the SM-like Higgs, the CP-even Higgs  $h$  can be light:  $m_h < m_{H^\pm} - m_W$ . The branching fractions can reach values up to 10% [59] in some regions of parameter space. In the NMSSM, where the Higgs sector is enlarged by an additional singlet, decays of  $H^\pm \rightarrow A_i W/H_i W$  can be significant in certain regions of parameter space [60, 61].

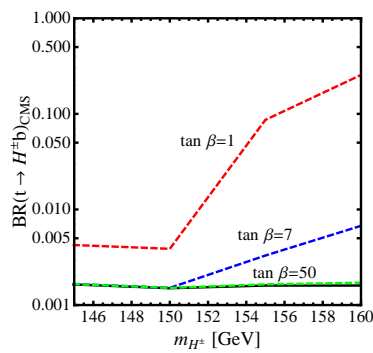
#### 4.2 LITERATURE REVIEW

Searches for a light charged Higgs boson have been performed by both ATLAS and CMS [32, 33] with  $19.7 \text{ fb}^{-1}$  of integrated luminosity at 8 TeV and  $4.6 \text{ fb}^{-1}$  of integrated luminosity at 7 TeV. The production mechanism considered in these searches is top pair production, with one top quark decaying to  $bH^\pm$  while the other decays to  $bW^\pm$ . These studies focus on the  $H^\pm \rightarrow \tau\nu$  decay channel, which is dominant in most parts of the parameter space in the absence of decays into lighter Higgses. Assuming a branching fraction  $\text{BR}(H^\pm \rightarrow \tau\nu) = 100\%$ , the null search results from CMS [33] imply upper bounds for the top quark branching fraction  $\text{BR}(t \rightarrow H^\pm b)$  ranging from 1.2% to 0.16% for charged Higgs masses between 80 and 160 GeV. This result can be translated into bounds on the MSSM parameter space. The obtained exclusion limits for the MSSM  $m_h^{\max}$  scenario can be seen in figure 4.5 (region to the left of red line). Only charged Higgs masses in the small region between 155 and 160 GeV around  $t_\beta = 8$  are still allowed. The results from ATLAS [32] are similar.

A search with the  $H^\pm \rightarrow cs$  decay channel has been performed by ATLAS [34] using  $4.7 \text{ fb}^{-1}$  integrated luminosity at 7 TeV and by CMS [35] using  $19.7 \text{ fb}^{-1}$  integrated luminosity at 8 TeV. Assuming  $\text{BR}(H^\pm \rightarrow cs) = 100\%$ , the ATLAS results imply an upper bound for  $\text{BR}(t \rightarrow bH^\pm)$  around 5% to 1% for charged Higgs masses between 90 and 150 GeV, while the CMS searches imply an upper bound of around 2% to 7% for a charged Higgs masses between 90 and 160 GeV.

These limits get weaker once we consider realistic branching fractions that are smaller than 100%. In figure 4.4, we show how the CMS limits on the branching fraction  $\text{BR}(t \rightarrow H^\pm b)$  can change significantly in the presence of an additional light neutral Higgs. The black curve shows the CMS limits presented in [33] assuming a  $\text{BR}(H^\pm \rightarrow \tau\nu) = 100\%$ . The modified limits assuming the existence of a 70 GeV CP-odd neutral Higgs are shown for  $t_\beta = 1$  (red), 7 (blue) and 50 (green). We can see that for large  $t_\beta$ , the limits stay almost unchanged since  $H^\pm \rightarrow \tau\nu$  is the dominant decay channel, but for smaller values of  $t_\beta$  these limits are weakened significantly.

Figure 4.4: CMS limits on the branching fraction of the top quark to the charged Higgs



Here, we are assuming a  $\text{BR}(H^\pm \rightarrow \tau\nu) = 100\%$  (black line) [33], as well as the weakened limits in the Type II 2HDM in the presence of a light neutral Higgs for various values of  $t_\beta$ .

Similarly, figure 4.5 shows how the CMS limits in the  $m_{H^\pm} - t_\beta$  plane weaken in the presence of an additional light Higgs. The union of the yellow and cyan regions is excluded by CMS assuming  $\text{BR}(H^\pm \rightarrow \tau\nu) = 100\%$ , while only the cyan region is excluded assuming the branching fractions predicted by a Type II 2HDM in the presence of a CP-odd neutral Higgs with mass 70 GeV. This weakening is most prominent in the low  $t_\beta$  region - the lower limit on charged Higgs masses reduces to about 150 GeV for  $t_\beta < 15$ . Therefore, the presence of exotic decay modes substantially weakens the current and future limits based on searches based on the conventional  $H^\pm \rightarrow \tau\nu, cs$  decay modes.

A light charged Higgs could have a large impact on precision and flavor observables as well [62]. For example, for a Type II 2HDM, the bounds on the rate of the decay  $b \rightarrow s\gamma$  restrict the charged Higgs to be heavier than 300 GeV. A detailed analysis of precision and flavor bounds in the 2HDM can be found in refs. [49, 50]. Flavor constraints on the Higgs sector are however typically model-dependent, and could be alleviated by contributions from other new particles in a model [56]. Since our focus in this work is on collider searches for light charged Higgses, we consider the scenario of a light charged Higgs as long as it satisfies the direct bounds set by collider searches for Higgs bosons.

Our study also assumes the existence of a light neutral Higgs  $A/H$ . This type of Higgs has been constrained by the  $A/H \rightarrow \tau\tau$  searches at the LHC [30, 31], in particular, for  $m_{A/H} > 90$  GeV and relatively large  $t_\beta$ . No limit, however, exists for  $m_{A/H} < 90$  GeV due to the difficulties in the identification of the relatively soft taus and the overwhelming SM backgrounds for soft leptons and  $\tau$ -jets. Furthermore, LEP limits [29] based on  $VH$  associated production do not apply to the CP-odd  $A$  or the non-SM like CP-even Higgs. LEP limits based on  $AH$  pair production also do not apply, as long as  $m_A + m_H > 208$  GeV. Therefore, in our analyses below, we choose the daughter (neutral) Higgs mass to be 70 GeV<sup>3</sup>.

There have been other theoretical studies on light charged Higgses as well - the authors of [63] and [64] analyzed light charged Higgses produced via single top production and decaying to the  $\tau\nu$  final state, while the authors of [65] and [66] investigate light charged Higgses that are produced via the top pair production channel, and decay to  $\mu\nu$  and  $\gamma\gamma W$  final states.

Charged Higgses heavier than the top quark have been analyzed in detail in [40], which considers the associated production channel  $H^\pm tb$  and the exotic decay channel  $H^\pm \rightarrow AW/HW^\pm$ . Given that our study considers the same final state ( $bbWWA/H$ ) as the one in [40], we can use a similar search strategy to find light charged Higgses that come from the decay of pair-produced top quarks.

<sup>3</sup>The mass of 70 GeV is also chosen to be less than half the mass of the SM Higgs. This prohibits the decay channel  $h_{\text{SM}} \rightarrow AA$  and enforces consistency with the current measurements of branching ratios of the SM Higgs.

### 4.3 COLLIDER ANALYSIS

In our analysis we study the exotic decay  $H^\pm \rightarrow AW/HW$  of light charged Higgs bosons ( $m_{H^\pm} < m_t$ ) produced via top decay. We consider two production mechanisms for the parent top quarks:  $t$ -channel single top production<sup>4</sup> ( $tj$ ) and top pair production ( $t\bar{t}$ ) [67].

The light neutral Higgs boson can either be the CP-even  $H$  or the CP-odd  $A$ . In the analysis that follows, we use the decay  $H^\pm \rightarrow AW^\pm$  as an illustration. Since we do not use angular correlations of the charged Higgs decay, the bounds obtained for  $H^\pm \rightarrow AW^\pm$  will apply to  $H^\pm \rightarrow HW^\pm$  as well.

The neutral Higgs boson  $A$  itself will decay further. In this analysis we look at the decay  $A \rightarrow \tau\tau$  for single top production and both the fermionic  $\tau\tau$  and the hadronic  $bb$  modes for top pair production. While the  $bb$  mode has the advantage of a large branching fraction  $\text{BR}(A \rightarrow bb)$ , the  $\tau\tau$  case has smaller SM backgrounds and therefore leads to a cleaner signal. We study both leptonic ( $\tau_{\text{lep}}$ ) and hadronic ( $\tau_{\text{had}}$ ) decays of the tau lepton, and consider the following cases:  $\tau_{\text{had}}\tau_{\text{had}}$ ,  $\tau_{\text{lep}}\tau_{\text{had}}$  and  $\tau_{\text{lep}}\tau_{\text{lep}}$ . The  $\tau_{\text{lep}}\tau_{\text{had}}$  case is particularly promising since we can utilize the same sign dilepton signal with the leptons from the decays of the  $W$  and the  $\tau$ .

We use Madgraph 5/MadEvent v1.5.11 [22] to generate our signal and background events. These events are passed to Pythia v2.1.21 [68] to simulate initial and final state radiation, showering and hadronization. The events are further passed through Delphes 3.07 [25] with the Snowmass combined LHC detector card [69] to simulate detector effects. The discovery reach and exclusion bounds have been determined using RooStats [70] and theta-auto [71].

In this section, we will present model *independent* limits on the  $\sigma \times \text{BR}$  for both 95% C.L. exclusion and  $5\sigma$  discovery for both single top and top pair production with possible final states  $\tau\tau bWj$  and  $\tau\tau bbWW/bbbbWW$ . We consider parent charged Higgses with masses between 150 and 170 GeV and a daughter Higgs  $A$  with a mass of 70 GeV.

#### *Single Top Production*

For single top production, we consider the channel

$$pp \rightarrow tj \rightarrow H^\pm bj \rightarrow AW^\pm bj \rightarrow \tau\tau Wbj.$$

The dominant SM backgrounds are  $W\tau\tau$  production, which we generate with up to two additional jets (including  $b$  jets); and top pair production with both fully leptonic and semileptonic decay chains, which we generate with up to one additional jet. We also take into account the SM backgrounds  $tj\tau\tau$  and  $tlll$  with  $l = (e, \mu, \tau)$ . Our approach is to perform a traditional ‘cut-and-count’ analysis, with the following selection cuts.

1. *Identification cuts:*

- *Case A* ( $\tau_{\text{had}} \tau_{\text{had}}$ ): We select events with exactly one lepton ( $e$  or  $\mu$ ), two  $\tau$  tagged jets, fewer than two  $b$  tagged jets, and at least one untagged jet. We also require the  $\tau$ -tagged jets to have opposite-sign charges.
- *Case B* ( $\tau_{\text{lep}} \tau_{\text{had}}$ ): Same as case A, except that we require exactly two leptons instead of one. Additionally, we require that both of these leptons have charges of the same sign, which is opposite to the sign of the  $\tau$  tagged jet.
- *Case C* ( $\tau_{\text{lep}} \tau_{\text{lep}}$ ): Same as case A, except that we require exactly three leptons instead of one. No conditions are placed on the signs of the charges for this case.

The following criteria were also required for the identification of leptons, and jets:  $|\eta_{l,b,\tau}| < 2.5$ ,  $|\eta_j| < 5$ ,  $p_T(l_1, j, b) > 20$  GeV and  $p_T(l_2) > 10$  GeV.

2. *Neutrino reconstruction:* We reconstruct the momentum of the neutrino using the missing transverse momentum and the momentum of the hardest lepton as described in [72], assuming that the missing energy is solely from the decay  $W \rightarrow l\nu$ .
3. *Neutral Higgs candidate:* The  $\tau$  jets (case A), the  $\tau$  jet and the softer lepton (case B) or the two softer leptons (case C) are combined to form the neutral Higgs candidate. The reconstruction of the neutrino and the neutral Higgs candidate are relatively poor in cases B and C due to additional missing energy from the neutrino associated with the leptonic  $\tau$  decay.
4. *Charged Higgs candidate:* The momenta of the neutral Higgs candidate, the reconstructed neutrino and the hardest lepton are combined to form the charged Higgs candidate.
5. *Mass cuts:* We place upper limits on the masses of the charged and neutral Higgs candidates, optimized for each mass combination. For  $m_{H^\pm} = 160$  GeV and  $m_A = 70$  GeV, we impose the cuts  $m_{\tau\tau} < 48$  GeV, and  $m_{\tau\tau W} < 148$  GeV.
6. *Angular correlation:* A unique kinematical signature of single top production is the distribution of the angle  $\theta^*$ , which is the angle between the top momentum in the  $tj$  system's rest frame and the  $tj$  system's momentum in the lab frame. This variable was first introduced in [73]. The differential distribution for  $\cos \theta^*$  is shown in figure 4.6 for the signal (red), and the backgrounds  $t\bar{t}$  (blue) and  $W\tau\tau$  (green). The signal distribution tends to peak around  $\cos \theta^* \approx -1$  while the background distribution is flat for  $W\tau\tau$  and  $t\bar{t}$ .<sup>5</sup> In our analysis we require  $\cos \theta^* < -0.8$ .
7. *Top and recoil jet system momentum:* In single top production, we expect that the transverse momentum of the top quark and recoil jet should balance each other, as shown in figure 4.7 by the red curve. We require that the transverse momentum of the  $tj$  system,  $p_{T,tj}$ , must be less than 30 GeV. This further suppresses the top

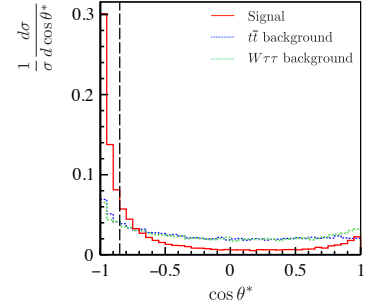


Figure 4.6: Normalized distribution of  $\cos \theta^*$ , for case A with  $m_{H^\pm} = 160$  GeV. The imposed cuts are indicated by the vertical dashed lines.

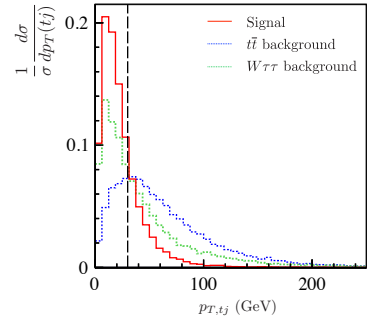


Figure 4.7: Normalized distribution of the transverse momentum of the  $tj$  system  $p_{T,tj}$ , for case A with  $m_{H^\pm} = 160$  GeV. The imposed cuts are indicated by the vertical dashed lines.

<sup>5</sup>As shown in [73], the  $\cos \theta^*$  distribution for  $t\bar{t}$  background would peak around  $\cos \theta^* = 1$  if the top quark could be reliably identified. However, in this study we approximate the top quark momentum by the momentum of the charged Higgs candidate, which results in a flat distribution of  $\cos \theta^*$  for the  $t\bar{t}$  system.

Table 4.1: Representative cut flow table for the benchmark point with  $m_{H^\pm} = 160$  GeV and  $m_A = 70$  GeV at the 14 TeV LHC.

Case	Cut	$\sigma_{\text{Signal}}$	$\sigma_{W(W)\tau\tau}$	$\sigma_{t\bar{t}}$	$\sigma_{tj\tau\tau/ttll}$	$S/B$	$S/\sqrt{B}$
	Original	100	2000	$6.3 \times 10^5$	257	-	-
A	Identification	0.29	5.36	130	1.39	0.002	0.43
	Mass cuts	0.16	0.34	2.62	0.04	0.05	1.55
	$\cos\theta^*$ and $p_{T,tj}$	0.07	0.03	0.07	0.001	0.67	3.72
B	Identification	0.25	4.45	2.46	1.33	0.03	1.51
	Mass cuts	0.11	0.31	0.20	0.05	0.19	2.48
	$\cos\theta^*$ and $p_{T,tj}$	0.06	0.04	0.02	0.002	0.91	3.99
C	Identification	0.18	3.07	6.77	6.74	0.01	0.78
	Mass cuts	0.12	0.55	0.94	0.28	0.07	1.63
	$\cos\theta^*$ and $p_{T,tj}$	0.07	0.08	0.10	0.01	0.38	2.84

All cross sections are given in femtobarns. We have chosen a nominal value for  $\sigma \times \text{BR}(pp \rightarrow tj \rightarrow H^\pm jb \rightarrow \tau\tau Wbj)$  of 100 fb to illustrate the cut efficiencies for the signal process. The significance,  $S/\sqrt{B}$  is calculated for an integrated luminosity of 300  $\text{fb}^{-1}$ .

pair background in the presence of additional jets coming from the second top quark.

In table 4.1, we show a representative cut flow table for a signal benchmark point with  $m_{H^\pm} = 160$  GeV and  $m_A = 70$  GeV at the 14 TeV LHC. The first row shows the total cross section before cuts, calculated using MadGraph. The following rows show the cross sections for the signal and major backgrounds after applying the selection cuts discussed above. We have chosen a nominal value for  $\sigma \times \text{BR}(pp \rightarrow H^\pm jb \rightarrow \tau\tau Wbj)$  of 100 fb to illustrate the cut efficiencies.<sup>6</sup>

We can see that the dominant background contributions after particle identification are  $t\bar{t}$  for cases A and C, and  $W\tau\tau$  for case B. The reach is slightly better in case B since the same sign dilepton signature can efficiently reduce the  $t\bar{t}$  background. Nevertheless, soft leptons from underlying events or  $b$ -decay can mimic the same sign dilepton signal. The obtained results are sensitive to the  $\tau$  tagging efficiency as well as the misidentification rate. In our analyses, we have used a  $\tau$  tagging efficiency of 60% and a mistagging rate of 0.4%, as suggested in [69]. A better rejection of non- $\tau$  initiated jets would increase the significance of this channel.

### Top Pair Production

We now turn to the top pair production channel,

$$pp \rightarrow tt \rightarrow H^\pm tb \rightarrow AbbWW \rightarrow \tau\tau bbWW/bbbbWW. \quad (4.3)$$

As mentioned earlier, a detailed collider study with the same final states has been performed in [40] with a focus on high charged Higgs masses.

<sup>6</sup>This is consistent with the Type II 2HDM the top branching fraction into a charged Higgs for  $m_{H^\pm} = 160$  GeV, which is typically between 0.1% and 1% (see figure 4.1). Using the single top production cross section,  $\sigma_{tj} = 248$  pb [67] and assuming the branching fractions  $\text{BR}(H^\pm \rightarrow AW^\pm) = 100\%$  and  $\text{BR}(A \rightarrow \tau\tau) = 8.6\%$  leads to the stated  $\sigma \times \text{BR}$  of around 21 – 210 fb.

Table 4.2: Representative cut flow table for benchmark point with  $m_{H^\pm} = 160$  GeV and  $m_A = 70$  GeV at the 14 TeV LHC, for the decay mode  $A \rightarrow \tau\tau$ .

Case	Cut	$\sigma_{\text{Signal}}$	$\sigma_{t\bar{t}}$	$\sigma_{t\bar{t}ll}$	$\sigma_{W(W)\tau\tau}$	$S/B$	$S/\sqrt{B}$
Original		1000	$6.3 \times 10^5$	247	2000	-	-
	Identification	4.1	23.3	0.58	0.078	0.17	14.9
A	$m_{\tau\tau}$ vs $m_{\tau\tau W}$	0.6	0.31	0.021	0.003	1.9	18.8
	Identification	3.3	0.35	0.697	0.072	3.0	55.3
B	$m_{\tau\tau}$ vs $m_{\tau\tau W}$	0.69	0.035	0.042	0.007	8.1	41.1
	Identification	3.1	2.35	5.11	0.058	0.41	19.9
C	$m_{\tau\tau}$ vs $m_{\tau\tau W}$	0.62	0.25	0.16	0.006	1.4	16.5

We have chosen a nominal value for  $\sigma \times \text{BR}(pp \rightarrow tt \rightarrow H^\pm tb \rightarrow \tau\tau bb WW)$  of 1000 fb to illustrate the cut efficiencies for the signal process. The significance,  $S/\sqrt{B}$  is calculated for an integrated luminosity of 300 fb<sup>-1</sup>. See [40] for the details of the selection cuts used.

We adopt the same strategy for the light charged Higgs case and refer to [40] for the details of the analysis.

To analyze this channel, we consider the same decay modes for the neutral Higgs as we did for the single top production case:  $\tau_{\text{had}}\tau_{\text{had}}$ ,  $\tau_{\text{had}}\tau_{\text{lep}}$ ,  $\tau_{\text{lep}}\tau_{\text{lep}}$ , along with the additional mode  $A \rightarrow bb$ . We require that one of the two  $W$  bosons from the decays of the charged Higgses decay leptonically, and the other hadronically, to strike a balance between reducing backgrounds and keeping a substantial production cross section.

The dominant SM background for the  $\tau\tau$  channel is top pair production with semi and fully leptonic decay chains. We also take into account  $t\bar{t}ll$  production with  $l = (e, \mu, \tau)$ , as well as  $WW$  and  $WW\tau\tau$ . We ignored the subdominant backgrounds from single vector boson production,  $WW$ ,  $ZZ$ , single top production, as well as multijet QCD background. Those backgrounds are either small or can be sufficiently suppressed by the cuts imposed. Similar backgrounds are considered for the  $bb$  process.

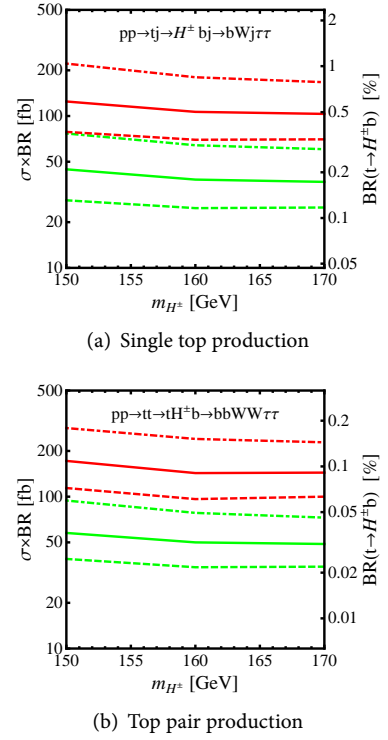
In table 4.2, we show a representative cut flow table for a signal benchmark point with  $m_{H^\pm} = 160$  GeV and  $m_A = 70$  GeV and the decay  $A \rightarrow \tau\tau$  at the 14 TeV LHC, similar to table 4.1. We have chosen a nominal value for  $\sigma \times \text{BR}(pp \rightarrow tt \rightarrow H^\pm tb \rightarrow \tau\tau bb WW)$  of 1000 fb to illustrate the cut efficiencies for the signal process.

After the cuts, the dominant background contributions are  $t\bar{t}$  ( $\tau_{\text{had}}\tau_{\text{had}}$ ,  $\tau_{\text{lep}}\tau_{\text{lep}}$ ) as well as  $t\bar{t}ll$  ( $\tau_{\text{had}}\tau_{\text{lep}}$ ) while the backgrounds including vector bosons do not contribute much. Similar to the single top case, we find that the  $\tau_{\text{lep}}\tau_{\text{had}}$  case gives the best reach.

#### Model-independent limits

Figure 4.8 displays the exclusion (green) and discovery (red) limits at the 14 TeV LHC for the single top production and top pair channels,

Figure 4.8: Exclusion and discovery limits on  $\sigma \times \text{BR}(t \rightarrow H^\pm b)$



The upper panel represents the single top channel and the lower panel represents the top pair production channel. The left vertical axis represents the limit on the quantity  $\sigma \times \text{BR}$ , while the right vertical axis represents the corresponding limits on the branching ratio of the top quark to the charged Higgs boson.

assuming  $\text{BR}(H^\pm \rightarrow AW^\pm) = 100\%$  and  $\text{BR}(A \rightarrow \tau\tau) = 8.6\%$ , and a systematic error of 10%. The dot-dashed, solid and dashed lines show the results for integrated luminosities of 100, 300, and  $1000 \text{ fb}^{-1}$  respectively. The left vertical axis shows limits on  $\sigma \times \text{BR}$ , and the right vertical axis shows the corresponding limits on  $\text{BR}(t \rightarrow H^\pm b)$ . In these plots we have combined all three cases of  $\tau$  decays. While in the single top channel, cases A, B, and C contribute roughly the same to the overall significance, the sensitivity achieved in case B is substantially greater than in cases A and B in the top pair production channel. Due to the small number of events in both channels, the statistical error dominates over the systematic error in the background cross sections. Therefore, higher luminosities lead to better reaches. Assuming  $300 \text{ fb}^{-1}$  of integrated luminosity, the exclusion limits on  $\sigma \times \text{BR}$  are about 35 and 55 fb for the single top and top pair production processes respectively. The discovery reaches are about three times higher.

Assuming that the branching fraction  $\text{BR}(H^\pm \rightarrow AW)$  is 100% and  $\text{BR}(A \rightarrow \tau\tau) = 8.6\%^7$ , we can reinterpret the limits on  $\sigma \times \text{BR}$  as limits on the branching fraction  $\text{BR}(t \rightarrow H^\pm b)$  as indicated by the vertical axes on the right. While the cross section limits are better in the single top channel, the corresponding limits on the branching fraction  $\text{BR}(t \rightarrow H^\pm b)$  are weaker due to the smaller single top production cross section. The achievable upper limit on  $\text{BR}(t \rightarrow H^\pm b)$  is about 0.2% for the single top process and 0.03% for the top pair production process, respectively.

A study of the  $A \rightarrow bb$  decay using the top pair production channel leads to worse results due to the significantly higher SM backgrounds. For the 14 TeV LHC with  $300 \text{ fb}^{-1}$ , the exclusion limit on  $\sigma \times \text{BR}$  is about 7 pb for a charged Higgs with a mass of 160 GeV, assuming the existence of a light neutral Higgs with a mass of 70 GeV. Thus, given the typical ratio of  $\text{BR}(A/H \rightarrow bb) : \text{Br}(A/H \rightarrow \tau\tau) \sim 3m_b^2/m_\tau^2$ , we conclude that the reach in the  $bb$  case is much worse than that of the  $\tau\tau$  case.

We reiterate here that the limits on  $\sigma \times \text{BR}$  are completely model independent. Whether or not discovery/exclusion is actually feasible in this channel should be answered within the context of a particular model, in which the theoretically predicted cross sections and branching fractions can be compared with the model-independent limits. We will do this in [section 4.4](#) for a Type II 2HDM.

#### 4.4 IMPLICATIONS FOR THE TYPE II 2HDM

Two-Higgs Doublet Models allow us to interpret the observed Higgs signal either as the lighter CP-even Higgs ( $h_{-126}$ ) or the heavier CP-even Higgs ( $H_{-126}$ ). The authors of [50] have identified the parameter space of Type II 2HDMs that survives all the existing experimental and theoretical constraints in both of these cases, assuming  $m_{12}^2 = 0$ . In the  $h_{-126}$  case, we are restricted to either a SM-like region at  $s_{\beta-\alpha} = \pm 1$  with  $t_\beta < 4$  or an extended region with  $0.6 < s_{\beta-\alpha} < 0.9$  and  $1.5 < t_\beta < 4$  with relatively unconstrained masses. In the  $H_{-126}$  case, a SM-like region

<sup>7</sup>Assuming  $bb$  and  $\tau\tau$  are the dominant decay modes of a light  $A$ ,  $\text{BR}(A \rightarrow \tau\tau) = 8.6\%$  in a Type II 2HDM or the MSSM at medium to large  $t_\beta$ . This branching fraction decreases for small  $t_\beta$  when the  $cs$ -channel is enhanced.

Masses (GeV)	Kinematically allowed?		Favored Region
	$H^\pm \rightarrow AW$	$H^\pm \rightarrow hW$	
{ $m_{H^\pm}, m_A, m_h, m_H$ }			
BP1: {160, 70, 126, 700}	Yes	No	$s_{\beta-\alpha} \approx \pm 1$
BP2: {160, 700, 70, 126}	No	Yes	$s_{\beta-\alpha} \approx 0$

around  $s_{\beta-\alpha} = 0$  and  $t_\beta < 8$ , and an extended region with  $-0.8 < s_{\beta-\alpha} < 0.05$  and  $t_\beta$  up to 30 or higher, survive all constraints.

We can interpret the results of the previous section in two ways: the light neutral Higgs that the charged Higgs decays to could either be either CP-even Higgs  $h$  or the CP-odd Higgs  $A$ . The decay mode  $H^\pm \rightarrow HW$  is not possible given that  $m_H \geq 126$  GeV. The decay  $H^\pm \rightarrow AW$  is possible in both the  $h$ -126 and  $H$ -126 case and the partial decay width is independent of  $s_{\beta-\alpha}$ . However, the branching fraction depends on whether  $H^\pm \rightarrow hW$  is open or not. For simplicity, we choose a benchmark point BP1, with  $\{m_{H^\pm}, m_A, m_h, m_H\} = \{160, 70, 126, 700\}$  such that only the decay mode  $H^\pm \rightarrow AW$  is kinematically accessible. The decay width  $H^\pm \rightarrow hW$  depends on  $s_{\beta-\alpha}$  and is only sizable in the  $h$ -126 case. We illustrate this case with a second benchmark point, BP2:  $\{m_{H^\pm}, m_A, m_h, m_H\} = \{160, 700, 70, 126\}$ , assuming that the CP-odd Higgs  $A$  decouples. We list the benchmark points in table 4.4.

In figure 4.9, we show the branching fraction  $\text{BR}(H^\pm \rightarrow AW)$  for BP1, which is independent of  $s_{\beta-\alpha}$  and decreases with increasing  $t_\beta$  due to the enhancement of the  $\tau\nu$  mode. The branching fraction can reach values of 90% or larger for small  $t_\beta < 4$  and stays the dominant channel until  $t_\beta = 12$ .

Figure 4.10 shows the branching fraction,  $\text{BR}(H^\pm \rightarrow hW)$ , for BP2. It reaches maximal values around  $s_{\beta-\alpha} = 0$  and decreases for larger  $|s_{\beta-\alpha}|$  compared to BP1 due to the suppressed  $H^\pm hW$  coupling.

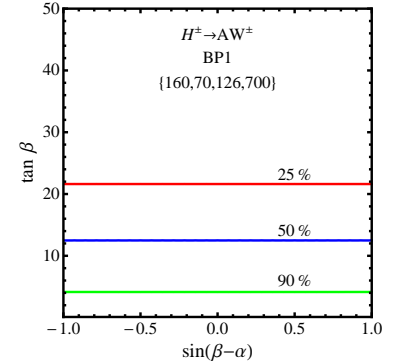
In figure 4.11, we display the regions that can be excluded (yellow regions enclosed by the solid lines as well as the cyan regions) and discovered (cyan regions enclosed by the dashed lines) for BP1 (left panel) and BP2 (right panel) at the 14 TeV LHC with  $300 \text{ fb}^{-1}$  integrated luminosity. The red lines represent the limits from the top pair production channel, and the blue lines represent the limits from the single top production channel.

For the benchmark point BP1 with  $H^\pm \rightarrow AW^\pm$ , the exclusion reach based on top pair production covers the entire parameter space, while discovery is possible for small  $t_\beta < 6$  and large  $t_\beta > 18$ , independent of  $s_{\beta-\alpha}$ . Intermediate values of  $t_\beta$  have a reduced branching fraction  $\text{BR}(t \rightarrow H^\pm b)$  (see figure 4.1) and therefore the total  $\sigma \times \text{BR}$  is suppressed. At high  $t_\beta$ ,  $\text{BR}(t \rightarrow H^\pm b)$  is enhanced enough to overcome the reduced branching fraction  $\text{BR}(H^\pm \rightarrow AW)$ . The search based on single top production is only effective in the small  $t_\beta$  region, with an exclusion reach of  $t_\beta < 4$  and a discovery reach of  $t_\beta < 2$ .

The right panel of figure 4.11 shows the reach for BP2. The exclusion

Table 4.3: Benchmark points used for illustrating the discovery and exclusion limits in the context of the Type II 2HDM. Also shown are the typical favored regions of  $s_{\beta-\alpha}$  for each case (see [50]).

Figure 4.9: Contours of branching fractions for the benchmark point BP1.



The branching fraction is independent of  $s_{\beta-\alpha}$ , and is dominated by the  $\tau\nu$  mode at high values of  $t_\beta$ . For small  $t_\beta$  less than 12, it is the dominant channel, reaching values of 90% or larger for  $t_\beta < 4$ .

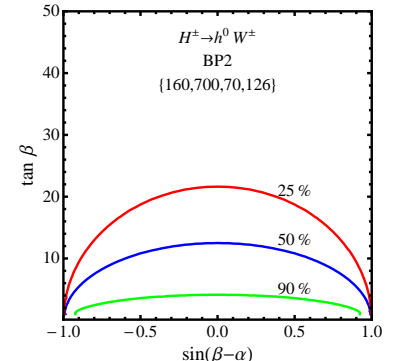


Figure 4.10: Contours of branching fractions  $\text{BR}(H^\pm \rightarrow hW^\pm)$  for the benchmark point BP2.

This branching fraction reaches its maximum at  $s_{\beta-\alpha}=0$ , since larger values of  $|s_{\beta-\alpha}|$  lead to the suppression of the  $H^\pm hW^\pm$  coupling.

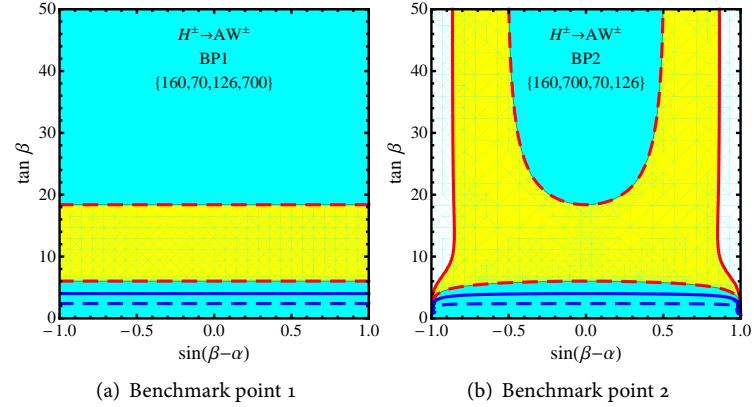


Figure 4.11: The exclusion (yellow and cyan regions combined, bounded by dashed lines) and discovery (cyan region only bound by solid lines) reach achievable in the  $t_\beta$  versus  $\sin(\beta-\alpha)$  plane for the benchmark points 1 and 2, with an integrated luminosity of  $300 \text{ fb}^{-1}$  at the 14 TeV LHC. The red lines represent the reach achievable by the top pair production channel, while the blue lines represent the reach achievable by the single top channel.

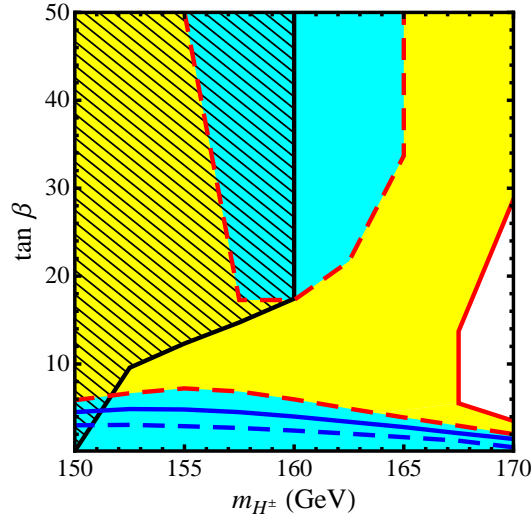


Figure 4.12: Exclusion (yellow regions bounded by solid lines as well as the cyan regions) and discovery (cyan regions bounded by the dashed lines) imposed by the  $tj$ -channel (blue) and  $tt$ -channel (red) in the  $m_{H^\pm} - t_\beta$  parameter space for  $300 \text{ fb}^{-1}$  luminosity with  $m_A = 70 \text{ GeV}$ . The same limits apply for  $m_h = 70 \text{ GeV}$  and  $s_{\beta-\alpha} = 0$  if  $A$  is decoupled. The black hatched region indicates the region excluded by the CMS search based on  $H^\pm \rightarrow \tau\nu$  [33].

region for top pair production covers the entire parameter space except for  $|s_{\beta-\alpha}| > 0.85$  and  $t_\beta > 4$ . Discovery is possible for large  $t_\beta > 18$  with  $|s_{\beta-\alpha}| < 0.5$  and for small  $t_\beta < 6$ . The reach for single top production is limited to the small  $t_\beta$  region.

In figure 4.12, we show the reach in the  $m_{H^\pm} - t_\beta$  plane for  $H^\pm \rightarrow AW$  with  $m_A = 70 \text{ GeV}$  with decays of  $H^\pm$  to both  $h$  and  $H$  kinematically disallowed. These limits also apply for  $H^\pm \rightarrow hW$  with  $m_h = 70 \text{ GeV}$  and  $s_{\beta-\alpha} = 0$  with a decoupled  $A$ . We display the exclusion (yellow regions enclosed by the solid lines as well as the cyan regions) and discovery limits (cyan regions enclosed by the dashed lines) for an integrated luminosity of  $300 \text{ fb}^{-1}$  at the 14 TeV LHC. Superimposed are the current CMS limits (black hatched region) [33] which exclude the large  $t_\beta$  region

at  $m_{H^\pm} < 160$  GeV.

The best reach is obtained by the top pair channel, as indicated by regions enclosed by the red lines. Charged Higgs masses can be excluded up to 167 GeV for all  $t_\beta$  and up to 170 GeV for  $t_\beta < 4$  or  $t_\beta > 29$ . Discovery is possible for both low  $t_\beta < 6$  with  $m_{H^\pm}$  between 150 and 170 GeV and high  $t_\beta > 17$  with  $m_{H^\pm}$  between 155 and 165 GeV. The reach is weakened for intermediate  $t_\beta$  due to the reduced branching fraction  $\text{BR}(t \rightarrow H^\pm b)$ . The single top channel (blue lines) only provides sensitivity in the low  $t_\beta$  region and permits exclusion for  $t_\beta \lesssim 4$  and discovery for  $t_\beta < 3$ .

We conclude this section with the following observations:

- Both the  $H^\pm \rightarrow AW$  channel for the  $h\text{-126}$  case and the  $H^\pm \rightarrow hW$  channel in the  $H\text{-126}$  case permit exclusion and discovery in large regions of the parameter space.
- While the top pair production channel covers a large region of parameter space, the single top channel permits discovery/exclusion in the low  $t_\beta$  region.

#### 4.5 CONCLUSION

After the discovery of the first fundamental scalar by both the ATLAS and CMS collaboration, it is now time to carefully measure its properties to determine the nature of this particle. Current measurements still permit the possibility that the discovered signal is not the SM Higgs particle, but just one scalar particle contained in a larger Higgs sector, as predicted by many extensions of the SM.

In this chapter we consider the prospects of discovering a charged Higgs lighter than the top quark, produced via top decay  $t \rightarrow H^\pm b$ . Due to the large single top and top pair production cross sections at the LHC, such a charged Higgs can be produced copiously. Assuming that the light charged Higgs predominantly decays into  $\tau\nu$ , both ATLAS and CMS exclude a light charged Higgs for most regions of the MSSM and Type II 2HDM parameter spaces. The branching fraction  $\text{BR}(H^\pm \rightarrow \tau\nu)$  can be significantly reduced once the exotic decay channel into a light Higgs,  $H^\pm \rightarrow AW/HW$ , is open. In this case, the exclusion bounds from the  $\tau\nu$  search get weakened, in particular for small and intermediate  $t_\beta$ , leaving the possibility of a light charged Higgs open. This loophole, however, can be closed when we consider the alternative charged Higgs decay channel:  $H^\pm \rightarrow AW/HW$ .

Our analysis examines the decay mode  $H^\pm \rightarrow AW/HW$  decay mode assuming that the lighter Higgs  $A/H$  decays into either  $\tau\tau$  or  $bb$ . While the top pair channel benefits from a large production cross section, the single top channel permits a cleaner signal due to its unique kinematic features. Assuming the existence of a light neutral Higgs of mass 70 GeV, the model independent exclusion limits on  $\sigma \times \text{BR}$  based on the  $\tau\tau$  channel are about 35 fb for the single top channel and 55 fb for the top pair channel. The discovery reaches are about three times higher.

Assuming  $\text{BR}(H^\pm \rightarrow AW/HW) = 100\%$  and  $\text{BR}(A/H \rightarrow \tau\tau) = 8.6\%$ , the exclusion limits on  $\text{BR}(t \rightarrow H^+ b)$  are about 0.2% and 0.03% for single top and top pair production, respectively. A significantly worse reach is obtained in the  $bb$  channel.

We discuss the implications of the obtained exclusion and discovery bounds in the context of the Type II 2HDM, focusing on two scenarios: the decay  $H^\pm \rightarrow AW$  with a light  $A$  in the  $h$ -126 case and the decay  $H^\pm \rightarrow hW$  in the  $H$ -126 case. The top pair channel provides the best reach and permits discovery for both large  $t_\beta > 17$  around  $m_{H^\pm} = 160$  GeV and small  $t_\beta < 6$  over the entire mass range, while exclusion is possible in the entire  $t_\beta$  versus  $m_{H^\pm}$  plane except for charged Higgs masses close to the top threshold. The single top channel is sensitive in the low  $t_\beta$  region and permits discovery for  $t_\beta < 3$ . In particular, the low  $t_\beta$  region is not constrained by searches in  $\tau\nu$  channel, making  $H^\pm \rightarrow AW/hW$  a complementary channel for charged Higgs searches.

While most of the searches for additional Higgs bosons have focused on conventional decay channels, searches using exotic decay channels have started to garner additional interest [37–48]. Studying all of the possibilities for the non-SM Higgs decays will allow us to exploit the full potential of the LHC and future colliders to improve our understanding of the nature of electroweak symmetry breaking.

*Acknowledgments.* We would like to thank Baradhwaj Coleppa for his participation at the beginning of this project. We would also like to thank Peter Loch and Matthew Leone for helpful discussions. This work was supported in part by the Department of Energy under Grant DE-FG02-13ER41976.

# 5

## EXOTIC HIGGS DECAYS AT 14 AND 100 TEV

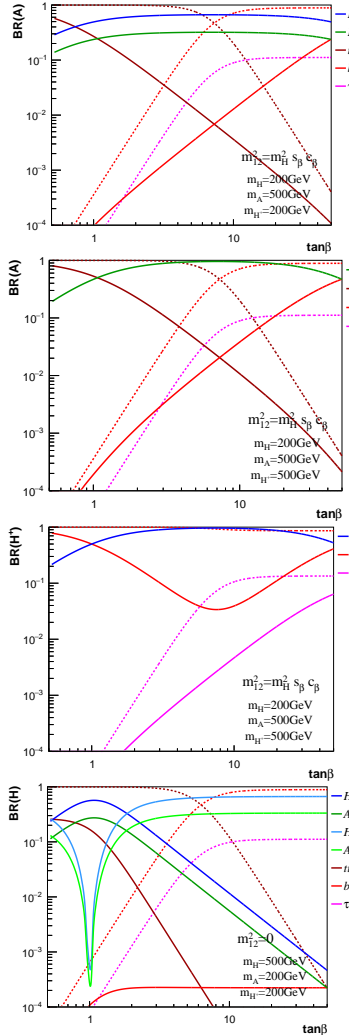
In chapter 4, we showed how exotic decay modes can offer an complementary avenue for discovering charged Higgs bosons at the LHC. While that analysis was performed for a single BSM Higgs and a single exotic decay mode, the project that forms the basis of this project aims to do something much more ambitious, namely, to perform a comprehensive set of collider analyses for all the exotic decay modes for heavy Higgses in Type II 2HDMs, both at the 14 TeV LHC, as well as a future 100 TeV hadron collider. The structure of this chapter is as follows. In section 5.1, we present the general case for considering large mass splittings among heavy higgses, thus motivating the consideration of exotic Higgs decay channels. We also briefly mention the physics potential of a future 100 TeV collider and provide references. In section 5.2, we summarize the most general decay modes for exotic Higgs, followed by a collection of benchmark planes corresponding to a set of exotic decay modes that satisfy theoretical and experimental constraints. In section 5.3, we enumerate some of the existing studies in the literature on exotic decays. In section 5.4, we describe the exotic decay modes we have studied so far, and the strategy we used to do so. In section 5.5, we present some of the preliminary results we have obtained. Finally, we conclude in section 5.6 with a summary and discussion of future work.

### 5.1 SETTING THE STAGE

As pointed out in chapter 4, most experimental analyses aimed at discovering BSM Higgses focus on conventional decay modes to Standard Model Particles. The reason for this is that most studies assume the *decoupling limit*, where the states  $H, A, H^\pm$  are much heavier than  $h$ . Decoupling implies the phenomenon of *alignment*, that is, the field  $h$  is the SM Higgs boson, or equivalently, the angles  $\beta$  and  $\alpha$  satisfy the condition  $\beta - \alpha = \pi/2$  [74]. The limit of decoupling with alignment is an attractive one, since it implies that the undiscovered Higgses are all much heavier than the SM Higgs, thus accounting for why they have not been found yet. However, in the decoupling limit, the splitting between the squared masses of heavy Higgses is constrained to be small, on the order of  $\sim O(v^2)$ , by the following conditions [75]:

- The quartic scalar self-couplings must be sufficiently small to maintain perturbativity.
- The S-matrix for tree-level scattering processes involving scalars must be unitary.
- The scalar potential  $V(\Phi_1, \Phi_2)$  must be bounded from below.

This constraint on the size of the mass splittings implies that decays of heavy Higgses into final states that contain other heavy Higgses will be kinematically disfavored, and thus they will dominantly decay to final states with SM particles.



The relation between decoupling and alignment is not bidirectional, though - alignment does not necessarily imply decoupling. In the limit of alignment without decoupling, it is possible to have sizable mass splittings between the heavy Higgses. While this scenario is necessarily less generic than the decoupling limit, it is well worth considering, especially given that large mass splittings are consistent with a strongly first order electroweak phase transition [42]. This type of phase transition is necessary for the mechanism of electroweak baryogenesis, which can explain the observed level of baryon asymmetry in the universe. It is also possible to generate such mass splittings away from the alignment limit. While this scenario is experimentally disfavored [76], it has not been excluded, and so we study it for completeness.

The presence of large mass splittings opens up the possibility that the heavy Higgses could decay into final states containing other heavy Higgses, that is, they could decay via exotic decay channels. As mentioned when we studied the exotic decay mode  $H^\pm AW^\pm$  in chapter 4, in certain regions of parameter space, once the exotic decay modes are allowed, they will dominate the conventional decay modes. This is illustrated in figure 5.1 for a few scenarios. The first two panels from the top show the branching fractions for the decays of  $A$ , with  $m_{12}^2 = m_H^2 s_\beta c_\beta$ . The next two panels show similar plots, this time for the branching fractions of  $H^\pm$ , with  $m_{12}^2$  equal to  $m_H^2 s_\beta c_\beta$  and 0 respectively. The dashed lines indicate the branching fractions to SM particles in the absence of the exotic decay modes. These channels have begun to garner additional interest in recent years, with the publication of a number of original studies on the topic [3, 38, 40–42, 77–84].

A 100 TeV collider would open up an immense number of physics opportunities not afforded to a 14 TeV collider [85]. Such a collider would be a natural next step after the LHC, and is being actively discussed in the particle physics community, with two major proposals being the FCC-hh by CERN [86], and the SppC by IHEP in China [87]. Executing a project of this size requires an immense amount of planning, over many years. Now is an opportune time to begin to fully explore the physics potential of a 100 TeV collider. There have been a number of studies conducted already, and more are coming out in the literature on a regular basis. We will not attempt to enumerate them all, and instead point the interested reader to the references sections of the review papers [74, 85, 88, 89].

## 5.2 CLASSIFYING EXOTIC DECAYS

Taking all the possible combinations of parent and daughter Higgses yields the complete list of exotic decay modes in 2HDMs, shown along with the dominant SM final states in table 5.1.

Given the large number of degrees of freedom in generic 2HDMs, it is important for us to whittle down the number of possible scenarios to a more manageable number by imposing some kinds of constraints.

Figure 5.1: Branching fractions for exotic decays in Type II 2HDMs, as a function of  $t_\beta$ , with  $c_{\beta-\alpha} = 0$ . Source: [4].

Table 5.1: Summary of all the possible exotic decay modes and the dominant final states for non-SM Higgs bosons

Parent Higgs	Decay type	Channels in 2HDM	Main Final States
Neutral Higgs $H, A$	$HH$	$H \rightarrow AA, hh$	$(bb/\tau\tau/WW/ZZ/\gamma\gamma)(bb/\tau\tau/WW/ZZ/\gamma\gamma)$
	$HZ$	$H \rightarrow AZ, A \rightarrow HZ, hZ$	$(ll/qq/vv)(bb/\tau\tau/WW/ZZ/\gamma\gamma)$
	$H^+ H^-$	$H \rightarrow H^+ H^-$	$(tb/\tau\nu/cs)(tb/\tau\nu/cs)$
	$H^\pm W^\mp$	$H/A \rightarrow H^\pm W^\mp$	$(lv/qq')(tb/\tau\nu/cs)$
Charged Higgs	$HW^\pm$	$H^\pm \rightarrow hW^\pm/HW^\pm/AW^\pm$	$(lv/qq')(bb/\tau\tau/WW/ZZ/\gamma\gamma)$

Here, we do not experimental and theoretical constraints into account. In the second column,  $H$  refers to any of the neutral Higgs bosons  $h, H$ , and  $A$ . Source: [74].

Name	Plane	Decays	$m_{12}^2$
IA	$m_A > m_H = m_{H^\pm}$	$A \rightarrow H^\pm W^\mp$	$m_H^2 s_\beta c_\beta$
		$A \rightarrow HZ$	0
IB	$m_A < m_H = m_{H^\pm}$	$H \rightarrow AZ/AA$	0
		$H^\pm \rightarrow AW^\pm$	
IIA	$m_H > m_A = m_{H^\pm}$	$H \rightarrow AZ/AA$	0
		$H \rightarrow H^+ H^- / H^\pm W^\pm$	
IIB	$m_H < m_A = m_{H^\pm}$	$A \rightarrow HZ$	$m_H^2 s_\beta c_\beta$
		$H^\pm \rightarrow HW^\pm$	0
III	$m_A = m_H = m_{H^\pm}$ vs $c_{\beta-\alpha}$	$A \rightarrow hZ, H^\pm \rightarrow hW^\pm$	$m_H^2 s_\beta c_\beta$
		$H \rightarrow hh$	0

Table 5.2: Summary of benchmark planes for exploring exotic Higgs decays in 2HDMs that survive theoretical and experimental constraints. Source: [4].

The authors of [4] have systematically categorized the scenarios (with differing mass orderings, splittings, values of the parameter  $m_{12}$ , and degrees of deviation from alignment) that are still viable after imposing all the relevant theoretical and experimental constraints. Based on this categorization, they have presented a number of benchmark planes to guide searches for new scalars at the LHC via exotic decay modes. These planes are summarized in table 5.2.

Even after this constraining, there remain a plethora of possible final states, as evidenced by the last column of table 5.1. In this work, we aim to answer the questions: which among these final states are the most promising to find new physics, and what are the best strategies to do so at a collider? In the next section, we outline some of the details of our approach.

### 5.3 LITERATURE REVIEW

There are a number of theoretical studies in the literature that examine exotic Higgs decays. We summarize some of the more recent ones. In [79], the exotic decay a heavy neutral Higgs,  $A \rightarrow HZ/H \rightarrow AZ$  is studied. The same authors subsequently study the exotic decay of a heavy charged Higgs:  $H^\pm \rightarrow (A/H)W^\pm$ . The prospects of finding a charged Higgs boson lighter than the top quark are examined in [3]

(which forms the basis of chapter 4). The study in [41] examines the exotic decay of a neutral heavy Higgs:  $A/H \rightarrow W^\pm H^\mp$ . All of these studies are performed for the 14 TeV LHC. Constraints are derived in the  $m_{H^\pm} - t_\beta$  plane for the decay chain  $H \rightarrow H^\pm W^\pm \rightarrow W^+ W^- A$  in [82], while the authors of [81] examine heavy charged Higgses produced in association with a  $W$  boson and decaying into a lighter neutral Higgs. In [80] the signals for a fermiophobic charged Higgs arising in a 2HDM with right handed neutrinos are examined. Finally, the whitepaper [38] investigates the prospects of discovering a heavy neutral Higgs through the decay  $A/H \rightarrow ZZ/Zh$ , with the  $Z$  decaying leptonically, and the  $h$  decaying to either the  $bb$  or  $\tau\tau$  final states.

#### 5.4 CRAFTING FEATURES FOR OUR CLASSIFIER

Preliminary analyses have been carried out for two of the benchmark planes described in table 5.2: benchmark plane IB, with  $m_A < m_H = m_{H^\pm}$ , and benchmark plane IIB,  $m_H < m_A = m_{H^\pm}$ , both assuming  $m_{12}^2 = m_H^2 s_\beta c_\beta$ . For benchmark plane IB, we examine the production and decay chains for the neutral Higgs  $H$ :

$$\begin{aligned} bb &\rightarrow H \rightarrow AZ \rightarrow \tau\tau ll, \\ gg &\rightarrow H \rightarrow AZ \rightarrow \tau\tau ll. \end{aligned}$$

For benchmark plane IIB, we consider the following production and decay chains for the neutral Higgs  $A$ :

$$\begin{aligned} bb &\rightarrow A \rightarrow HZ \rightarrow \tau\tau ll, \\ gg &\rightarrow A \rightarrow HZ \rightarrow \tau\tau ll. \end{aligned}$$

In addition, we examine the following production and decay chain for a heavy charged Higgs  $H^\pm$  in benchmark plane IIB:

$$pp \rightarrow tbH^\pm \rightarrow (Wb)b(HW) \rightarrow (Wb)b((\tau\tau)W),$$

where one of the  $W$  bosons decays leptonically, and the other hadronically. This production and decay chain has been previously considered in [79]. Recognizing the power of statistical learning techniques to efficiently find non-linear decision boundaries in feature space, we use boosted decision tree classifiers to discriminate between signal and background events. For each channel, we provide the classifier with a mixture of low-level and high-level features. Low-level features include readily available information such as the momenta of the final state particles, whereas high-level features are functions of the low-level features designed to exploit kinematic relations unique to each decay topology. In practice, using high and low level features in conjunction with each other yields better results than using either of them alone.

#### *Exotic decays of neutral Higgses A/H*

For the exotic decay modes  $(A/H) \rightarrow (H/A)Z$  with the final state  $\tau\tau ll$ , the following strategy was taken to prepare feature arrays for the boosted

decision tree classifier. We consider two possibilities for the decay of the  $Z$  boson:  $Z \rightarrow bb$  (case A), and  $Z \rightarrow l^+l^-$  (case B).

1. *Trigger.* We selected events that passed one of the following trigger criteria:
  - a) At least one lepton with  $p_T > 30$  GeV.
  - b) Two leptons, with the hardest lepton having  $p_T > 20$  GeV and the second hardest lepton having  $p_T > 10$  GeV.
  - c) A minimum missing energy of 100 GeV.
2. *Identification.* We required events have at least two  $b$ -tagged jets (case A), or at least one pair of oppositely charged  $\tau$ -tagged jets (case B). For both cases, we require exactly two leptons (electrons or muons) with the same flavor and opposite sign.
3. *Calculate and collect features.* For events that pass the trigger and identification criteria above, we construct the following set of features:
  - a)  $Z$  candidate. We combine the momenta of the two same flavor, opposite sign leptons to form the  $Z$  candidate, and calculate its invariant mass,  $m_{ll}$ .
  - b) Lighter neutral Higgs candidate. We combine the momenta of the two leading  $b$ -tagged jets (case A) or the two  $\tau$ -tagged jets (case B) to form the lighter neutral Higgs candidate, and calculate its invariant mass, denoted either  $m_{bb}$  or  $m_{ll}$ .
  - c) Heavier (parent) neutral Higgs candidate. We combine the momenta of the  $Z$  candidate and the  $A/H$  candidate to form the charged Higgs candidate  $H^\pm$ , and calculate its invariant mass, denoted  $m_{llbb}$  (case A) or  $m_{ll\tau\tau}$  (case B).
  - d) We also collect the following set of features: the transverse momenta of the leptons, and  $b$ -tagged jets (case A), or the  $\tau$ -tagged jets (case B). Finally, we collect the missing and hadronic transverse energies of the event.

#### *Exotic decays of the charged Higgs $H^\pm$*

The search channel involving the charged Higgs, has the production and decay chain:

$$pp \rightarrow tbH^+ \rightarrow (Wb)b(HW) \rightarrow l\nu bb\tau_h\tau_l jj,$$

Here, one of the  $W$ 's and one of the  $\tau$ s decays hadronically, and the other decays leptonically. We employed the following strategy to construct input features for our classifier.

1. *Identification.* We required events have exactly one or two  $b$ -tagged jets, at least two untagged jets, exactly one  $\tau$ -tagged jet, and exactly two leptons (electrons or muons) with the same charge which is opposite to that of the  $\tau$ -tagged jet.
2. *Calculate and collect features.* As a test of the software setup, we analysed this channel with only the following low-level features: the transverse momenta of the leptons, the leading  $b$ -tagged jet,

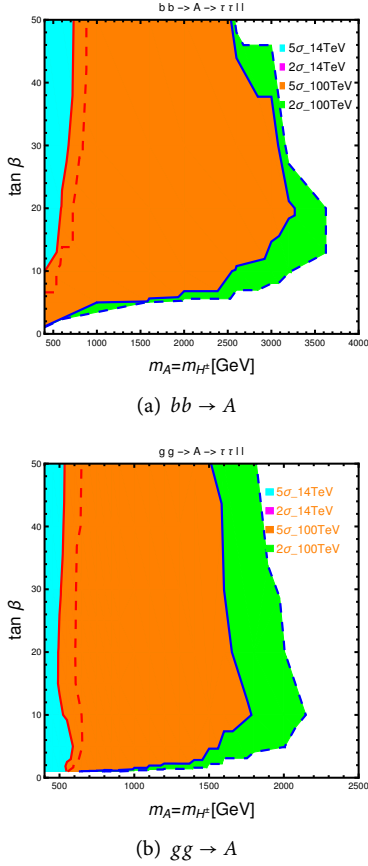


Figure 5.2: Exclusion and discovery limits for the channel  $A \rightarrow HZ \rightarrow \tau\tau ll$ , for the 14 TeV LHC with  $100 \text{ fb}^{-1}$  (solid red line) and  $300 \text{ fb}^{-1}$  (dashed red line) and a 100 TeV collider with  $1000 \text{ fb}^{-1}$  (solid blue line) and  $3000 \text{ fb}^{-1}$  (dashed blue line). Here we assume  $m_{12}^2 = m_H^2 s_\beta c_\beta$ . The top panel represents the  $bb \rightarrow A$  production channel, while the lower one represents the  $gg \rightarrow A$  production channel.

and the untagged jets, and the missing and hadronic transverse energies of the event. In the future, we aim to reconstruct the lighter Higgs  $H$  and the charged Higgs  $H^\pm$ , building upon the strategy in [79], and using the calculated invariant masses as input features for the classifier.

### 5.5 PRELIMINARY RESULTS

In this section, we will present some of the preliminary results of this project. In figure 5.2, we see the reach obtainable in the  $A \rightarrow HZ \rightarrow \tau\tau ll$  channels in the  $m_A = m_{H^\pm} - t_\beta$  plane, with  $m_H = 200 \text{ GeV}$ . The results are shown separately for the  $A$  produced via  $bb \rightarrow A$  (top panel), and  $gg \rightarrow A$  (bottom panel). The  $bb$  production channel has a significantly higher reach, being able to exclude points with  $m_A = m_{H^\pm} + i$  up to 3.5 TeV for  $t_\beta$  between 15 and 20, for a 100 TeV collider (combined green, brown, and cyan regions). The corresponding reach for the  $gg$  production channel is only up to about 2 TeV. In figure 5.3, we see the reach obtainable in the  $H \rightarrow AZ \rightarrow \tau\tau ll$  channels, with  $m_A = 200 \text{ GeV}$ . Similar to the results for  $A \rightarrow HZ$ , the results for the  $bb$  production channel (upper panel) are significantly better than those for the  $gg$  production channel (lower panel). The  $bb$  production channel will be able to exclude points in the  $m_H = m_{H^\pm} - t_\beta$  plane up to 3.5 TeV for a wide range of values of  $t_\beta$  between 10 and 50. The reach for the  $gg$  production channel is seen to be low for intermediate values of  $t_\beta$  of about 20. This plane simply represents the region along the diagonal of benchmark plane IIB - this region was chosen since it survives all the theoretical and experimental constraints. Varying  $\tan \beta$  does not vary the kinematics of the final state particles, just the total  $\sigma \times \text{BR}$ .

For the charged Higgs channel  $H^\pm \rightarrow HW$  described in the previous section, the reach for a 100 TeV collider is shown in figure 5.4, in the  $m_{H^\pm} = m_H$  vs  $m_H$  plane. We see that with the simple set of input features described in section 5.4, we are able to exclude charged Higgses with masses up to 2 TeV for neutral Higgses  $H$  with masses up to 500 GeV. We

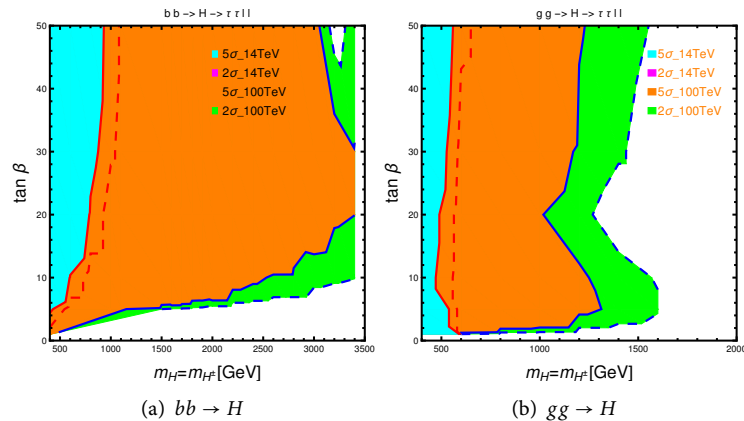


Figure 5.3: Exclusion and discovery limits for the channel  $H \rightarrow AZ \rightarrow \tau\tau ll$  for the 14 TeV LHC with  $100 \text{ fb}^{-1}$  (solid red line) and  $300 \text{ fb}^{-1}$  (dashed red line) and a 100 TeV collider with  $1000 \text{ fb}^{-1}$  (solid blue line) and  $3000 \text{ fb}^{-1}$  (dashed blue line). Here we assume  $m_{12}^2 = m_H^2 s_\beta c_\beta$ . The left panel represents the  $bb \rightarrow H$  production channel, while the right represents the  $gg \rightarrow H$  production channel.

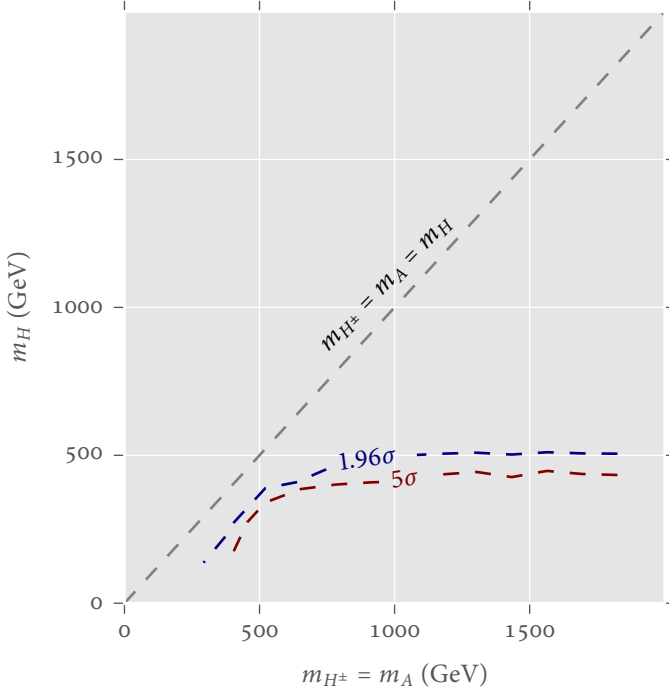


Figure 5.4: Exclusion and discovery reaches in the  $m_{H^\pm} - m_H$  plane for the exotic decay  $H^\pm \rightarrow HW^\pm$ , at a 100 TeV collider with an integrated luminosity of  $3 \text{ ab}^{-1}$ . Here we assume  $m_{12}^2 = m_H^2 s_\beta c_\beta$ .

expect that the addition of high-level features such as invariant masses will substantially improve the results. In all cases, the significance is calculated using the formula  $S/\sqrt{B}$ . For the 14 TeV LHC, we consider an integrated luminosity of  $300 \text{ fb}^{-1}$ , and for a 100 TeV collider, we consider an integrated luminosity of  $3000 \text{ fb}^{-1}$ .

## 5.6 CONCLUSIONS AND OUTLOOK

In this chapter, we have provided some preliminary results from a project aimed at evaluating the prospects of discovering new heavy scalars from 2HDMs at the 14 TeV LHC and a 100 TeV collider, in the physically well-motivated but underexamined scenario where they can have large mass splittings. The approach we take is to examine the resulting ‘exotic’ decay modes of these heavy scalars, since they can dominate over the conventional decay modes, once kinematically allowed. We began by examining two of the benchmark planes suggested in [4]. The first, benchmark plane IB, with  $m_A < m_H = m_{H^\pm}$  was probed using the exotic decay  $H \rightarrow AZ$ , with the subsequent decays  $A \rightarrow \tau\tau, Z \rightarrow ll$ . The second plane, labeled IIB, with  $m_H < m_A = m_{H^\pm}$ , was investigated using the exotic decay modes  $A \rightarrow HZ$  and  $H^\pm \rightarrow HW^\pm$ . For the first mode, we consider the final state  $\tau\tau ll$ , similar to the  $H \rightarrow AZ$  case, while for the second, we consider the more complicated final state  $bbWW\tau\tau$ , where one  $\tau$  and one  $W$  decay hadronically, and the other  $\tau$  and  $W$  decay leptonically. We used boosted decision tree classifiers to separate signal and background events, using a mixture of low-level features and

physically inspired high-level features that are unique to each of the channels. For the benchmark plane IB, we found that we are able to exclude points with  $m_A = m_H^\pm$  up to 3.5 TeV at optimal points in the  $m_A = m_{H^\pm}$  plane, with a fixed  $m_H = 200$  GeV, for a 100 TeV collider. For benchmark plane IIB, we found that the reach is higher - we can discover points with  $m_H = m_{H^\pm}$  up to 3.5 TeV, again for the same mass difference between the parent and daughter Higgs. Preliminary results for the charged Higgs channel  $H^\pm \rightarrow HW^\pm \rightarrow \tau\tau W^\pm$  show an exclusion reach in benchmark plane IIB up to charged Higgs masses of about 2 TeV, for  $m_H$  up to 500 GeV. This region is complementary to the region explored by the channel  $A \rightarrow HZ$  discussed in section 5.4 in the benchmark plane IIB. These preliminary results look promising, and we aim to complete our investigation of all the benchmark planes in the near future. An extended scalar sector arises frequently in theories beyond the Standard Model, and would have important implications for the electroweak phase transition, electroweak baryogenesis, as well as the hierarchy problem. Thus, understanding its structure is vital, and exotic decays provide a complementary avenue to do so.

## 6.1 DARK MATTER

In 1933, the Swiss astronomer Fritz Zwicky turned his telescope to the night sky to measure the velocities of galaxies in a particular galaxy cluster known as the Coma cluster. He discovered that the visible matter in this cluster could not account for the speeds at which the galaxies were moving. He postulated that there must be some matter that does not emit light, but has mass and interacts only gravitationally with known matter. He termed this ‘Dunkle materie’, or *dark matter*. The evidence for dark matter has only continued to grow since then, and we now know that there is far more of it in the universe than there is regular, or *baryonic* matter. The nature of dark matter is one of the most compelling mysteries in physics today.

Over the years, there have been many dark matter candidates, but the most widely accepted view today is that dark matter is comprised of a completely new kind of particle that interacts only weakly with the particles of the Standard Model and moves at non-relativistic speeds.

One of the most tantalizing clues to the nature of dark matter is the so-called ‘WIMP miracle’ - the remarkable coincidence that the observed dark matter density in the universe can arise naturally from a particle with mass and couplings comparable to the weak scale. This raises the hope that such particles might feasibly be detected at colliders or direct detection experiments.

There are three main methods of detecting WIMP dark matter. The first, direct detection, involves constructing a well shielded, giant vat of a relatively inert substance, and waiting for dark matter particles to interact with that substance. The second, termed indirect detection, involves searching for signs of dark matter particles annihilating each other in the cosmos. The third method, collider detection, involves producing dark matter through high energy particle collisions and searching for their associated signatures. The three methods are depicted in figure 6.1, where  $\chi$  and SM represent dark matter and SM states respectively, and the arrows represent the flow of time. The first two methods place relatively stringent constraints on the nature of dark matter, but have their own limitations. The smallest interaction cross-section between dark matter and regular matter that direct detection can measure is limited from below by the background of neutrinos from the sun, though there are creative methods that are being developed to deal with this background. Indirect detection suffers from large astrophysical uncertainties [90]. Collider detection, therefore, is competitive with, and can even possibly surpass the other two methods.

WIMPs arise naturally in many extensions of the SM. Of these extensions, one of the most studied is the Minimal Supersymmetric Standard

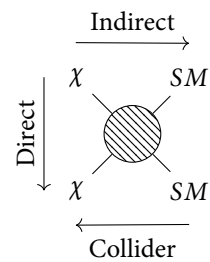


Figure 6.1: DM detection, three ways

Model (MSSM), introduced in [section 2.3](#). In the MSSM, the lightest supersymmetric partner (LSP) is predicted to be absolutely stable, making it a good candidate for dark matter. The identity of the LSP is determined by the mass hierarchy of the superpartners, which in turn depends on how supersymmetry is broken. However, taking into account experimental constraints and phenomenological considerations, the lightest neutralino emerges as the most attractive candidate for the LSP [\[91\]](#).

Though a natural MSSM spectrum has the potential to tame the hierarchy problem, it is under siege from recent data from the LHC. A compelling alternative scenario comes in the form of split supersymmetry [\[92–94\]](#). In this scenario, the lightest superpartners are the fermionic ones (gauginos and higgsinos), on the scale of 1–10 TeV, while the scalar superpartners can be much heavier, on the scale of 100 – 1000 TeV. In exchange for accepting some level of fine-tuning, we obtain numerous benefits, including the suppression of flavor-changing neutral currents and greater compatibility with data from CP-violation experiments [\[92\]](#).

The most interesting regions of the split SUSY parameter space lies beyond the reach of the LHC. Consider, for example the case in which the dark matter candidate is a nearly-pure bino. Even though the simplicity of its gauge singlet structure makes it an attractive DM candidate, It is well known that heavy bino LSPs heavier than about 200 GeV result in an overabundance of dark matter in the universe, in conflict with experimental observations. However, if the bino is nearly mass-degenerate with another supersymmetric particle, such as the gluino, stau, or a squark, it can coannihilate with it (see [figure 6.2](#) for a Feynman diagram depicting the coannihilation with a stau), thereby reducing the dark matter abundance to acceptable levels [\[95\]](#). Coannihilation with a gluino would raise the acceptable bino mass to  $\sim 7$  TeV, and coannihilation with a stop or squark raises the acceptable bino mass to  $\sim 2$  TeV. Bringing one of these particles down to the low-energy spectrum should not affect the branching ratio of the higgsinos too much. Gluino coannihilators would not change the branching ratios of the neutral higgsinos, since they are uncharged under  $SU(3)$ <sup>1</sup>. Higgsino-fermion-sfermion couplings are Yukawa-like, and are proportional to the mass of the fermion in the interaction vertex. Thus, this coupling will be relatively small (with the possible exception of the higgsino-top-stop case). In this study, we will simply assume that a scalar can be brought down into the low-energy spectrum to be nearly mass-degenerate with the bino, thus satisfying the relic density requirement. Such heavy binos are out of the reach of the 14 TeV LHC, but well within the reach of a 100 TeV collider.

This study aims to add to the corpus an assessment of the prospects of finding pair-produced neutral higgsinos that decay to binos via intermediate  $Z$  and  $h$  bosons, at a future 100 TeV collider. Razor variables [\[96\]](#) were originally designed for searches involving two heavy, mass-degenerate pair-produced particles, each of which decays into a visible and invisible set of particles. This topology matches that of our search channel, making this set of variables a natural choice for our analysis.

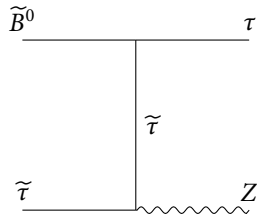


Figure 6.2: Feynman diagram for bino-stau coannihilation.

<sup>1</sup>But doing so would reduce the importance of electroweak search channels in comparison, as gluinos would then be abundantly produced.

Finding higgsinos has traditionally been more challenging than finding winos, due to their lower production rate - it is thus important to devise innovative strategies to do so. In addition, the higgsino mass parameter  $\mu$  that governs the mass of the higgsino plays an important role in electroweak symmetry breaking [97]. This combination of NLSP (next-to-lightest supersymmetric partner) and LSP has been studied earlier in [98] with intermediate vector dibosons and multi-lepton final states. In this study, however, we attempt to exploit the relatively high branching ratio of the SM Higgs boson to  $b$  quarks (as suggested in [99]), and choose the decay modes  $Z \rightarrow ll$  and  $h \rightarrow bb$  for the intermediate  $Z$  and  $h$  bosons in our search channel.

At a 100 TeV collider, the backgrounds are going to be even larger than at the LHC. We will need to harness all the possible tools we can to deal with them. An ancillary goal of this study is to investigate the potential for machine learning (ML) techniques to augment our analysis. with the advent of more powerful computers and simultaneous advances in the field of statistical learning in recent years, the usage of ML is rising in experimental particle physics. In fact, the discovery of the SM Higgs boson in 2012 was done with the help of neural networks [100] and boosted decision trees [101].

The rest of this chapter is structured as follows. In section 6.2, we describe our model and search channel in more detail, and list the existing experimental constraints on it. In section 6.3, we describe our analysis strategies and results obtained for both the traditional cut-and-count analysis and the analysis performed with boosted decision trees. Finally, we conclude with the implications in section 6.4.

## 6.2 MODEL AND EXPERIMENTAL CONSTRAINTS

In this section, we will elaborate a little more on the structure of the neutralino sector in the MSSM (and by extension, split SUSY), motivate our chosen search channel, and review some of the relevant experimental literature and limits.

### *The neutralino sector*

The neutralino sector consists of four mass eigenstates  $(\tilde{\chi}_1^0, \tilde{\chi}_2^0, \tilde{\chi}_3^0, \tilde{\chi}_4^0)$  that are mixtures of the gauge eigenstates  $(\tilde{B}^0, \tilde{W}^0, \tilde{H}_u^0, \tilde{H}_d^0)$  - the bino, the wino, and the two neutral higgsinos, originally encountered in section 2.3. In the basis of these gauge eigenstates, the mass matrix of the neutralino can be written as

$$\mathbf{M}_{\tilde{N}} = \begin{pmatrix} M_1 & 0 & -c_\beta s_W m_Z & s_\beta s_W m_Z \\ 0 & M_2 & c_\beta c_W m_Z & s_\beta c_W m_Z \\ -c_\beta s_W m_Z & c_\beta c_W m_Z & 0 & -\mu \\ s_\beta s_W m_Z & -s_\beta c_W m_Z & -\mu & 0 \end{pmatrix}, \quad \text{Neutralino mass matrix}$$

where  $s_\beta = \sin \beta$ ,  $c_\beta = \cos \beta$ ,  $s_W = \sin \theta_W$ , and  $c_W = \cos \theta_W$ . The angle  $\beta$  is a central parameter of the theory - it parameterizes the mixing between

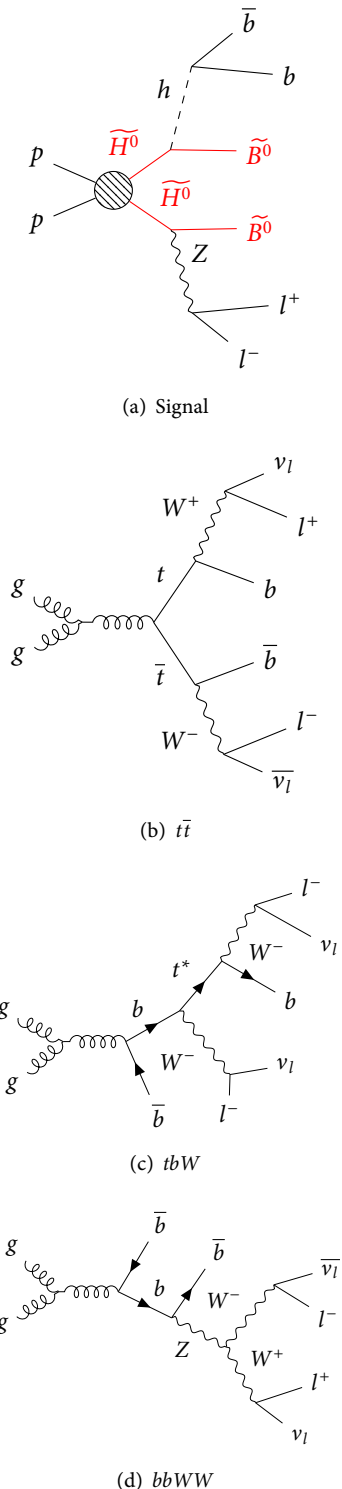


Figure 6.3: Feynman diagrams for the signal and background processes (Generated using [102].)

the two Higgs doublets,  $\tilde{H}_u$  and  $\tilde{H}_d$ . It is defined as  $\tan \beta = v_u/v_d$ , where  $v_u$  and  $v_d$  are the vacuum expectation values of  $H_u^0$  and  $H_d^0$ . The parameters  $M_1$ ,  $M_2$ , and  $\mu$  are the coefficients of bino, wino, and higgsino mass terms in the soft supersymmetry breaking Lagrangian.

This matrix can be diagonalized with the unitary matrix  $\mathbf{N}$  to obtain

$$\mathbf{N}^* \mathbf{M}_{\tilde{N}} \mathbf{N}^{-1} = \begin{pmatrix} m_{\tilde{\chi}_1^0} & 0 & 0 & 0 \\ 0 & m_{\tilde{\chi}_2^0} & 0 & 0 \\ 0 & 0 & m_{\tilde{\chi}_3^0} & 0 \\ 0 & 0 & 0 & m_{\tilde{\chi}_4^0} \end{pmatrix},$$

where  $m_{\tilde{\chi}_i^0}$  are the masses of the neutralino mass eigenstates.

In the limit of  $m_Z \ll |\mu \pm M_1|, |\mu \pm M_2|$ , the mass eigenstates are, to good approximation, a nearly pure bino,  $\tilde{B}^0$ , with mass  $M_1$ , a nearly pure wino,  $\tilde{W}^0$ , with mass  $M_2$ , and nearly pure higgsinos  $\tilde{H}_{1,2}^0 = (\tilde{H}_u^0 \pm \tilde{H}_d^0)/\sqrt{2}$ , with mass  $|\mu|$ . This limit is well-motivated, since we are considering heavy electroweakinos that are out of the reach of the LHC - the minimum mass of the higgsinos considered is 500 GeV, and the wino is decoupled to 5 TeV.

The optimal search strategy for finding electroweakinos is highly dependent on the mass difference between them. Phenomenological collider studies on finding electroweakinos separated by about 0.1 - 50 GeV at a 100 TeV collider can be found in [90, 103–105], while well-separated spectra have been studied in [97, 98].

So far, the well-separated spectra have been studied using multi-lepton channels, of the form

$$pp \rightarrow \tilde{\chi}_{\text{NLSP}} \tilde{\chi}_{\text{LSP}} \rightarrow VV + \tilde{\chi}_{\text{LSP}} \tilde{\chi}_{\text{LSP}} \rightarrow 2l/3l + \cancel{E}_T + \tilde{\chi}_{\text{LSP}} \tilde{\chi}_{\text{LSP}}$$

where  $\tilde{\chi}_{\text{NLSP}}$  can be a neutralino or chargino, and  $\tilde{\chi}_{\text{LSP}}$  is the lightest neutralino. These searches work well since the large mass difference between the electroweakinos can lead to energetic leptons that can be easily identified. Among the multi-lepton searches, the trilepton searches (with  $W$  and  $Z$  as the intermediate dibosons) have the best reach, due to the high production cross-section of chargino-neutralino pairs combined with the large reduction in  $t\bar{t}$  and QCD backgrounds obtained by requiring three leptons. Multilepton searches with  $Zh$  and  $ZZ$  as the intermediate dibosons are unlikely to be as powerful, due to the lower pair-production cross-section of neutral higgsinos, combined with the low branching

Stage	$\tilde{\chi}_{2,3}^0 \tilde{\chi}_2^\pm$	$\tilde{\chi}_2^0 \tilde{\chi}_3^0$
Pair production cross section	60 fb	16 fb
Intermediate diboson contribution	( $WZ$ ) 30 fb	( $Zh$ ) 8 fb
Applying $BR(W \rightarrow l\nu)$ , $BR(Z \rightarrow ll)$ & $BR(h \rightarrow bb)$	0.42 fb	0.32 fb

Table 6.1: Comparison of cross-sections for  $(\tilde{\chi}_{2,3}^0 \tilde{\chi}_2^\pm)$  and  $(\tilde{\chi}_2^0 \tilde{\chi}_3^0)$ , for  $|\mu| \approx 1$  TeV, at a 100 TeV  $pp$  collider. The pair-production cross sections are taken from [98], and the branching ratios are taken to be the same as the SM ones listed in the PDG [62].

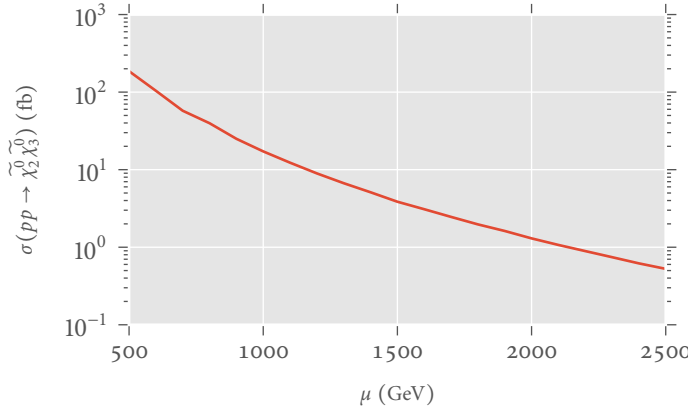


Figure 6.4: Higgsino pair production cross section as a function of  $\mu$ , for a  $M_1 = 25$  GeV.

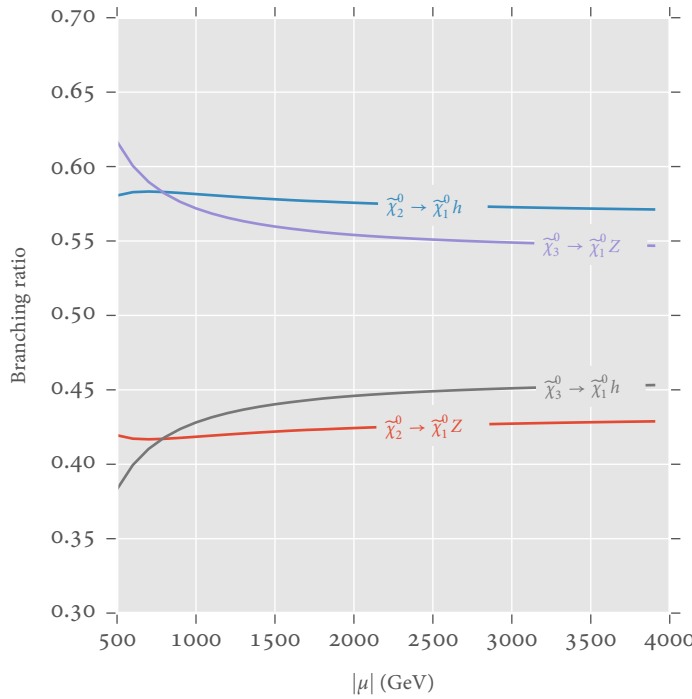


Figure 6.5: Higgsino decay branching ratios of  $\mu$ , for a  $M_1 = 25$  GeV.

ratio of  $Z$  to leptons. However, if we move beyond multilepton searches, the channel with  $Zh$  as the intermediate dibosons emerges as a possible competitor to the  $WZ$  channel. If the  $Z$  decays leptonically and  $h$  decays to a pair of  $bs$ , then after applying the relevant branching ratios, the signal cross sections become comparable (for details, see table 6.1).

In this study, we will focus on a well-separated electroweakino spectrum, with  $M_2 \gg |\mu|, M_1$ , and study the process:

$$pp \rightarrow \tilde{\chi}_2^0 \tilde{\chi}_3^0 \rightarrow (Z\tilde{\chi}_1^0)(h\tilde{\chi}_1^0) \rightarrow ((l^+l^-)\tilde{B}^0)((b\bar{b})\tilde{B}^0),$$

*Our signal process*

which is manifested at colliders as a final state with two  $b$ -jets, two same

flavor, opposite sign leptons, and missing transverse energy. Note that  $\tilde{\chi}_{2,3}$  represents neutral higgsino-like NLSPs, and  $\tilde{\chi}_0$  represents bino-like LSPs. The main backgrounds for this process are:  $t\bar{t}$ ,  $t b W$  with the  $b$  and  $W$  not coming from a  $t$ , and  $bbWW$  with no intermediate  $s$ -channel top quarks. See [figure 6.3](#) for representative Feynman diagrams for the signal and background processes. The typical pair-production cross section for the higgsino-like NLSPs is on the order of less than 10 fb for  $|\mu| > 1$  TeV, as can be seen in [figure 6.4](#).

#### *Couplings and branching ratios*

The mixing of the neutralino gauge eigenstates gives rise to complicated expressions for the couplings involving the mass eigenstates. For consistency, We use SUSY-HIT to calculate the branching ratios  $BR(\tilde{\chi}_{2,3}^0 \rightarrow h\tilde{\chi}_1^0)$ ,  $BR(\tilde{\chi}_{2,3}^0 \rightarrow Z\tilde{\chi}_1^0)$ , and  $BR(h \rightarrow bb)$ . For all our benchmark points, we decouple the neutral wino, setting  $M_2 = 5$  TeV.

#### *Review of experimental searches and limits*

While the majority of the existing searches for supersymmetry focus on gluino pair production, there are a number of analyses involving electroweakino pair production as well, which we will attempt to briefly review here. Searches involving multiple leptons and missing energy ( $2l/3l/4l + \cancel{E}_T$ ) in the final state are described in [\[106–109\]](#), assuming a wino-like NLSP and a bino-like LSP. The best reach is obtained in the  $4l$  channel, with NLSP masses up to 1.14 TeV excluded for LSP masses greater than about 500 GeV. The trilepton channel is a close second-best, with NLSP masses up to 1 TeV excluded for a massless LSP. Both of these results have been calculated with  $13.3 \text{ fb}^{-1}$  of 13 TeV LHC data by ATLAS.

Topologies with one or two hadronically-decaying tau leptons and missing energy in the final state have been studied in [\[110, 111\]](#), with the greatest reach obtained by ATLAS in [\[110\]](#), using 13 TeV data - they are able to exclude wino-like NLSPs up to a mass of 700 GeV for a massless bino-like LSP.

Photon signatures with the final states  $\gamma\gamma/\gamma b/\gamma j/\gamma l/\gamma jj + \cancel{E}_T$  been used to probe gauge mediated supersymmetry breaking models in [\[112–116\]](#). Winos are excluded below 710 GeV for nearly bino-like LSPs that are nearly mass-degenerate with them in [\[116\]](#). The study [\[114\]](#) excludes winos up to a mass of 590 GeV in the final state  $\gamma\gamma + \cancel{E}_T$ . The final state  $\gamma l + \cancel{E}_T$  is used to exclude winos up to 360 GeV in [\[113\]](#).

Searches with a combination of leptons and jets in the final states can be found in [\[117–119\]](#). Winos up to 465 GeV are excluded in the  $2l + 0/2j$  final states in [\[117\]](#). A compressed mass spectrum is studied in [\[118\]](#), with a mass difference of about 50 GeV between winos and binos. This study uses the vector boson fusion channel, with a final state of  $2l + 2j + \cancel{E}_T$ , and excludes winos up to a mass of 170 GeV. Of particular interest to us is the analysis in [\[119\]](#), where higgsinos can be excluded

up to a mass of 380 GeV using the  $bbl + \cancel{E}_T$  final state, but cannot be discovered in any region of the relevant parameter space. As we shall see, a 100 TeV collider will enable us to greatly improve upon these limits.

### 6.3 ANALYSIS DETAILS

In this section, we will describe our strategies for both the traditional cut-and-count analysis, as well as the analysis carried out with boosted decision trees.

#### *Simulation*

We simulated parton-level events using `MadGraph5 v2.3.2.2` and `MadEvent` [22], then passed those events to `Pythia 6` [23] for showering and hadronization. Finally, we used `Delphes 3` [25] to perform a fast, parametrized detector simulation, with the detector card devised by the FCC-hh working group<sup>2</sup>. For the backgrounds, we allowed up to one additional jet in the final state, to approximate NLO QCD effects, and performed MLM matching with the `xqcut` parameter set to 40 GeV. The Higgsino pair production cross sections were calculated using `Prospino2` [120]. To decouple the wino, we set its mass parameter  $M_2$  to 5 TeV.

One of the challenges we faced while performing this analysis was dealing with the sheer number of background events to generate and analyze. At a 100 TeV collider, the background cross-sections grow very large compared to their 14 TeV counterparts. For example, the cross section for the inclusive production of top quark pairs increases from  $\sim 975$  pb (N<sup>3</sup>LO) to  $\sim 34,000$  pb (NLO) [89], that is, increasing the collision energy by about seven times increases the number of events by a factor of more than 30! Multiplying this by  $3\text{ ab}^{-1}$  (the expected integrated luminosity from the first 10 years of running the FCC), gives us 96 billion top pair production events. Simulating this many events would require enormous amounts of computing time as well as huge amounts of storage. To alleviate the first problem, we generated events on the University of Arizona cluster, leveraging the power of many computing nodes to perform event generation simultaneously. But this alone would not be enough.

Since we expect our signal process to have a dilepton resonance from an on-shell  $Z$  boson, we restricted the phase space for event generation for backgrounds to the region where the invariant mass of dilepton pairs lies between 80 and 100 GeV. Additionally, the bino dark matter that escapes the detector would result in a large amount of missing transverse energy ( $\cancel{E}_T$ ), so we required a minimum  $\cancel{E}_T$  of 100 GeV at the parton level for the backgrounds as well.

At the reconstructed level, we relaxed the lepton isolation criterion in the `Delphes` detector card from  $\Delta R_{\min}$  from 0.4 to 0.05. This is motivated by the fact that due to the large mass difference between the higgsino NLSP and the bino LSP in our search channel, the intermediate

<sup>2</sup><https://github.com/HEP-FCC/FCCSW/tree/master/Sim/Sim/Delphes/Interface/data>

$Z$  bosons will be highly boosted, and the leptons to which they decay will be highly collimated. The value of 0.05 is consistent with what is suggested in previous 100 TeV studies ([97, 98, 121]) and will allow for easier comparison between strategies.

### Rectangular cuts

For the cut-and-count analysis, we implemented successive one-dimensional cuts on the variables listed below, using the MadAnalysis 5 package [122].

1. **Trigger:** Events were selected if they had at least one lepton with  $p_T > 100$  GeV.
2. **Identification:**
  - We required that events contain exactly two leptons of the same flavor and with opposite charges, with  $p_T > 15$  GeV, and  $|\eta| < 2.5$ .
  - We required that events contain at least two  $b$ -tagged jets with  $p_T > 30$  GeV and  $|\eta| < 2.5$ .
3. **Invariant mass of  $Z$ -candidate:** We required that the invariant mass of the two leptons,  $m_{l^+l^-}$ , lie between 85 and 95 GeV.
4. **Invariant mass of  $h$ -candidate:** We combine the two  $b$ -tagged jets with the highest  $p_T$  to form a  $h$  candidate and require that its invariant mass,  $m_{bb}$ , lies between 75 and 150 GeV.
5. **Missing Transverse Energy:** We required events to have  $\cancel{E}_T > 400$  GeV.
6. **Razor variables:** Consider the pair production of two massive particles  $S_1$  and  $S_2$  that decay into the particles  $(Q_1, \chi_1)$  and  $(Q_2, \chi_2)$  respectively, where  $\chi_{1,2}$  are invisible and have the same mass. The first razor variable,  $M_R$ , inherits the knowledge of the mass difference between the parent particle (the Higgsino), and the invisible particle (the bino).

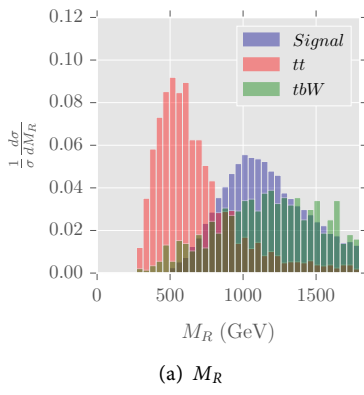
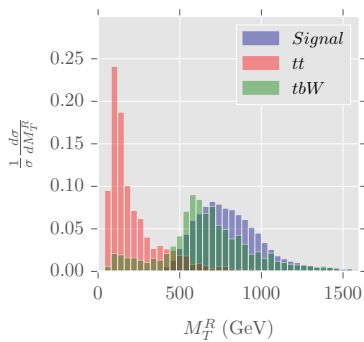
(a)  $M_R$ (b)  $M_T^R$ 

Figure 6.6: Normalized distributions of the razor kinematical variables  $M_R$  (top) and  $M_T^R$  (bottom) for a 1 TeV higgsino NLSP and 25 GeV bino LSP

$$M_R = \sqrt{(E_1 + E_2)^2 - (q_1^z + q_2^z)^2}$$

where  $E_i$  are the energies of the visible particles  $Q_i$ , and  $q_i^z$  are the  $z$ -components of their momenta. The second razor variable,  $M_T^R$ , can be thought of as a longitudinally-invariant analogue of the transverse mass.

$$M_T^R = \sqrt{\frac{1}{2} \left[ \cancel{E}_T (|\vec{q}_{1T}| + |\vec{q}_{2T}|)^2 - \cancel{E}_T \cdot (\vec{q}_{1T} + \vec{q}_{2T}) \right]}$$

For our process, the visible particles  $Q_i$  correspond to the reconstructed SM Higgs and  $Z$  bosons, and the invisibles  $\chi_i$  correspond to the bino LSPs. We scanned across a range of minimum values of these variables to find the ones that yielded the greatest significance. Representative kinematic distributions of these variables for a 1 TeV higgsino and a 25 GeV bino are shown in figure 6.6, after the trigger, identification, and  $\cancel{E}_T$  cuts. We can see that  $M_R$

	$\sigma_{\text{signal}}$	$\sigma_{tt}$	$\sigma_{tbW}$	$\sigma_{bbWW}$	$\sigma_{\text{tot, BG}}$	$S/B$	$S/\sqrt{B}$
Original	0.37	35,998	4,176	7.8	40,182	9.1e-06	0.10
Trigger	0.31	5,321	1,058	2.5	6,382	4.9e-05	0.21
SFOS leptons	0.25	1,774	360	0.88	2,135	1.2e-04	0.30
2 $b$ jets	0.04	290	62	0.09	352	1.3e-04	0.13
$MET < 400$	0.03	5.3	6.8	0.007	12	0.003	0.49
$85 < m_{ll} < 95$	0.03	2.1	3.3	0.004	5.3	0.005	0.62
$75 < m_{bb} < 150$	0.02	0.59	0.30	8.2e-04	0.90	0.02	1.3
$m_R > 800$	0.02	0.03	0.20	3.3e-04	0.23	0.09	2.2
$m_T^R > 400$	0.02	0.008	0.18	1.9e-04	0.19	0.10	2.4

Table 6.2: Representative cut flow table for the benchmark point  $|\mu| = 1 \text{ TeV}$ ,  $M_1 = 25 \text{ GeV}$ , for a traditional cut-and-count analysis. All cross sections are given in femtobarns, and the units for the missing energy, invariant mass, and razor variable cuts are GeV. The significance,  $S/\sqrt{B}$ , is calculated for an integrated luminosity of  $3 \text{ ab}^{-1}$ .

is peaked around 1 TeV for the signal, which is what we would expect, since it corresponds to the mass difference between the NLSP and LSP. The distribution for the  $bbWW$  background is not shown, since it is negligible in comparison to the others. For this mass combination, requiring  $M_R > 800 \text{ GeV}$  and  $M_T^R > 400 \text{ GeV}$  yields the greatest significance.

In table 6.2, we show the cut efficiencies for a representative signal benchmark point with a  $|\mu| = 1 \text{ TeV}$  and  $M_1 = 25 \text{ GeV}$ . The initial signal cross-section is calculated using Prospino2 at next-to-leading order, and is then multiplied by the branching ratios calculated using SUSY-HIT. The cross-sections of the backgrounds are averages of the cross-sections output by MadEvent after performing the MLM matching procedure. Their small size reflects the  $m_{ll}$  and  $\cancel{E}_T$  cuts we imposed at the parton level. For all the benchmark points, we require a minimum of 5 signal events left over after cuts. We can see that, after applying our cuts,  $tt$  and  $tbW$  remain as the dominant backgrounds. The values of the razor variable cuts were chosen to maximize the significance,  $S/\sqrt{B}$  (calculated for an integrated luminosity of  $3000 \text{ fb}^{-1}$ ), shown in the last column.

#### Optimizing using gradient boosted decision trees

For each signal benchmark point and background process, we pre-selected events that passed the lepton trigger, contained two SFOS leptons and two  $b$ -tagged jets, and calculated a number of features for each event. We then placed these features in an array, with each row corresponding to an event, and the columns corresponding to the features. A mixture of low-level and high level features was seen to have the greatest effectiveness. The features chosen were  $m_{ll}$ ,  $m_{bb}$ ,  $M_R$ ,  $M_T^R$ ,  $\cancel{E}_T$ , the total hadronic transverse energy  $THT$ , and transverse momenta of individual final state leptons and  $b$ -quarks:  $p_T(l_1)$ ,  $p_T(l_2)$ ,  $p_T(b_1)$ , and  $p_T(b_2)$ .

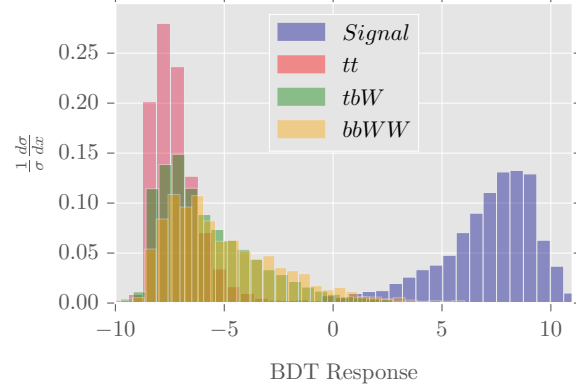


Figure 6.7: Distribution of the decision function of the gradient boosted decision tree classifier algorithm for the signal ( $|\mu| = 1 \text{ TeV}$ ,  $M_1 = 25 \text{ GeV}$ ) and backgrounds.

	$\sigma_{\text{signal}}$	$\sigma_{\text{tt}}$	$\sigma_{\text{tbW}}$	$\sigma_{\text{bbWW}}$	$\sigma_{\text{tot,BG}}$	$S/B$	$S/\sqrt{B}$
Original	0.37	35,998	4,176	7.8	40,182	9.1e-06	0.10
Preselection	0.04	290	62	0.09	352	1.3e-04	0.13
BDT response $> 5.1$	0.04	0.02	0.04	4.8e-04	0.06	0.63	8.4

Table 6.3: Representative cut flow table for the same benchmark point and integrated luminosity as in [table 6.2](#), but using a boosted decision tree (BDT) analysis instead. The preselection is equivalent to the trigger and identification cuts listed in [table 6.2](#). As before, all the cross sections are in femtobarns.

We then divided the events into training and test sets, with the training set comprising 75% of signal events and 30% of background events. We used the `scikit-learn` package [123] to implement our analysis. A boosted decision tree classifier was trained with 1000 weak learners and a learning rate of 0.025. After the classifier is trained, we use it to assign scores to individual events. A more negative score indicates a more background-like event, and a more positive score denotes a more signal-like event. After the scores have been assigned to the events in the test sets, we can use this score just as we would a regular kinematical variable, that is, we apply a cut that selects events with a minimum of this score. The value of the cut is chosen to maximize the significance for each signal benchmark point. The distribution of scores for the specific benchmark point ( $|\mu| = 1 \text{ TeV}$ ,  $M_1 = 25 \text{ GeV}$ ) is shown in [figure 6.7](#). We observe that there is an appreciable separation between the signal and background distributions.

[Table 6.3](#) shows the cut efficiencies for the same representative benchmark point as in [table 6.2](#), but this time for a boosted decision tree analysis. We observe that the statistical significance we can achieve goes up from 2.4 to 8.4, a roughly four-fold increase.

*Note on low event counts and statistics.* For certain values of the cuts on kinematical variables or the score of the ML classifier, no MC events survived for one or more of the background components. To guard against overly optimistic estimates of the significance  $S/\sqrt{B}$ , we set

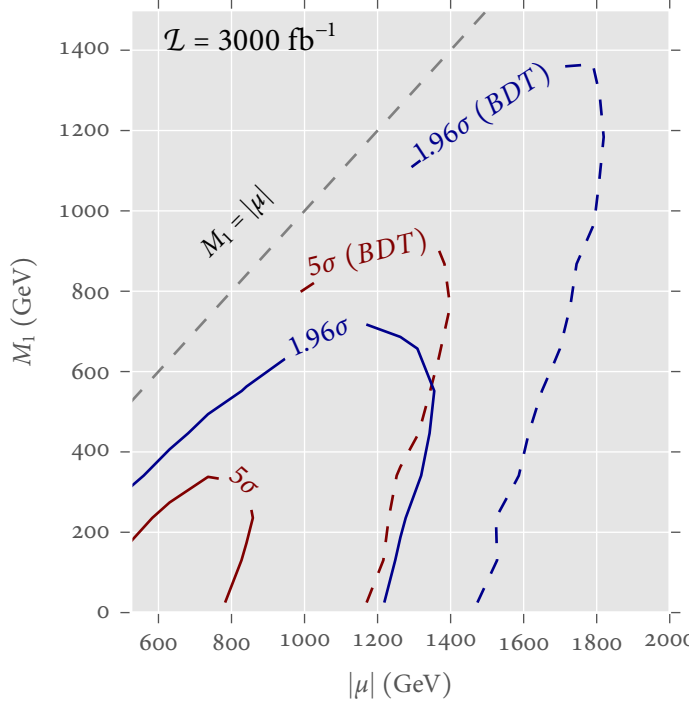


Figure 6.8: Discovery (red) and exclusion (blue) contours for the traditional cut-and-count analysis (solid) and boosted decision tree analysis (dashed), for an integrated luminosity of  $3000 \text{ fb}^{-1}$ .

a lower bound of 3 for the number of MC events after cuts for each background component.

#### *Reach in parameter space*

Figure 6.8 shows the expected reach in parameter space for exclusion and discovery. The cut-and-count strategy is able to discover higgsinos up to 750 GeV and exclude them up to 1.3 TeV. The boosted decision tree analysis, improves this reach - it is able to discover higgsinos up to 1.3 TeV, and exclude them up to 1.8 TeV in favorable points in parameter space. Similarly, binos can be discovered up to 300 GeV and excluded up to 800 GeV with the rectangular cut analysis, and the BDT analysis can discover them up to about 900 GeV and exclude them up to 1.3 TeV. Table 6.4 contains a summary of these results. We do not include systematic errors in these estimates.

This improvement is substantial, but perhaps not spectacular. However, it should be kept in mind that this is probably a conservative estimate. Since we reserve 30% of the data for training purposes, and impose the condition that the minimum number of MC events after cuts for the backgrounds must be 3 (see note at the end of section 6.3), the true rate of background rejection by the classifier is likely underestimated, and the expected significance from the BDT analysis will improve. This extrapolation is qualitatively supported by the high degree of separation between signal and background events seen in figure 6.7, and the fact

Table 6.4: Discovery reaches and expected exclusion limits (in TeV) for the parameters ( $|\mu|, M_1$ ) for the rectangular cuts and boosted decision tree analyses.

Analysis type	$5\sigma$ (discovery)	$1.96\sigma$ (exclusion)
Rectangular cuts	(0.75, 0.30)	(1.3, 0.8)
BDT Analysis	(1.3, 0.90)	(1.8, 1.3)

that a larger fraction of the signal events are preserved with the BDT approach compared to the rectangular cut approach, as can be seen in tables 6.2 and 6.3.

In regions with large mass differences between the LSP and NLSP, the reach is not as good, since the intermediate SM higgs boson will be highly boosted, and thus decay into a highly collimated pair of  $b$ -jets. The extent to which this affects our results can be estimated from table 6.2. We see that requiring two  $b$ -tagged jets reduces our signal cross-section by roughly 87%. This is far more than the 28% reduction that might be naively expected from the  $b$ -tagging efficiency of about 85% specified in our Delphes card.

#### 6.4 CONCLUSION

In this study, we examined the potential for a 100 TeV collider to discover pair-produced heavy higgsino neutralinos that decay to bino LSPs via intermediate  $Z$  and  $h$  bosons that decay to a pair of leptons and  $b$  quarks respectively. More specifically, we examined a split-SUSY like scenario where the scalar superpartners and the wino are heavy and decoupled, reducing the number of available decay channels for the higgsinos.

To do this, we pursued two analysis strategies. One was more traditional, using rectangular selection cuts on kinematical variables, while the other strategy used a boosted decision tree classifier trained with a number of low and high level features. We expected that the machine learning approach would be able to more efficiently determine the optimal decision boundary between signal and background events in feature space than the traditional rectangular cuts.

Overall, we find that the reach of our analysis strategy is a significant improvement over the current limits from the LHC. We found that the rectangular cut strategy has the potential to discover higgsino LSPs up to a mass of 750 GeV, and exclude them up to a mass of 1.3 TeV. As expected, the boosted decision tree classifier performs better, with the ability to discover higgsino NLSPs up to 1.3 TeV and exclude them up to a mass of 1.8 TeV. With this analysis, bino dark matter candidates can be discovered up to 900 GeV, and excluded up to 1.3 TeV. In the process, we highlighted the importance of generating enough Monte Carlo events to estimate the huge backgrounds at a 100 TeV collider.

Additionally, we found that the reach for both strategies is considerably reduced when the difference  $M_1 - |\mu|$  is high, since it results in a highly boosted  $h$  that decays to a collimated pair of  $b$ 's that will most likely be identified as a single jet. This is not an insurmountable difficulty - there are ways to deal with collimated jets, although they are beyond

the scope of this work. This issue does, however, highlight the necessity of improving isolation performance at a 100 TeV machine, where large mass hierarchies can result in highly boosted and collimated decay products. For a review of currently used methods to determine jet substructure, see [124]. In the future, machine learning techniques might be profitably applied to this area as well - for a review of developments along this line, see [125]. The collimation of the b-jets, along with the fact that we take into account detector effects using Delphes, result in a lower reach in the high  $|\mu|$ , low  $M_1$  region than the multilepton analysis in [98], which is able to exclude higgsinos up to a mass of 2.9 TeV for massless binos. The reach of our analysis is slightly higher in the region where the difference between  $|\mu|$  and  $M_1$  is smaller. This is consistent with our usage of the razor variable  $M_R$ , which is sensitive to the mass difference between the parent and daughter particles.

A 100 TeV proton-proton collider represents an excellent opportunity to discover physics beyond the standard model. The extremely high energies and luminosities involved will present new challenges for particle physicists, and it is likely that machine learning will play an important part in facing them.

*Acknowledgments.* We would like to thank Matthew Leone and Ken Johns for helpful discussions. An allocation of computer time from the UA Research Computing High Performance Computing (HPC) and High Throughput Computing (HTC) at the University of Arizona is also gratefully acknowledged. This work was supported in part by the Department of Energy (DoE) under Grant DE-FG02-13ER41976 / de-sc0009913.



# 7

## CONCLUSION

---

The discovery of the Higgs boson in 2012 completed the framework of the Standard Model of particle physics, which has been verified to unprecedent levels of precision. However, the journey is not yet over - the Standard Model either provides unsatisfactory answers to issues such as the hierarchy problem, or is silent on other questions such as the nature of dark matter. Clearly, it is not the final word on the subject of particle physics. To address the issues that the SM does not, we must go beyond it, constructing new theories that provide satisfactory explanations of physics at high energy scales.

Two-Higgs Doublet Models (2HDMs) are physically well-motivated extensions to the scalar sector of the SM. They predict a collection of Higgs bosons, (as opposed to the single Higgs boson of the SM): two CP-even states  $h$  and  $H$ , a CP-odd state  $A$ , and a charged state  $H^\pm$ . Traditional searches for these Higgses at particle colliders focus on them via their decays to SM final states. However, there are compelling scenarios in which these heavy scalars decay predominantly through exotic modes to non-SM final states. In certain regions of parameter space, these exotic modes can dominate the conventional decay modes to SM final states, and thus provide a complementary avenue for discovery.

In [chapter 4](#), we presented an analysis aimed at discovering light charged Higgses produced via top quark decay at the 14 TeV LHC. We found that the exotic decay channel  $H^\pm \rightarrow AW^\pm$  is able to probe the low  $t_\beta$  region better than the conventional decay channels.

In [chapter 5](#), we presented preliminary results from a project aimed at systematically covering a number of exotic decay scenarios through collider analyses for both the 14 TeV LHC and a future 100 TeV collider. We find that the preliminary results are promising, and cover a large swathe of 2HDM parameter space, up to scalar masses of 3.5 TeV, for a wide range of values of  $\tan\beta$ , at a 100 TeV collider.

In addition, we also present an analysis aimed at discovering pair produced higgsino-like neutralinos that decay to bino-like neutralino LSPs at a 100 TeV collider. Both of these particles arise from the Minimal Supersymmetric Standard Model, described in [section 2.3](#). This heavily-studied model can be viewed a special case of a 2HDM that incorporates supersymmetry, a symmetry that connects fermions and bosons. This analysis is performed using the razor variables and boosted decision trees. We find that we are able to exclude Higgsinos up to 1.8 TeV for binos up to 1.3 TeV with this analysis.

In some ways, the three analyses presented in this dissertation can be viewed as a progression on two fronts. On the one hand, they involve increasingly high collider energies, going from 14 TeV to 100 TeV. On the other, they involve an increasing use of machine learning techniques. The first analysis solely uses rectangular selection cuts, the second qual-

tatively compares rectangular cut and machine learning strategies, and the third uses machine learning exclusively. The author believes that it is likely that this trend will be reflected in experimental particle physics research in the future, as we attempt to grapple with increasingly difficult questions at the frontier of the field. Increasing collider energies will be required to probe physically well-motivated scenarios with a TeV scale mass spectrum, while machine learning techniques will be increasingly needed to tackle the extremely large backgrounds and small signal rates at future colliders.

*Open Science.* The author strongly believes in the value of reproducible research and open science. In this spirit, the source code for the dissertation document has been made freely available online at

<https://github.com/adarshp/dissertation>.

The code for the analysis in [chapter 6](#) can be found at

<https://github.com/adarshp/Dark-Matter-at-100-TeV>

while the code for the analysis of the  $H^\pm \rightarrow HW^\pm$  decay channel in [chapter 5](#) can be found at

<https://github.com/adarshp/ExoticHiggs>.

In addition, the code for both of these analyses utilizes a Python-based software framework, `clusterpheno`, written by the author during the course of his graduate work, for the purpose of performing large-scale event generation and analysis on the University of Arizona cluster. The source code for this framework can be found online at

<https://github.com/adarshp/clusterpheno>.

## BIBLIOGRAPHY

---

- [1] Georges Aad et al. “Observation of a new particle in the search for the Standard Model Higgs boson with the ATLAS detector at the LHC”. In: *Phys. Lett.* B716 (2012), pp. 1–29. arXiv: [1207.7214 \[hep-ex\]](#) (cited on page [19](#)).
- [2] Serguei Chatrchyan et al. “Observation of a new boson at a mass of 125 GeV with the CMS experiment at the LHC”. In: *Phys. Lett.* B716 (2012), pp. 30–61. arXiv: [1207.7235 \[hep-ex\]](#) (cited on page [19](#)).
- [3] Felix Kling, Adarsh Pyarelal, and Shufang Su. “Light charged Higgs bosons to AW/HW via top decay”. In: *Journal of High Energy Physics* 2015.11 (Nov. 2015), p. 51. ISSN: 1029-8479 (cited on pages [21](#), [64](#), [65](#)).
- [4] Felix Kling, Jose Miguel No, and Shufang Su. “Anatomy of Exotic Higgs Decays in 2HDM”. In: (Apr. 2016). arXiv: [1604.01406](#) (cited on pages [21](#), [22](#), [64](#), [65](#), [69](#)).
- [5] Ta-Pei Cheng, Ling-Fong Li, and David Gross. “Gauge Theory of Elementary Particle Physics”. In: *Physics Today* 38.12 (1985), p. 78. ISSN: 00319228 (cited on page [23](#)).
- [6] Matthew Schwartz. *Quantum Field Theory and the Standard Model*. Cambridge University Press, 2014, p. 850. ISBN: 9781107034730 (cited on page [23](#)).
- [7] A. Zee. *Quantum Field Theory in a Nutshell*. Princeton, N. J.: Princeton University Press, 2010. ISBN: 9780691140346 (cited on page [23](#)).
- [8] Michael E Peskin and Daniel V Schroeder. *An Introduction to quantum field theory*. 1995. ISBN: 9780201503975 (cited on page [23](#)).
- [9] G. C. Branco, P. M. Ferreira, L. Lavoura, M. N. Rebelo, Marc Sher, and Joao P. Silva. “Theory and phenomenology of two-Higgs-doublet models”. In: *Physics Reports* 516.1 (2012), pp. 1–102. ISSN: 03701573. arXiv: [1106.0034](#) (cited on page [23](#)).
- [10] Stephen P. Martin. “A Supersymmetry Primer”. In: (Sept. 1997), p. 152. arXiv: [9709356 \[hep-ph\]](#) (cited on pages [23](#), [33](#), [34](#)).
- [11] *The most precise picture of the proton* (cited on page [27](#)).
- [12] Felix Kling. “Exotic Higgs Decays”. PhD thesis. 2016, p. 223 (cited on page [32](#)).
- [13] Sidney Coleman and Jeffrey Mandula. “All possible symmetries of the S matrix”. In: *Physical Review* 159.5 (1967), pp. 1251–1256. ISSN: 0031899X (cited on page [34](#)).
- [14] Jeffrey Mandula. “Coleman-Mandula theorem”. In: *Scholarpedia* 10.2 (2015), p. 7476. ISSN: 1941-6016 (cited on page [34](#)).

- [15] Julius Wess and Jonathan Bagger. *Supersymmetry and supergravity*. Princeton, N.J, 1992 (cited on page 34).
- [16] Rudolf Haag, Jan T. Łopuszański, and Martin Sohnius. “All possible generators of supersymmetries of the S-matrix”. In: *Nuclear Physics B* 88.2 (Mar. 1975), pp. 257–274. ISSN: 05503213 (cited on page 34).
- [17] J. Wess and B. Zumino. “Supergauge transformations in four dimensions”. In: *Nuclear Physics B* 70.1 (Feb. 1974), pp. 39–50. ISSN: 05503213 (cited on page 34).
- [18] Abdus Salam and J. Strathdee. “Super-gauge transformations”. In: *Nuclear Physics B* 76.3 (July 1974), pp. 477–482. ISSN: 05503213 (cited on page 34).
- [19] Daniel Froidevaux and Paris Sphicas. “General-Purpose Detectors for the Large Hadron Collider”. In: *Annual Review of Nuclear and Particle Science* 56.1 (Nov. 2006), pp. 375–440. ISSN: 0163-8998 (cited on page 40).
- [20] CMS-doc-4172-v2: *Interactive Slice of the CMS detector*. 2010 (cited on page 41).
- [21] Adarsh Pyarelal. “A Reggeized model for  $\eta(548)$  meson production in high energy proton/proton collisions - Reed College”. PhD thesis. Reed College, 2011, p. 50 (cited on page 42).
- [22] J Alwall, R Frederix, S Frixione, V Hirschi, F Maltoni, and O Mattelaer. “The automated computation of tree-level and next-to-leading Order Differential Cross Sections , and Their Matching To Parton Shower Simulations”. In: (2014). arXiv: [arXiv:1405.0301v1](https://arxiv.org/abs/1405.0301v1) (cited on pages 42, 54, 77).
- [23] Torbjörn Sjöstrand, Stephen Mrenna, and Peter Skands. “PYTHIA 6.4 physics and manual”. In: *Jhep* 2006.05 (2006), pp. 026–026. ISSN: 1029-8479. arXiv: [0603175 \[hep-ph\]](https://arxiv.org/abs/0603175) (cited on pages 42, 77).
- [24] S. Agostinelli et al. “GEANT4 - A simulation toolkit”. In: *Nuclear Instruments and Methods in Physics Research, Section A: Accelerators, Spectrometers, Detectors and Associated Equipment* 506.3 (2003), pp. 250–303. ISSN: 01689002. arXiv: [1005 . 0727v1](https://arxiv.org/abs/1005.0727v1) (cited on page 42).
- [25] J. De Favereau, C. Delaere, P. Demin, A. Giammanco, V. Lemaître, A. Mertens, and M. Selvaggi. “DELPHES 3: A modular framework for fast simulation of a generic collider experiment”. In: *Journal of High Energy Physics* 2014.2 (2014). ISSN: 11266708. arXiv: [arXiv:1307.6346v3](https://arxiv.org/abs/1307.6346v3) (cited on pages 42, 54, 77).
- [26] Joel Heinrich. *Hypothesis Testing* (cited on page 43).
- [27] Kyle Cranmer. “Practical Statistics for the LHC”. In: *Statistics* (2015). arXiv: [1503 . 07622](https://arxiv.org/abs/1503.07622) (cited on page 43).

- [28] Trevor Hastie, Robert Tibshirani, and Jerome Friedman. “The Elements of Statistical Learning: Data Mining, Inference, and Prediction, Second Edition (Springer Series in Statistics) (9780387848570): Trevor Hastie, Robert Tibshirani, Jerome Friedman: Books”. In: *The elements of statistical learning: dta mining, inference, and prediction*. 2011, pp. 501–520 (cited on page 47).
- [29] *LEP Higgs Working Group Home Page* (cited on pages 49, 53).
- [30] Georges Aad et al. “Search for neutral Higgs bosons of the minimal supersymmetric standard model in pp collisions at  $\sqrt{s} = 8$  TeV with the ATLAS detector”. In: *JHEP* 11 (2014), p. 056. arXiv: [1409.6064 \[hep-ex\]](#) (cited on pages 49, 53).
- [31] Vardan Khachatryan et al. “Search for neutral MSSM Higgs bosons decaying to a pair of tau leptons in pp collisions”. In: *JHEP* 10 (2014), p. 160. arXiv: [1408.3316 \[hep-ex\]](#) (cited on pages 49, 53).
- [32] The ATLAS collaboration. “Search for charged Higgs bosons in the  $\tau + \text{jets}$  final state with pp collision data recorded at  $\sqrt{s} = 8$  TeV with the ATLAS experiment”. In: (2013) (cited on pages 49, 52).
- [33] CMS Collaboration. “Search for charged Higgs bosons with the  $H^+$  to tau nu decay channel in the fully hadronic final state at  $\sqrt{s} = 8$  TeV”. In: (2014) (cited on pages 49, 52, 60).
- [34] Georges Aad et al. “Search for a light charged Higgs boson in the decay channel  $H^+ \rightarrow c\bar{s}$  in  $t\bar{t}$  events using pp collisions at  $\sqrt{s} = 7$  TeV with the ATLAS detector”. In: *Eur. Phys. J. C* 73.6 (2013), p. 2465. arXiv: [1302.3694 \[hep-ex\]](#) (cited on pages 49, 52).
- [35] CMS Collaboration. “Search for  $H^+$  to  $c\bar{s}$ -bar decay”. In: (2014) (cited on pages 49, 52).
- [36] Vardan Khachatryan et al. “Search for a Higgs boson in the mass range from 145 to 1000 GeV decaying to a pair of W or Z bosons”. In: *JHEP* 10 (2015), p. 144. arXiv: [1504.00936 \[hep-ex\]](#) (cited on page 49).
- [37] David Curtin et al. “Exotic decays of the 125 GeV Higgs boson”. In: *Phys. Rev. D* 90.7 (2014), p. 075004. arXiv: [1312.4992 \[hep-ph\]](#) (cited on pages 49, 62).
- [38] Eric Brownson, Nathaniel Craig, Ulrich Heintz, Gena Kukartsev, Meenakshi Narain, Neeti Parashar, and John Stupak. “Heavy Higgs Scalars at Future Hadron Colliders (A Snowmass Whitepaper)”. In: (2013). arXiv: [1308.6334 \[hep-ex\]](#) (cited on pages 49, 62, 64, 66).
- [39] Baradhwaj Coleppa, Felix Kling, and Shufang Su. “Exotic Decays Of A Heavy Neutral Higgs Through HZ/AZ Channel”. In: *JHEP* 09 (2014), p. 161. arXiv: [1404.1922 \[hep-ph\]](#) (cited on pages 49, 62).

- [40] Baradhwaj Coleppa, Felix Kling, and Shufang Su. “Charged Higgs search via  $AW^\pm/HW^\pm$  channel”. In: *JHEP* 12 (2014), p. 148. arXiv: [1408.4119 \[hep-ph\]](#) (cited on pages 49, 53, 56, 57, 62, 64).
- [41] Tong Li and Shufang Su. “Exotic Higgs Decay via Charged Higgs”. In: *JHEP* 11 (2015), p. 068. arXiv: [1504.04381 \[hep-ph\]](#) (cited on pages 49, 62, 64, 66).
- [42] G. C. Dorsch, S. J. Huber, K. Mimasu, and J. M. No. “Echoes of the Electroweak Phase Transition: Discovering a second Higgs doublet through  $A_0 \rightarrow ZH_0$ ”. In: *Phys. Rev. Lett.* 113.21 (2014), p. 211802. arXiv: [1405.5537 \[hep-ph\]](#) (cited on pages 49, 62, 64).
- [43] Ning Chen, Chun Du, Yaquan Fang, and Lan-Chun Lü. “LHC Searches for The Heavy Higgs Boson via Two B Jets plus Diphoton”. In: *Phys. Rev.* D89.11 (2014), p. 115006. arXiv: [1312.7212 \[hep-ph\]](#) (cited on pages 49, 62).
- [44] Ning Chen, Jinmian Li, Yandong Liu, and Zuowei Liu. “LHC searches for the CP-odd Higgs by the jet substructure analysis”. In: *Phys. Rev.* D91.7 (2015), p. 075002. arXiv: [1410.4447 \[hep-ph\]](#) (cited on pages 49, 62).
- [45] Rikard Enberg, William Klemm, Stefano Moretti, Shoaib Munir, and Glenn Wouda. “Charged Higgs boson in the  $W^\pm$  Higgs channel at the Large Hadron Collider”. In: *Nucl. Phys.* B893 (2015), pp. 420–442. arXiv: [1412.5814 \[hep-ph\]](#) (cited on pages 49, 62).
- [46] Georges Aad et al. “Search for a CP-odd Higgs boson decaying to Zh in pp collisions at  $\sqrt{s} = 8$  TeV with the ATLAS detector”. In: *Phys. Lett.* B744 (2015), pp. 163–183. arXiv: [1502.04478 \[hep-ex\]](#) (cited on pages 49, 62).
- [47] CMS Collaboration. “Search for a pseudoscalar boson A decaying into a Z and an h boson in the llbb final state”. In: (2014) (cited on pages 49, 62).
- [48] CMS Collaboration. “Search for extended Higgs sectors in the H to hh and A to Zh channels in  $\sqrt{s} = 8$  TeV pp collisions with multileptons and photons final states”. In: (2013) (cited on pages 49, 62).
- [49] Farvah Mahmoudi and Oscar Stal. “Flavor constraints on the two-Higgs-doublet model with general Yukawa couplings”. In: *Phys. Rev.* D81 (2010), p. 035016. arXiv: [0907.1791 \[hep-ph\]](#) (cited on pages 50, 53).
- [50] Baradhwaj Coleppa, Felix Kling, and Shufang Su. “Constraining Type II 2HDM in Light of LHC Higgs Searches”. In: *JHEP* 01 (2014), p. 161. arXiv: [1305.0002 \[hep-ph\]](#) (cited on pages 50, 51, 53, 58, 59).

- [51] C. D. Froggatt, R. G. Moorhouse, and I. G. Knowles. “Leading radiative corrections in two scalar doublet models”. In: *Phys. Rev.* D45 (1992), pp. 2471–2481 (cited on page 50).
- [52] C. D. Froggatt, R. G. Moorhouse, and I. G. Knowles. “Two scalar doublet models with softly broken symmetries”. In: *Nucl. Phys.* B386 (1992), pp. 63–114 (cited on page 50).
- [53] Alex Pomarol and Roberto Vega. “Constraints on CP violation in the Higgs sector from the rho parameter”. In: *Nucl. Phys.* B413 (1994), pp. 3–15. arXiv: [hep-ph/9305272 \[hep-ph\]](#) (cited on page 50).
- [54] Abdul Wahab El Kaffas, Per Osland, and Odd Magne Ogreid. “Constraining the Two-Higgs-Doublet-Model parameter space”. In: *Phys. Rev.* D76 (2007), p. 095001. arXiv: [0706.2997 \[hep-ph\]](#) (cited on page 50).
- [55] Howard E. Haber and Deva O’Neil. “Basis-independent methods for the two-Higgs-doublet model III: The CP-conserving limit, custodial symmetry, and the oblique parameters S, T, U”. In: *Phys. Rev.* D83 (2011), p. 055017. arXiv: [1011.6188 \[hep-ph\]](#) (cited on page 50).
- [56] Tao Han, Tong Li, Shufang Su, and Lian-Tao Wang. “Non-Decoupling MSSM Higgs Sector and Light Superpartners”. In: *JHEP* 11 (2013), p. 053. arXiv: [1306.3229 \[hep-ph\]](#) (cited on pages 50, 53).
- [57] David Eriksson, Johan Rathsman, and Oscar Stal. “2HDMC: Two-Higgs-Doublet Model Calculator Physics and Manual”. In: *Comput. Phys. Commun.* 181 (2010), pp. 189–205. arXiv: [0902.0851 \[hep-ph\]](#) (cited on page 50).
- [58] John F. Gunion, Howard E. Haber, Gordon L. Kane, and Sally Dawson. “The Higgs Hunter’s Guide”. In: *Front. Phys.* 80 (2000), pp. 1–404 (cited on page 51).
- [59] J R Andersen et al. “Handbook of LHC Higgs Cross Sections: 3. Higgs Properties”. In: (2013). Ed. by S Heinemeyer, C Mariotti, G Passarino, and R Tanaka. arXiv: [1307.1347 \[hep-ph\]](#) (cited on page 52).
- [60] Neil D. Christensen, Tao Han, Zhen Liu, and Shufang Su. “Low-Mass Higgs Bosons in the NMSSM and Their LHC Implications”. In: *JHEP* 08 (2013), p. 019. arXiv: [1303.2113 \[hep-ph\]](#) (cited on page 52).
- [61] Manuel Drees, Monoranjan Guchait, and D. P. Roy. “Signature of charged to neutral Higgs boson decay at the LHC in SUSY models”. In: *Phys. Lett.* B471 (1999), pp. 39–44. arXiv: [hep-ph/9909266 \[hep-ph\]](#) (cited on page 52).

- [62] K.A. Olive and Particle Data Group. “Review of Particle Physics”. In: *Chinese Physics C* 40.10 (Oct. 2016), p. 100001. ISSN: 1674-1137 (cited on pages 53, 74).
- [63] Renato Guedes, Stefano Moretti, and Rui Santos. “Charged Higgs bosons in single top production at the LHC”. In: *JHEP* 10 (2012), p. 119. arXiv: 1207.4071 [hep-ph] (cited on page 53).
- [64] Majid Hashemi. “Single Top Events as a Source of Light Charged Higgs in the Fully Hadronic Final State at LHC”. In: *JHEP* 05 (2013), p. 112. arXiv: 1305.2096 [hep-ph] (cited on page 53).
- [65] Majid Hashemi. “Observability of Light Charged Higgs Decay to Muon in Top Quark Pair Events at LHC”. In: *Eur. Phys. J.* C72 (2012), p. 1994. arXiv: 1109.5356 [hep-ph] (cited on page 53).
- [66] Debottam Das, Lukas Mitzka, and Werner Porod. “Discovery of Charged Higgs through  $\gamma\gamma$  final states”. In: (2014). arXiv: 1408.1704 [hep-ph] (cited on page 53).
- [67] Nikolaos Kidonakis. “Differential and total cross sections for top pair and single top production”. In: *Proceedings, 20th International Workshop on Deep-Inelastic Scattering and Related Subjects (DIS 2012): Bonn, Germany, March 26-30, 2012*. [,831(2012)]. 2012, pp. 831–834. arXiv: 1205.3453 [hep-ph] (cited on pages 54, 56).
- [68] Torbjorn Sjostrand, Stephen Mrenna, and Peter Z. Skands. “PYTHIA 6.4 Physics and Manual”. In: *JHEP* 05 (2006), p. 026. arXiv: hep-ph/0603175 [hep-ph] (cited on page 54).
- [69] Jacob Anderson et al. “Snowmass Energy Frontier Simulations”. In: *Proceedings, Community Summer Study 2013: Snowmass on the Mississippi (CSS2013): Minneapolis, MN, USA, July 29-August 6, 2013*. 2013. arXiv: 1309.1057 [hep-ex] (cited on pages 54, 56).
- [70] Lorenzo Moneta, Kevin Belasco, Kyle S. Cranmer, S. Kreiss, Alfonso Lazzaro, Danilo Piparo, Gregory Schott, Wouter Verkerke, and Matthias Wolf. “The RooStats Project”. In: *PoS ACAT2010* (2010), p. 057. arXiv: 1009.1003 [physics.data-an] (cited on page 54).
- [71] *theta: Introduction to theta-auto* (cited on page 54).
- [72] Georges Aad et al. “Measurement of the  $t$ -channel single top-quark production cross section in  $pp$  collisions at  $\sqrt{s} = 7$  TeV with the ATLAS detector”. In: *Phys. Lett.* B717 (2012), pp. 330–350. arXiv: 1205.3130 [hep-ex] (cited on page 55).
- [73] Felix Kling, Tilman Plehn, and Michihisa Takeuchi. “Tagging single Tops”. In: *Phys. Rev.* D86 (2012), p. 094029. arXiv: 1207.4787 [hep-ph] (cited on page 55).

- [74] R. Contino et al. “Physics at a 100 TeV pp collider: Higgs and EW symmetry breaking studies”. In: (2016). arXiv: [1606.09408 \[hep-ph\]](#) (cited on pages [63–65](#)).
- [75] John F. Gunion and Howard E. Haber. “The CP conserving two Higgs doublet model: The Approach to the decoupling limit”. In: *Phys. Rev.* D67 (2003), p. 075019. arXiv: [hep-ph/0207010 \[hep-ph\]](#) (cited on page [63](#)).
- [76] Georges Aad et al. “Constraints on new phenomena via Higgs boson couplings and invisible decays with the ATLAS detector”. In: *JHEP* 11 (2015), p. 206. arXiv: [1509.00672 \[hep-ex\]](#) (cited on page [64](#)).
- [77] G. C. Dorsch, S. J. Huber, K. Mimasu, and J. M. No. “Hierarchical versus degenerate 2HDM: The LHC run 1 legacy at the onset of run 2”. In: *Phys. Rev.* D93.11 (2016), p. 115033. arXiv: [1601.04545 \[hep-ph\]](#) (cited on page [64](#)).
- [78] Baradhwaj Coleppa, Felix Kling, and Shufang Su. “Exotic Higgs Decay via AZ/HZ Channel: a Snowmass Whitepaper”. In: (2013), pp. 1–9. arXiv: [1308.6201](#) (cited on page [64](#)).
- [79] Baradhwaj Coleppa, Felix Kling, and Shufang Su. “Exotic decays of a heavy neutral Higgs through HZ/AZ channel”. In: *Journal of High Energy Physics* 2014.9 (Sept. 2014), p. 161. ISSN: 1029-8479. arXiv: [1404.1922](#) (cited on pages [64–66](#), [68](#)).
- [80] Ushoshi Maitra, Biswarup Mukhopadhyaya, S. Nandi, Santosh Kumar Rai, and Ambresh Shivaji. “Searching for an elusive charged Higgs boson at the Large Hadron Collider”. In: *Phys. Rev.* D89.5 (2014), p. 055024. arXiv: [1401.1775 \[hep-ph\]](#) (cited on pages [64](#), [66](#)).
- [81] L. Basso, A. Lipniacka, F. Mahmoudi, S. Moretti, P. Osland, G. M. Pruna, and M. Purmohammadi. “Probing the charged Higgs boson at the LHC in the CP-violating type-II 2HDM”. In: *JHEP* 11 (2012), p. 011. arXiv: [1205.6569 \[hep-ph\]](#) (cited on pages [64](#), [66](#)).
- [82] Radovan Dermisek, Jonathan P. Hall, Enrico Lunghi, and Seodong Shin. “A New Avenue to Charged Higgs Discovery in Multi-Higgs Models”. In: *JHEP* 04 (2014), p. 140. arXiv: [1311.7208 \[hep-ph\]](#) (cited on pages [64](#), [66](#)).
- [83] B. Mohn, N. Gollub, and K. A. Assamagan. “The ATLAS discovery potential for a heavy Charged Higgs boson in a large mass splitting MSSM scenario”. In: (2005) (cited on page [64](#)).
- [84] K. A. Assamagan. “Signature of the charged Higgs decay  $H^+ \rightarrow W^+ \nu_W$  with the ATLAS detector”. In: *Acta Phys. Polon.* B31 (2000), pp. 881–893 (cited on page [64](#)).

- [85] Nima Arkani-Hamed, Tao Han, Michelangelo Mangano, and Lian-Tao Wang. “Physics Opportunities of a 100 TeV Proton-Proton Collider”. In: *arXiv:1511.06495 [hep-ph]* (Nov. 2015) (cited on page 64).
- [86] *The FCC-hh Homepage* (cited on page 64).
- [87] *CEPC Homepage* (cited on page 64).
- [88] T. Golling et al. “Physics at a 100 TeV pp collider: beyond the Standard Model phenomena”. In: *Submitted to: Phys. Rept.* (2016). arXiv: [1606.00947 \[hep-ph\]](#) (cited on page 64).
- [89] M. L. and others Mangano. *Physics at a 100 TeV pp collider: Standard Model Processes*. Tech. rep. 2016. arXiv: [1607.01831](#) (cited on pages 64, 77).
- [90] Matthew Low and Lian-Tao Wang. “Neutralino dark matter at 14 TeV and 100 TeV”. In: *Journal of High Energy Physics* 2014.8 (Aug. 2014), p. 161. ISSN: 1029-8479. arXiv: [1404.0682](#) (cited on pages 71, 74).
- [91] Gianfranco Bertone, Dan Hooper, and Joseph Silk. *Particle dark matter: Evidence, candidates and constraints*. 2005. arXiv: [0404175 \[hep-ph\]](#) (cited on page 72).
- [92] James D Wells. “Implications of supersymmetry breaking with a little hierarchy between gauginos and scalars”. In: (2003). arXiv: [hep-ph/0306127 \[hep-ph\]](#) (cited on page 72).
- [93] S Dimopoulos, G F Giudice, and A Romanino. “Aspects of Split Supersymmetry arXiv : hep-ph / 0409232v2 19 Oct 2004”. In: September (2004). arXiv: [0409232v2 \[arXiv:hep-ph\]](#) (cited on page 72).
- [94] G. F. Giudice. “Split supersymmetry”. In: *AIP Conference Proceedings*. Vol. 794. 2005, pp. 150–156. ISBN: 073540285X. arXiv: [0406088 \[hep-ph\]](#) (cited on page 72).
- [95] Kim Griest and David Seckel. “Three exceptions in the calculation of relic abundances”. In: *Phys. Rev. D* 43 (1991), pp. 3191–3203 (cited on page 72).
- [96] Christopher Rogan. “Kinematical variables towards new dynamics at the LHC”. In: *arXiv:1006.2727 [hep-ex, physics:hep-ph]* (June 2010) (cited on page 72).
- [97] Bobby S. Acharya, Krzysztof Bozek, Chakrit Pongkitivanichkul, and Kazuki Sakurai. “Prospects for observing charginos and neutralinos at a 100 TeV proton-proton collider”. In: (Oct. 2014), p. 19. arXiv: [1410.1532](#) (cited on pages 73, 74, 78).
- [98] Stefania Gori, Sungsoon Jung, Lian-Tao Wang, and James D Wells. “Prospects for Electroweakino Discovery at a 100 TeV Hadron Collider”. In: *JHEP* 1412 (2014), p. 108. arXiv: [1410.6287 \[hep-ph\]](#) (cited on pages 73, 74, 78, 83).

- [99] Tao Han, Sanjay Padhi, and Shufang Su. “Electroweakinos in the light of the Higgs boson”. In: *Physical Review D* 88.11 (Dec. 2013), p. 115010. ISSN: 1550-7998. arXiv: [1309.5966](#) (cited on page 73).
- [100] ATLAS Collaboration. “Observation of a new particle in the search for the Standard Model Higgs boson with the ATLAS detector at the LHC”. In: *Physics Letters B* 716.1 (2012), pp. 1–29. ISSN: 03702693. arXiv: [1207.7214 \[hep-ex\]](#) (cited on page 73).
- [101] CMS Collaboration. “Observation of a new boson at a mass of  $125\{\text{GeV}\}$  with the {CMS} experiment at the {LHC}”. In: *Phys. Lett. B* 716 (2012), pp. 30–61. ISSN: 03702693. arXiv: [1207.7235 \[hep-ex\]](#) (cited on page 73).
- [102] Joshua Ellis. “TikZ-Feynman: Feynman diagrams with TikZ”. In: January (2016), p. 31. arXiv: [1601.05437](#) (cited on page 74).
- [103] Tilman Plehn. “Lectures on LHC physics”. In: *Lecture Notes in Physics* 886 (2015), pp. 1–340. ISSN: 00758450. arXiv: [0910.4182](#) (cited on page 74).
- [104] Asher Berlin, Tongyan Lin, Matthew Low, and Lian-Tao Wang. “Neutralinos in Vector Boson Fusion at High Energy Colliders”. In: (Feb. 2015). arXiv: [1502.05044](#) (cited on page 74).
- [105] Marco Cirelli, Filippo Sala, and Marco Taoso. “Wino-like Minimal Dark Matter and future colliders”. In: (July 2014), p. 28. arXiv: [1407.7058](#) (cited on page 74).
- [106] The ATLAS collaboration. “Search for supersymmetry with two and three leptons and missing transverse momentum in the final state at  $\sqrt{s} = 13 \text{ TeV}$  with the ATLAS detector”. In: (2016) (cited on page 76).
- [107] The ATLAS collaboration. “Search for supersymmetry in events with four or more leptons in  $\sqrt{s} = 13 \text{ TeV}$  pp collisions using  $13.3\text{fb}^{-1}$  of ATLAS data.” In: (2016) (cited on page 76).
- [108] Vardan Khachatryan et al. “Searches for electroweak production of charginos, neutralinos, and sleptons decaying to leptons and W, Z, and Higgs bosons in pp collisions at 8 TeV”. In: *Eur. Phys. J.* C74.9 (2014), p. 3036. arXiv: [1405.7570 \[hep-ex\]](#) (cited on page 76).
- [109] Serguei Chatrchyan et al. “Search for electroweak production of charginos and neutralinos using leptonic final states in pp collisions at  $\sqrt{s} = 7 \text{ TeV}$ ”. In: *JHEP* 11 (2012), p. 147. arXiv: [1209.6620 \[hep-ex\]](#) (cited on page 76).
- [110] The ATLAS collaboration. “Search for electroweak production of supersymmetric particles in final states with tau leptons in  $\sqrt{s} = 13 \text{ TeV}$  pp collisions with the ATLAS detector”. In: (2016) (cited on page 76).

- [111] Vardan Khachatryan et al. “Search for electroweak production of charginos in final states with two tau leptons in pp collisions at  $\sqrt{s} = 8$  TeV”. In: *Submitted to: JHEP* (2016). arXiv: [1610.04870 \[hep-ex\]](#) (cited on page 76).
- [112] Serguei Chatrchyan et al. “Search for new physics in events with photons, jets, and missing transverse energy in  $pp$  collisions at  $\sqrt{s} = 7$  TeV”. In: *JHEP* 03 (2013), p. 111. arXiv: [1211.4784 \[hep-ex\]](#) (cited on page 76).
- [113] Vardan Khachatryan et al. “Search for supersymmetry in events with a photon, a lepton, and missing transverse momentum in pp collisions at  $\sqrt{s} = 8$  TeV”. In: *Phys. Lett. B* 757 (2016), pp. 6–31. arXiv: [1508.01218 \[hep-ex\]](#) (cited on page 76).
- [114] Georges Aad et al. “Search for photonic signatures of gauge-mediated supersymmetry in 8 TeV pp collisions with the ATLAS detector”. In: *Phys. Rev. D* 92.7 (2015), p. 072001. arXiv: [1507.05493 \[hep-ex\]](#) (cited on page 76).
- [115] Vardan Khachatryan et al. “Search for supersymmetry with photons in pp collisions at  $\sqrt{s}=8$ TeV”. In: *Phys. Rev. D* 92.7 (2015), p. 072006. arXiv: [1507.02898 \[hep-ex\]](#) (cited on page 76).
- [116] Vardan Khachatryan et al. “Search for supersymmetry in electroweak production with photons and large missing transverse energy in pp collisions at  $\sqrt{s} = 8$  TeV”. In: *Phys. Lett. B* 759 (2016), pp. 479–500. arXiv: [1602.08772 \[hep-ex\]](#) (cited on page 76).
- [117] Georges Aad et al. “Search for direct production of charginos, neutralinos and sleptons in final states with two leptons and missing transverse momentum in  $pp$  collisions at  $\sqrt{s} = 8$  TeV with the ATLAS detector”. In: *JHEP* 05 (2014), p. 071. arXiv: [1403.5294 \[hep-ex\]](#) (cited on page 76).
- [118] Vardan Khachatryan et al. “Search for supersymmetry in the vector-boson fusion topology in proton-proton collisions at  $\sqrt{s} = 8$  TeV”. In: *JHEP* 11 (2015), p. 189. arXiv: [1508.07628 \[hep-ex\]](#) (cited on page 76).
- [119] Vardan Khachatryan et al. “Searches for electroweak neutralino and chargino production in channels with Higgs, Z, and W bosons in pp collisions at 8 TeV”. In: *Phys. Rev. D* 90.9 (2014), p. 092007. arXiv: [1409.3168 \[hep-ex\]](#) (cited on page 76).
- [120] W. Beenakker, M. Klasen, M. Krämer, T. Plehn, M. Spira, and P. M. Zerwas. “The Production of Charginos/Neutralinos and Sleptons at Hadron Colliders”. In: (June 1999). arXiv: [9906298 \[hep-ph\]](#) (cited on page 77).
- [121] Joseph Bramante, Patrick J Fox, Adam Martin, Bryan Ostdiek, and Tilman Plehn. “The Relic Neutralino Surface at a 100 TeV collider”. In: (2015). arXiv: [arXiv : 1412.4789v1](#) (cited on page 78).

- [122] Eric Conte, Benjamin Fuks, and Guillaume Serret. “MadAnalysis 5, a user-friendly framework for collider phenomenology”. In: *Computer Physics Communications* 184.1 (2013). ISSN: 00104655. arXiv: [1206.1599](#) (cited on page 78).
- [123] Fabian Pedregosa and G Varoquaux. *Scikit-learn: Machine learning in Python*. Vol. 12. 2011, pp. 2825–2830. ISBN: 9781783281930. arXiv: [arXiv:1201.0490v2](#) (cited on page 80).
- [124] Jessie Shelton. “Jet Substructure”. In: *Proceedings, Theoretical Advanced Study Institute in Elementary Particle Physics: Searching for New Physics at Small and Large Scales (TASI 2012): Boulder, Colorado, June 4-29, 2012*. 2013, pp. 303–340. arXiv: [1302.0260 \[hep-ph\]](#) (cited on page 83).
- [125] A. Schwartzman, M. Kagan, L. Mackey, B. Nachman, and L. De Oliveira. “Image Processing, Computer Vision, and Deep Learning: new approaches to the analysis and physics interpretation of LHC events”. In: *J. Phys. Conf. Ser.* 762.1 (2016), p. 012035 (cited on page 83).

## COLOPHON

This thesis was designed using L<sup>A</sup>T<sub>E</sub>X and the `memoir` package. The inspiration for the layout comes from the works of Edward Tufte and Robert Bringhurst. Minion Pro is used for serif text, and Bitstream Vera Mono for monospaced text.